Detrital zircon U-Pb and Hf constraints on provenance and timing of deposition of the Mesoproterozoic to Cambrian sedimentary cover of the East European Craton, Belarus

Mariusz Paszkowski[1,*], Bartosz Budzyń[1,*], Stanisław Mazur[1], Jiří Sláma[2], Leonid Shumlyanskyy[3,4], Jan Środoń[1], Bruno Dhuime[5,6], Artur Kędzior[1], Sirle Liivamägi[1], Agnieszka Pisarzowska[1,7]

[1] *Institute of Geological Sciences, Polish Academy of Sciences (ING PAN), Research Centre in Kraków, Senacka 1, PL–31002 Kraków, Poland*

[2] *The Czech Academy of Sciences, Institute of Geology, Rozvojová 269, Prague 6 16500, Czech Republic*

[3] *M.P. Semenenko Institute of Geochemistry, Mineralogy and Ore Formation, Palladina ave., 34, 03142, Kyiv, Ukraine*

[4] *School of Earth and Planetary Sciences, Curtin University, Perth, GPO Box U1987, WA 6845, Australia*

[5] *Bristol Isotope Group, School of Earth Sciences, University of Bristol, Wills Memorial Building, Queen's Road, Bristol BS8 1RJ, UK*

[6] *CNRS-UMR5243, Géosciences Montpellier, Université de Montpellier, 34095 Montpellier Cedex 05, France*

[7] *Faculty of Earth Sciences, University of Silesia, Będzińska 60, 41-200, Sosnowiec, Poland*

* Corresponding authors e-mails: ndpaszko@cyf-kr.edu.pl, ndbudzyn@cyf-kr.edu.pl

Abstract

The sedimentary cover of the East European Craton (EEC) is unique because of its low degree of diagenetic alteration that allows preservation of the original "source to sink" relationships. The present study provides U-Pb and Hf zircon data for the entire Proterozoic sedimentary section of the EEC based on samples from five boreholes in Belarus within the Volyn-Orsha Basin, one of the most important sedimentary basins of the craton. Twenty-one samples of mudstones and sandstones were selected for detrital zircon U-Pb geochronology, supplemented by the Hf isotope analyses of zircons from 6 samples representing different U-

Pb age spectra and bulk rock XRD mineralogy of all mudstone samples collected from the studied boreholes. Five clastic successions in the Volyn-Orsha Basin are characterized by different sources of detrital material: (1) The Mesoproterozoic Pinsk Suite with a narrow population of c. 2.0 Ga zircons, (2) The Orsha Suite with a broad 1.3–3.2 Ga zircon age distribution, (3) Glacial sediments of the Vilchitsy Series with an age spectra similar to the Orsha Suite, except for a c. 1.0 and 1.2 Ga cluster, (4) The Volyn and Valdai Series, including lowermost Cambrian, with a narrow trimodal population of 0.5, 1.5, and 1.8 Ga zircons, and (5) lower Cambrian (?) sediments with a diffused zircon age spectrum, including a 500–700 Ma cluster. Maximum depositional ages were constrained for the Vilchitsy Series at 977 ±6 Ma and for the Volyn Series at 579–545 ±4 Ma. Combined Hf zircon data indicate four episodes of new continental crust generation at 3.3, 2.8, 2.1–2.3 and 1.8 Ga, suggestive of source terrains within the crust of the present-day EEC. These sources experienced subsequent reworking of crust at c. 1.8 Ga and 550–600 Ma. Only a lower Cambrian sample lacks any trend or clustering within the Hf data probably due to mixing of zircons from exotic and local sources. Paleogeographic models, explaining these provenance signals, in terms of intracratonic erosion and sediment transport until to the beginning of Cambrian are presented.

Key-words: Baltica, Ediacaran, Hf isotopes, maximum depositional ages, Rodinia, zircon geochronology

1. Introduction

The East European Craton (EEC) is the coherent mass of the Precambrian continental crust that occupies the north-eastern half of the present-day European continent (Fig. 1). The EEC was assembled at c. 1.8–1.7 Ga through multiple terrane collisions and it has never been dismembered since then (Bogdanova et al., 1996, 2008). The sedimentary cover of the major

part of the EEC is unique because of its low degree of diagenetic alteration (Goryl et al., 2018; Liivamägi et al., 2018; Pehr et al., 2018) that assures preservation of the original sediment characteristics, indicative of the paleoenvironment and life on the planet at this fundamental evolutionary event. Having been deposited on a stable craton, the Precambrian sediments of the EEC keep record of the "source to sink" relationships from the time preceding the Ediacaran fragmentation of the Rodinia supercontinent.

The Proterozoic sedimentary cover of the EEC has been extensively drilled and studied since the 1950's when detailed lithological descriptions, petrographic observations and lithostratigraphic subdivisions of the sedimentary sequence were established (review in Makhnach et al., 2001). More recently the Neoproterozoic flood basalt ages were constrained by zircon U-Pb dating (Shumlyanskyy et al., 2016 and references therein). The youngest, post-eruptive sediments are widespread on the craton (Russia, Baltic States, Belarus, Ukraine, Moldova and Poland; Rozanov and Łydka, 1987), whereas older sediments are preserved only locally, mostly in Belarus and Russia. Their ages remain unconstrained by biostratigraphy due to the absence of fossils. U-Pb geochronological constraints are also lacking in Belarus.

In this contribution, a provenance study for the entire Proterozoic sedimentary column of the EEC was undertaken, using samples from five boreholes in Belarus, selected to represent the main sedimentary basin on the craton (Figs. 1, 2). The U-Pb geochronology of detrital zircon was supplemented by Hf isotope analysis of representative zircon groups and the bulk rock XRD mineralogy of the host rocks. Such a combined analytical approach is aimed at constraining changes in provenance and sources of sediments, particularly at the time of Rodinia break-up and the birth of Baltica, during the Ediacaran/Cambrian transition (e.g.,

Torsvik et al., 1992, 1996). In addition to the provenance information, the U-Pb zircon data is used to constrain maximum depositional ages, which offers a potentially more accurate age determination compared to the previously used general lithostratigraphy and acritarch-based biostratigraphy (Makhnach et al., 2001).

2. Geological background

2.1. Crystalline basement

The main lithotectonic units of the crystalline basement of Belarus are composed of medium- to high-grade metamorphic rocks of Paleoproterozoic age (Bogdanova et al., 2001; Claesson et al., 2001; Shumlyanskyy, 2014). They run NE–SW, parallel to the c. 1.8 Ga old tectonic suture between Sarmatia and Fennoscandia (Elming et al., 1998; Bogdanova et al., 2008; Lubnina et al., 2009) (Fig. 1a). The crystalline basement of Belarus on both sides of the suture was already deeply eroded and peneplained by the end of Paleoproterozoic. However, subsequent differentiated subsidence produced the Volyn-Orsha Aulacogen and Prypyat Trough, prominent cratonic basins reaching several kilometres in depth (e.g., Bogdanova et al., 2008).

2.2. Volcano-sedimentary cover

The volcano-sedimentary cover in Belarus (Fig. 1a) includes a large variety of lithostratigraphic units ranging in age from Mesoproterozoic to recent and are variable in the extent and thickness – from a few dozens of meters on the domal uplifts up to several kilometres in the cratonic basins, aulacogens, and troughs (Makhnach et al., 2001). The lithostratigraphic subdivision of the pre-Ordovician rocks used in this study (Figs. 2, 3) and their description below was compiled from data published by Chumakov and Semikhatov

105 (1981), Rundqvist and Mitrofanov (1993), Makhnach et al. (2005) and Pacześna (2010),
106 including their stratigraphic age assignments (Fig. 3).
107
108 *2.2.1. Belarus Series*
109 The oldest rocks studied belong to the Belarus Series that fills the Volyn-Orsha Aulacogen
110 (Fig. 1) and is subdivided into the Rogachev, Pinsk, Orsha and Lapichi Suites (Fig. 3). The
111 weighted average $^{207}Pb/^{206}Pb$ age of the youngest group of detrital zircons found in the
112 Polissya Series (Ukrainian equivalent of the Belarus Series) defines a maximum depositional
113 age of 1228 ± 15 Ma (Shumlyanskyy et al., 2015). This age is older than previously obtained
114 mica and feldspar K-Ar ages of 700–815 Ma and K-Ar whole-rock ages of 880–980 Ma
115 (Makhnach et al., 1976; Chebanenko et al., 1990) as well as whole-rock K-Ar age of 1055
116 Ma by Nechaev (1974).
117
118 *The Pinsk Suite* in the study area (Fig. 3) rests unconformably on Paleoproterozoic crystalline
119 basement and reaches 460 m in thickness. It is mainly composed of fine-grained
120 sandstones/coarse-grained siltstones with interbeds of oligomictic to mesomictic medium-
121 grained sandstones (quartz arenites are minor component), argillaceous siltstones and clays.
122 Rocks are weakly to moderately cemented by either clay minerals or rarely by dolomite. The
123 sediments are generally variegated, reddish with abundant reduction greyish spots, bands, and
124 interlayers. The sedimentary sequence is characterized by the rhythmic appearance of fining
125 upward sequences, each starting with an erosional surface.
126
127 *The Orsha Suite* with a well-developed basal horizon reaches 620 m in thickness and overlies
128 the eroded surface of the Pinsk Suite or, in peripheral areas of the Volyn-Orsha linear
129 depocenter, rests directly on the Paleoproterozoic crystalline basement. The Orsha Suite is

130 composed of predominantly red-coloured, loose, quartz arenites of well-rounded and well-
131 sorted framework with finely dispersed kaolinite. In the top part of the unit, quartz-cemented
132 sediments occur. Siltstones and argillites are rare. The sediments are usually horizontally or
133 cross-bedded. The Orsha Suite does not contain any organic remnants or trace fossils and its
134 monotonous composition makes correlations difficult.
135
136 *The Lapichi Suite* is absent from the studied wells (Fig. 2), but elsewhere it reaches 82 m in
137 thickness (Fig. 3) and occurs only locally in central Belarus. This unit is represented mainly
138 by mesomictic to oligomictic sandstones, siltstones, clays, dolomites, syngenetic dolomitic
139 breccias, rarely conglomerates. The rocks are red and variably coloured. The dolomites form
140 0.4 to 3 m thick beds of chemical and organic (microphytolitic and stromatolitic) origin
141 (Makhnach et al., 2001).
142
143 *2.2.2. Vilchitsy Series*
144 The Vilchitsy Series sediments are present mainly within the Volyn-Orsha Aulacogen,
145 although small outliers are also known from the adjacent areas (Ukrainian Brody Suite). The
146 Vilchitsy Series is up to 728 m thick terrigenous succession composed of tillites (unsorted
147 massive argillites-siltstones-sandstones with dispersed fine sand to pebble-sized clasts),
148 sandstones, fine-bedded argillites-siltstones and clays. Sandstones and sands are mainly
149 poorly sorted, oligomictic, often cross-bedded, whereas siltstones and clays are horizontally
150 laminated (varved clays) and contain numerous larger clasts.
151
152 In the southern part of the Orsha Basin the Vilchitsy Series is subdivided into two terrigenous
153 suites (Fig. 3): (i) lower – the Blon Suite, interpreted as moraine sediments comprising local
154 material, dominated by Orsha quartz arenite erratics, with a very small proportion of exotic

155 rocks, and (ii) the regionally more extensive Glusk Suite containing 3–4 tillite beds with a
156 thickness of 26–64 m each, alternated with the horizons of sandstones, siltstones, and clays.
157 The Vilchitsy Series is classified as Vendian, but its precise age is unknown (Chumakov,
158 2015). According to Chumakov (2010), the first (Blon) and second (Glusk) glacial levels of
159 the Vilchitsy Series/Lapland Horizon probably correspond to the global Marinoan and
160 Gaskiers glacial event, respectively.
161
162 *2.2.3. Ediacaran Volyn Series*
163 The Volyn Series sediments cover most of Belarus, also extending into western Ukraine
164 (upper Drevlyane Horizon), eastern Poland (Sławatycze Series) and Lithuania (Merkys
165 Formation). In the south-western Belarus, the thickness of the Volyn Series reaches 300–440
166 m, but it does not exceed 100 m in other parts of the country. In Belarus, the Volyn Series is
167 subdivided into three suites (Fig. 3).
168
169 The lower, *Gorbashi Suite*, 6 to 30 m thick, occurs in north-western Ukraine and south-
170 western Belarus. This unit of predominantly red colour is composed of unevenly-grained and
171 coarse-grained sandstones with interlayers of pebble-sized conglomerates and rarely
172 siltstones. Dating of detrital zircons isolated from conglomerate matrix revealed the presence
173 of a single population of 1422 ± 19 Ma igneous zircons (Shumlyanskyy et al., 2015).
174
175 *The Rataychitsy Suite* and its local equivalents (Lukomsk and Kletsk; Fig. 3) occur as a
176 sequence of volcanic and volcano-sedimentary rocks termed “Volyn flood basalt province”
177 (VFBP; Kuzmenkova et al., 2011; Shumlyanskyy, 2012; Shumlyanskyy et al., 2016). These
178 rocks are widely distributed in Belarus with a maximum thickness of 340 m in the Brest
179 Basin, and decreasing to 100 m elsewhere proportionally to the distance from the area of

180 volcanic activity. While volcanic rocks (basalts and tuffs with locally occurring felsic
181 volcanic rocks) prevail in the Brest Basin, pyroclastic rocks occur in the surrounding NE
182 areas, passing into terrigenous sediments with an admixture of ash in distal areas. According
183 to Shumlyanskyy et al. (2016), volcanic rocks of the VFBP were emplaced at 573 ± 14 Ma
184 (lower basalts) and 571 ± 13 Ma (rhyolitic dacite), while Compston et al. (1995) dated tuff
185 from SE Poland at 551±4 Ma.
186
187 The Rataychitsy Suite is overlaid by the *Girsk Suite* (Brest Basin) or *Lyozno Suite* (Orsha
188 Basin) and *Vidibor Suite* (Pripyat Trough, Eastern part of the Polissya Saddle). The Girsk
189 Suite is composed of red-coloured uneven-grained arkoses and polymictic sandstones with
190 numerous interlayers of pebble-sized conglomerates, and argillaceous siltstones. The rocks
191 contain abundant volcanomictic and pyroclastic material. The coarse-grained sediments are
192 cemented by clay minerals, often with admixture of iron oxides and hydroxides or ferrous
193 dolomite. The Lyozno Suite is composed of grey-coloured finer sediments (clays,
194 argillaceous siltstones) with interlayers and lenses of arkosic sandstones in the lower part of
195 the succession.
196
197 *2.2.4. Ediacaran Valdai Series*
198 The Valday Series transgressively overlays the older sedimentary rocks and crystalline
199 basement. In NE Belarus it occurs as extensive cover, whereas in SW Belarus it is limited to
200 isolated areas. The Valdai Series is composed of terrigenous deposits that occur as four large
201 sedimentary cycles: the Nizov, Selsk, and Tshernitse Suites, collectively defined as the
202 Redkino Horizon, and the youngest Kotlin Suite (Fig. 3).
203

The Redkino Horizon is up to 168 m thick. The lower part of each sedimentary cycle starts with unevenly-grained sandstones and conglomerates, passing upwards into arkosic medium-fine-grained sandstones with argillaceous and dolomitic cement of interstitial and basal types. To the top, they grade to heteroliths (interbedded sandstones and siltstones), and then into thin-layered micaceous and argillaceous siltstones and argillites. The Nizov Suite is enriched in volcanic material, probably derived from the underlying Volyn Series. The Selsk Suite contains a horizon of brown argillites. The upper part of this suite also contains a horizon of grey argillaceous siltstones enriched in organic matter. The Tshernitse Suite is enriched in thin laminae of heavy minerals. The transition to overlying Kotlin Suite is gradual and the subdivision is based on biostratigraphy.

The Kotlin Suite is characterised by highly variable thickness from a maximum of 220 m in the Orsha Basin to 50–140 m elsewhere. In the Orsha Basin, the Kotlin Suite shows clear tripartition being dominated by sand, argillaceous siltstones and clay in the lower, middle and upper part, respectively. In the western part of Belarus, the domination of coarse-grained terrigenous deposits with argillaceous siltstone interbeds is explained by the facial variability in the marginal parts of the basin and/or deep erosion that left only the lower, coarse-grained basal part of the suite with the total present thickness of 10–100 m.

2.2.5. Cambrian sediments

The thickness of lower and middle Cambrian sediments varies from more than 520 m in the southwest part of Belarus to 160 m (only lower Cambrian) in the northwest part. Cambrian rocks comprise clays, siltstones, and sandstones relatively poor in organic remains. The amount of fine-grained sediments (clays) gradually increases upward in the section and westwards, in the direction of deeper parts of the Cambrian sedimentary basin. Cambrian

229 sediments overlie the Ediacaran rocks with an unconformity that is consistent with
230 biostratigraphic data.
231
232 **3. Sample selection and analytical methods**
233 Quantitative XRD analyses of bulk rocks is an independent source of information to
234 characterise provenance. Such analyses were performed on all mudstone samples collected
235 from the boreholes. The XRD patterns of random samples, wet-ground with ZnO internal
236 standard to assure high reproducibility of intensities (Środoń et al., 2001), were recorded in
237 5–65 °2Θ range with 0.02 °2Θ step on Xtra diffractometer, equipped with Cu tube and solid-
238 state detector. After mineral identification, quantitative mineral analysis was performed using
239 in-house Q-Min software (M. Szczerba, unpublished).
240
241 Twenty-one samples of mudstones and sandstones from five boreholes in Belarus were
242 selected for zircon geochronology (Fig. 2; Table 1). Analytical strategy included selecting c.
243 40 most euhedral grains with sharp edges (named group A) and c. 100 grains representing
244 random detrital population for provenance analysis (named group B). Maximum depositional
245 ages were calculated using from 2 to 5 youngest zircons following Dickinson and Gehrels
246 (2009). These are presented as concordia ages calculated from the youngest zircons with
247 <2.0% discordance. The Pb/U and Pb isotopic ratios in zircons were measured using a
248 Thermo Scientific Element 2 sector field ICP-MS coupled to a 193 nm ArF excimer laser
249 (Teledyne Cetac Analyte Excite laser) at the Institute of Geology of the Czech Academy of
250 Sciences, Prague, Czech Republic. Analytical details are presented in Supplementary Data
251 (SD1 and SD2).
252

Hf isotopes were measured in zircons from 6 selected samples representing different U-Pb age spectra in order to shed more light on their provenance. The analyses were performed at the University of Bristol (Bristol Isotope Group) using a ThermoFinnigan Neptune plus multicollector inductively-coupled plasma mass spectrometer (MC-ICP-MS) coupled with a Photon-Machine Analyte G2 Excimer laser (193 nm wavelength). The new crust evolution curve of Dhuime et al. (2011) and chondritic values from Bouvier et al. (2008) were used for model age and initial ε_{Hf} calculations. See Supplementary Data (SD1 and SD3) for more details.

4. Results

4.1. Mineral composition

The largest difference in mineral composition was observed between pre-Volyn, Volyn and post-Volyn Series rocks. The pre-Volyn rocks contain >60% quartz, while the fraction of quartz in the sum of primary minerals exceeds 70% and plagioclase is lacking (Table S1; Fig. 4). Orthoclase and microcline, if present, occur in similar proportions (ratio of 0.7–1.4) and micas are minor components. The Orsha Suite differs from the rest of the pre-Volyn Series by extremely mature composition, exclusively quartz, kaolinite and hematite.

The Volyn Series is characterized by a quartz content <25% (38–48% of primary minerals), very high orthoclase/microcline ratio (3–10), high hematite and dioctahedral 2:1 clays, the presence of specific basaltic minerals (calcic plagioclase, occasionally pyroxene, zeolites, saponite, chlorite or mixed layer chlorite-smectite), trioctahedral mica, and the lack of muscovite. The lower part of the Volyn Series in the Vilchitsy borehole, some Volyn samples in the Pinsk borehole and the central part of the Volyn Series in the Kobryn borehole lack microcline, trioctahedral mica and kaolinite, which identifies pure, unweathered volcanic

material (tuffs in the Vilchitsy and Pinsk boreholes, tuffs and basalts in the Kobryn borehole). Tuffs differ from basalts by the much higher quartz and K-feldspar content and lack of pyroxene. Non-stoichiometric dolomite is characteristic of the Volyn Series.

Above the Volyn Series the mineral composition is different (Fig. 4): the low quartz content is slowly increasing, the high orthoclase/microcline ratio is preserved (except of the Kobryn borehole), hematite and the specific basaltic minerals are decreasing abruptly, while $2M_1$ mica and the sum of authigenic minerals are increasing. Na-plagioclase, trioctahedral mica and kaolinite reach the maximum values in Redkino and they are decreasing in the younger rocks, while the dioctahedral 2:1 clays increase from the Redkino minimum. Among authigenic minerals, berthierine and apatite exceed 3% from the Volyn Series to Cambrian, while siderite and dolomite are only present in the Kotlin Suite and in the Cambrian rocks.

4.2. LA-ICP-MS U-Pb zircon geochronology

The majority of zircon crystals of the group A in each sample have oscillatory zoning with some crystals containing euhedral inherited cores (Fig. 5). Homogeneous and patchy zoned crystals are less common. Zircons of the group B are predominantly oscillatory zoned with minor crystals having patchy or complex zoning. The Th/U ratio in the majority of the analysed zircon grains is well above 0.1 (mostly between c. 0.1–4.3) indicating that zircons probably crystallized in magmatic rocks (Hoskin and Black, 2000; Kelly and Harley, 2005; Rubatto, 2017). Because of the large amount of data, the following section presents U-Pb results for both A and B groups together. Inclusion of the euhedral population does not affect data presentation, i.e. there is no significant shift towards younger ages, except for a few samples (see discussion below). U-Pb data are filtered to remove analyses that are >10%

discordant. A full set of analytical results is provided in Table S2. Additional details concerning U-Pb results for groups A and B are presented in Supplementary Data (SD4).

4.2.1. Pre-Volyn rocks

The zircons from the Vilch-2 and Vilch-4 samples representing the Pinsk Suite (Figs. 2, 3) are dominated by Paleoproterozoic c. 2.00 Ga zircons (minor populations at 1.70–1.80 Ga and 2.10–2.15 Ga for Vilch-2; 1.75–1.84 Ga and 2.10 Ga for Vilch-4; Fig. 6), and contain several Archean grains (up to c. 2.90 Ga). Both samples are characterised, in contrast to all other analysed samples, by the limited proportion of euhedral grains. Concerning the latter along with uncertain geological significance of a few younger ages (c. 588 Ma, 980 Ma and 617 Ma, 954 Ma), a maximum depositional age for the Pinsk Suite is not calculated.

In contrast to the Pinsk Suite, samples from the Orsha Suite and Vilchitsy Series bear record of multiple events. Zircons from the Vilch-5B (Orsha Suite) yielded U-Pb ages nearly continuously distributed between 1.29 and 3.19 Ma with local maxima at 1.80 Ga, 1.90 Ga, 2.10 Ga and a dominant peak at 2.00 Ga (Fig. 6). The tillite samples Vilch-6A and Vilch-7A (Vilchitsy Series) contain zircons with U-Pb ages nearly continuously ranging from c. 941 Ma to 2.15 Ga with dominant age peaks at 2.00 Ga for the Vilch-6A, and 945 Ma to 2.20 Ga for the Vilch-7A. In all samples from the Orsha Suite and Vilchitsy Series a few Archean ages up to c. 3.20 Ga were identified. The maximum depositional ages of 977±6 Ma (n = 2, MSWD = 1.12) and 1056 ± 4 Ma (n = 4; MSWD = 1.9) have been constrained for samples Vilch-6A and Vilch-7A, respectively.

4.2.2. Volyn rocks

326 The Volyn Series rocks are represented by three samples of the Rataychitsy Suite (lower part
327 of the Volyn Series) and four samples of the Girsk/Lyozno Suites (upper part of the Volyn
328 Series; Fig. 2). The zircons from the lower part (samples Pinsk-45A, Pinsk-46A) show nearly
329 identical U-Pb age pattern with a dominant peak at c. 1.50 Ga with two smaller peaks at c.
330 590 Ma and 1.80 Ga, whereas in the Kob-10 sample the youngest c. 580 Ma peak dominates
331 over 1.50 and 1.80 Ga (Fig. 6). The maximum depositional ages for both the Pinsk-45A and
332 46A samples are constrained to 579 ± 4 Ma (n = 4, MSWD = 0.18; and n = 3, MSWD = 2.2,
333 respectively). For the Kob-10 sample, the PDP plot is shifted towards youngest ages due to c.
334 580 Ma dominance in group A zircons (for more details see Supplementary Data SD4). A
335 maximum depositional age of 569 ± 4 Ma (n = 4, MSWD = 0.72) is 10 Ma younger staying
336 slightly out of the error range (Fig. 6).
337
338 The samples from the upper part of the Volyn Series included brown, soft tuffite Kob-27A,
339 arkose/wacke Kob-32A, tuffite Kob-34A and arkose Kob-34B. Zircons from these samples
340 demonstrate a dominant U-Pb age peak at c. 1.50 Ga, along with smaller peaks at 1.80 Ga
341 and 550–570 Ma (except of sample Kob-34B with c. 1.50 Ga and 0.60 Ga peaks roughly of
342 the same size). Maximum depositional ages demonstrate decreasing trend up the profile, from
343 560 ± 5 Ma (Kob-27A; n = 3, MSWD = 2.3), and 567 ± 4 Ma (Kob-32A; n = 3, MSWD =
344 0.102) to ages 545 ± 4 Ma (Kob-34A; n = 3, MSWD = 3.7) and 550 ± 4 Ma (Kob-34B; n = 5,
345 MSWD = 0.045) staying within the error range (Fig. 6).
346
347 *4.2.3. Valdai Series rocks*
348 The Valdai Series rocks are represented by 4 samples from the Redkino Horizon (Nizov,
349 Selsk and Tshernitse Suites) and 3 samples from the Kotlin Suite (Fig. 2). The zircon ages

mainly range between c. 1.50 and 1.90 Ga, but without a younger group at c. 550–570 Ma that is present in the older Volyn Series rocks.

Zircons from the Nizov Suite (sample Bog-33A) yielded a dominant age peak at c. 1.50–1.70 Ga with two maxima at c. 1.58 and 1.64 Ga. Another large peak is identified at c. 1.83 Ga, with an additional minor age group at c. 1.91 Ga. Two zircons have older ages of 2.32 and 2.84 Ga. The age pattern of the Selsk Suite (sample Lep-12A) exhibits a dominant age peak at c. 1.84 Ga and smaller peaks at 1.47 and 1.59 Ga and contains only one zircon grain of older age at 2.37 Ga. The zircons from the Tshernitse Suite show an age pattern with a dominant peak at c. 1.50 Ga (minor age clusters at c. 1.62 and 1.83 Ga) in sample Bog-43A and c. 1.84 Ga (smaller peaks at 1.47 and 1.59 Ga; similarly to the age pattern recognised in the Selsk Suite) in sample Lep-20B. Both samples from the Tshernitse Suite contain grains of the older age, i.e. 2.18 Ga in Bog-43A and 2.05–2.32 Ga in Lep-20B.

The samples from the Kotlin Suite (Lep-28A, Bog-51A and Kob-40A) show a similar age pattern to those from the Redkino Horizon with a dominant age peak at c. 1.50–1.54 Ga and smaller peaks at c. 1.80–1.84 Ga. Additionally, the Bog-51A sample reflects also a small peak at c. 1.62 Ga. The older zircon single ages are between 1.96 and 2.75 Ga (Lep-28A and Bog-51A) or c. 3.28 Ga (Kob-40A).

4.2.4. Palaeozoic rocks

The lower Cambrian glauconite-bearing quartz arenite (sample Kob-54) contains most homogeneous age record in this study with a single peak at c. 1.49 Ga. Only five analyses yielded ages staying out of the main cluster, from c. 1.60 to 1.94 Ga. In contrast, the second lower Cambrian sample (Kob-57), a coarse-grained sandstone, contains a nearly continuous

spectrum of ages ranging from c. 542 to 3.41 Ga with dominant peaks at c. 550 and 620 Ma, and smaller older peaks at c. 2.04, 2.10, 2.66 and 2.71 Ga. Two zircons yielded a maximum depositional age of 543±4 Ma (MSWD = 0.91) staying within the error range of the Precambrian–Cambrian boundary.

4.3. Hf isotopes

Zircons from tillite Vilch-6A (Vilchitsy Series) analysed for Hf isotopes have U/Pb or Pb/Pb dates ranging between 683–3185 Ma and they display a wide range of initial ε_{Hf} values from -10.6 to 6.1 (Table 2; Fig. 7a). According to their pattern on the measured date versus ε_{Hf} plot, all zircons in this sample can be tentatively attributed to three groups (Fig. 7a). The first (oldest) group includes zircons with ages between 3.19 and 2.50 Ga, and ε_{Hf} from 2.5 to -6.5 (n = 6). These zircons plot along c. 3.3 Ga crust evolution line with $^{176}Lu/^{177}Hf = 0.019$; however, due to limited data points, they may also plot along a large number of evolution lines with different slopes corresponding to different $^{176}Lu/^{177}Hf$ ratios, and any scenario from felsic to mafic (0.009 and 0.022, respectively; Gardiner et al., 2018) crustal evolution is possible. The second, poorer defined group comprises zircons with ages ranging from 2.17 to 1.42 Ga, and ε_{Hf} from 5.2 to -10.2 (n = 14). The youngest group is well-defined and comprises zircons ranging in age from 1.53 to 0.68 Ga and ε_{Hf} from 6.1 to -2.8 (n = 8), most of them being juvenile. These zircons plot along a line of slope $^{176}Lu/^{177}Hf$ c. 0.016, which corresponds nearly to the average continental crust. The "new crust" model age (Dhuime et al., 2011) for this group is c. 1.8 Ga, which probably corresponds to a discrete crust-forming event.

Zircons from tuffite Pinsk-46A (Rataychitsy Suite) range in age from c. 1860 to 575 Ma, and initial ε_{Hf} from +4 to -13.9 (Table 2; Fig. 7b). These zircons belong to three age groups: the

oldest group (age 1.75–1.87 Ga, ε_{Hf} from 3.4 to -1.5; n = 9), the intermediate group (age c. 1.50 Ga, ε_{Hf} from -2.8 to -5.5; n = 13), and the youngest group (age 590–575 Ma, ε_{Hf} from -10.2 to -13.9; n = 4). All these zircons, irrespective of their age, plot along an evolution line with $^{176}Lu/^{177}Hf$ of c. 0.015 indicating average continental crust source, and with the new crust model age of c. 2.3 Ga.

Zircons from the arkose Kob-34B sample (Girsk Suite) were selected from three separate age groups: the oldest group (c. 1.75–1.85 Ga) comprises predominantly chondritic to slightly juvenile zircon with ε_{Hf} varying from 4.4 to -1.4 (n = 9), the intermediate group of zircons (1.46–1.57 Ga) have ε_{Hf} ranging from -1.6 to -4.1 (n = 12), and the youngest group have a narrow age interval (548–571 Ma with one date 708 Ma) and wide range of ε_{Hf} values – from -0.6 to -18.4 (n = 9; Fig. 7c; Table 2). Interestingly, the oldest and intermediate groups in the Rataychitsy and Girsk Suites coincide in age and ε_{Hf} se. The data from the Kob-34B sample also plot along an evolution line of slope $^{176}Lu/^{177}Hf$ 0.013, which intercepts the new crust evolution line at c. 2.2 Ga.

Zircons from quartz arenite/subarkose sample Bog-33A (Nizov Suite) form a coherent group that ranges in age from 1.93 to 1.49 Ga and initial ε_{Hf} from 5.8 to -4.3 (n = 24; Table 2; Fig. 7d). This group plots along a regression line of slope $^{176}Lu/^{177}Hf = 0.010$. A low $^{176}Lu/^{177}Hf$ ratio (i.e., 0.010) reflects evolution of felsic source reservoir with a mantle extraction age of c. 2.1 Ga. The c. 2.1 Ga crust-forming event is similar to the c. 2.1–2.3 Ga event observed in other Neoproterozoic sediments. Furthermore, three isolated zircons from this sample have either older ages or lower ε_{Hf} values (2.84 Ga and 4.1; 2.32 Ga and 0.4; 1.54 Ga and -9.2, respectively).

Two age groups occur in the arkose Lep-12A sample (Selsk Suite). The older group (1.72–1.89 Ga) ranges in ε_{Hf} from +2.3 to -1.6 (n = 10), and the younger group (1.42–1.67 Ga) ranges in ε_{Hf} from +5.3 to -5.4 (n = 13; Table 2; Fig. 7e). The large majority of the data plot along an evolution line of slope $^{176}Lu/^{177}Hf = 0.013$ indicating intermediate to felsic source and intercepting the new crust evolution line at c. 2.2 Ga, similar to the crust extraction age seen for the Volyn Series sediments.

Zircons from the lower Cambrian quartz arenite Kob-57 sample are extremely variable in terms of both their age (ranging from 3.41 Ga to 546 Ma) and Hf isotope composition (ε_{Hf} ranging from 5.1 to -20.0) (Table 2; Fig. 7f). Similarly, to sample Vilch-6A, such data scattering prevents distinguishing principal crust formation events with confidence.

5. Discussion

5.1. Pre-Rodinia provenance signal

The lower part of the sedimentary succession of the EEC consisting of the Pinsk and Orsha Suites, although not precisely dated, was deposited in a time interval of c. 1.32–1.0 Ga (Fig. 3). These sediments represent the time post-dating break-up of the Columbia/Nuna supercontinent (e.g., Rogers and Santosh, 2002; Zhao et al., 2002, 2004; Evans and Mitchell, 2011). According to most of currently accepted plate tectonic reconstructions the present-day EEC, a precursor of early Palaeozoic Baltica, was at that time attached to the Greenland margin of Laurentia, while both continents drifted together at low latitudes (Buchan et al., 2000; Ernst et al., 2000; Condie, 2002; Zhao et al., 2004; Pisarevsky et al., 2014).

Such reconstruction is consistent with our mineralogical data. The ratio of kaolinite to illite-smectite (originally a smectitic product of weathering; cf. Liivamägi et al., 2018) is proposed

here as a proxy for weathering intensity in the source areas (clay index; Table S1; Fig. 4). This value is not dependent on the percentage of primary minerals, used as a proxy for the grain size, thus it was not affected significantly by hydraulic sorting (cf. Środoń et al., 2014, their fig. 16). The ratio of quartz to all pre-weathering minerals can be considered as an alternative proxy for weathering intensity (primary minerals index; Table S1; Fig. 4). These indices offer some clues concerning the provenance of the Orsha Suite, where both weathering indices agree, indicating very intense kaolinitic-type weathering in a source area, implying warm and humid conditions.

The Pinsk Suite, with a current exposure of 150,000 km^2 (Makhnach et al., 2001), reveals nearly unimodal U-Pb age spectra in two samples analysed (c. 2.0 Ga; Fig. 6). Similar detrital age spectra have been reported from the Paleoproterozoic Ovruch Series in the Ukrainian Shield (dated as 1.76 Ga using zircons in the underlying rhyolites; Shumlyanskyy et al., 2017). However, the Ovruch Series can hardly be considered a source area for the Pinsk Suite sediments because of its rather minor extent (1000 km^2) and much higher maturity of mineral composition (pyrophyllite-grade; Sinyakovskaya et al., 2005). Therefore, the Osnitsk-Mikashevychi Igneous Belt (northern Ukraine – southern Belarus), dated at c. 2.0 Ga (Shumlyanskyy et al., 2016 and references therein), is a plausible candidate for a source area, even though it might have been partly buried beneath younger sediments at the time of the Pinsk Suite deposition. Since the Proterozoic basins located on the Ukrainian Shield contain formations with similar 2.0–2.1 Ga zircon age patterns (Shumlyanskyy et al., 2015) a common, voluminous and widespread source terrain is suggested. Such a narrow detrital age spectrum in a sedimentary cover of a craton remains a rare phenomenon that can be best explained by erosion of an extensive volcanogenic cover and relatively short detritus transport that prevents mixing of zircons from various sources. Therefore, a continental arc

475 producing sediments with a relatively narrow age range can be an alternative solution to the
476 Osnitsk-Mikashevychi Igneous Belt.
477
478 The Orsha Suite quartz arenite yielded a polymodal 1.3–3.2 Ga zircon age distribution,
479 indicating a complex provenance for the Orsha Suite (Fig. 6). The detritus distributary
480 systems and long-lasting weathering possibly lead to mixing and recycling of the material
481 from numerous, potentially distant sources. Clearly, the catchment area changed in
482 comparison to the Pinsk Suite.
483
484 ***5.2. Provenance of Rodinia-related sediments***
485 Only the Vilchitsy Series, traditionally ascribed to Cryogenian (720–635 Ma; Fig. 3), can be
486 correlated with the time, when the Rodinia supercontinent existed (1.0–0.63 Ma; e.g., Weil et
487 al., 1998; Meert and Torsvik, 2003; Pisarevsky et al., 2003; Torsvik 2003; Li et al., 2008).
488 The Rodinia reconstructions place the EEC (future Baltica) at high latitudes of the southern
489 hemisphere until 900 Ma (Pisarevsky et al., 2003; Li et al., 2008). From 750 Ma onwards, the
490 EEC occupied position at moderate latitudes until the break-up of Rodinia (630 Ma; e.g., Li
491 et al., 2008).
492
493 The composition of primary (pre-weathering) minerals, detectable by XRD, can be used as a
494 provenance indicator for the EEC sediments in Belarus. The Vilchitsy Series rocks are
495 characterized by similar proportions of orthoclase to microcline and biotite to muscovite, like
496 the Pinsk Suite (Fig. 4). These ratios, the high ratio of quartz to all pre-weathering minerals,
497 along with low ratio of kaolinite to illite-smectite imply glacial erosion of the underlying
498 sedimentary rocks, practically without chemical weathering.
499

500 The nearly continuous zircon age spectra (1.0–3.2 Ga; Fig. 6) from glacial sediments of the
501 Vilchitsy Series are similar to those from the Orsha Suite, except for a c. 1.0–1.3 Ga cluster
502 and more dominant 2.0 Ga peak in one of the Vilchitsy Series samples. These spectra indicate
503 that the main source area were the underlying Pinsk and Orsha Suites, supplemented by a
504 younger Grenvillian-age component. Such an interpretation is consistent with the mineral
505 composition of the bulk rock, intermediate between the Pinsk and Orsha Suites and without
506 measurable input of non-weathered material (Table S1). Since the maximum deposition age
507 of the Vilchitsy Series is constrained by the zircon age spectra to c. 1.0 Ga (Fig. 6), and the
508 oldest overlying basalts are dated at c. 570 Ma, the Vilchitsy tillites (Fig. 3) may represent
509 any of the Cryogenian glaciations as well as the Ediacaran Gaskiers glaciation. The centre of
510 glaciation must have been located SW from the glacial sediments of the Vilchitsy Series, as
511 indicated by the lateral facies trends in the Volyn-Orsha Basin: the glacial sediments thin out
512 towards the NE along the axis of the basin (Kheraskova et al., 2003). The glacial series was
513 deposited on the continent covered by kaolinitic redbeds: products of intense weathering in
514 hot and humid climate, *in situ* or redeposited (Orsha Suite). Therefore, the glacial character of
515 the Vilchitsy Series implies a major climate change compared to the time of deposition of the
516 Orsha Suite or, alternatively, a localised elevation of part of the craton. The former option is
517 possible due to a large time gap between deposition of the Orsha Suite (c. 1.3–1.0 Ga) and the
518 Vilchitsy Series. The latter interpretation is also reasonable since the addition of 1.0 Ga
519 zircons may suggest some post-Grenvillian (post-Sveconorwegian) elevated topography. C. 1
520 Ga dates obtained by Shumlyanskyy et al. (2015) for the Ukrainian Polissya Series indicate
521 delivery of the detritus from a comparable source terrain.
522
523 The Lu-Hf data show that the best-defined group of detrital zircons (Fig. 7a) with ages from
524 1.53 to 0.68 Ga and ε_{Hf} from 6.1 to -2.8 (n = 8) correspond to the average continental crust

525 with a model age of 1.8 Ga. This age represents a main crust-forming event in Fennoscandia
526 implying a local character of the source terrain. The admixture of zircons dated at 1.0 Ga is
527 notable, but these grains are characterized by only slightly positive ε_{Hf} values (0 to +2).
528 Therefore, they do not match a clearly positive ε_{Hf} signature (+5 to +7) of magmatic zircon
529 cores from the Grenvillian Oaxaquia Terrane (Weber et al., 2010).
530
531 ***5.3. Sedimentary record of Baltica***
532 The sediments sampled that were laid down after the break-up of Rodinia are included into
533 the Volyn and Valdai Series of the Ediacaran age (635–542 Ma) as well as the lower
534 Cambrian succession (542–530 Ma; Fig. 3). They were deposited during a time interval,
535 when Baltica was located at the equator (Popov et al., 2002; Li et al., 2008) or resided at
536 moderate southern latitudes (Torsvik and Rehnström, 2001).
537
538 Since the Lu-Hf data for all the zircons from the Volyn and Valdai Series correspond to
539 intermediate to felsic source with model ages of 2.1–2.3 Ga they suggest that the main
540 catchment area was located within Sarmatia (present-day Ukraine, SW part of the EEC).
541 Furthermore, the Mesoproterozoic zircons (c. 1.5 Ga) from the Volyn and Valdai Series
542 reveal ε_{Hf} values in the range of +5.8 to -5.5 that are comparable to those in the granites and
543 gneisses from the Danish island of Bornholm (Johansson et al., 2016) and rapakivi granites of
544 SW Fennoscandia (Heinonen et al., 2010, 2014). Abundant zircons of similar age (c. 1.5 Ga)
545 were documented in sedimentary rocks of the Ukrainian Shield and interpreted as detritus
546 supplied from the Fennoscandian Shield (Shumlanskyy et al., 2015).
547
548 In the volcanoclastic sediments of the Volyn Series orthoclase dominates over microcline and
549 they contain abundant biotite along with primary basalt minerals (Ca-plagioclase, pyroxene)

and their hydrothermal alteration products (trioctahedral clays and zeolites). This change reveals detritus derivation from sources comprising basalts and biotite-bearing rocks. Starting from the Redkino Horizon of the Valdai Series, the basaltic source is gradually diminished, whereas a biotite-rich source continues to supply material. Finally, contribution from a new source rich in muscovite continuously increases until early Cambrian (the youngest unit studied).

The Volyn Series mineral composition shows characteristics opposite to the Orsha Suite: both indices have the lowest values; clay index because of the lack of kaolinite (no weathering) and the primary mineral index because of low quartz content. Both mineral composition indices are the lowest in the area close to the centres of magmatic activity, where pure basalts or volcanoclastics occur. They increase in samples, where the admixture of non-volcanic material is the highest. The very low clay indices for the Volyn Series rocks with terrigenous addition indicate that they are approximate time equivalents to the basalts and tuffs, as they formed before the development of intense kaolinitic weathering of the top layer of basalts (Liivamägi et al., 2018).

The Redkino Horizon of the Valdai Series differs from the underlying Volyn Series by an abrupt increase of the clay index and a very small increase of the primary mineral index. Such relationships suggest that the Redkino Horizon contains a significant admixture of already weathered volcanic material. Indeed, in the Volyn region the Redkino Horizon sediments are deposited on kaolinitic palaeosols developed on basalts (Liivamägi et al., 2018). Above the Redkino Horizon, these indices evolve in reciprocal direction across the Ediacaran/Cambrian boundary: clay index decreases, accompanied by decrease of hematite, while primary mineral index increases. Such regularity seems to indicate a gradual decrease

575 of the contribution from the strongly weathered volcanic source (high in kaolinite and low in
576 quartz).
577
578 The zircon U-Pb record (Fig. 6), in samples from the Volyn and Valdai Series deposited in
579 the intraplate basin during c. 40 Ma of continuous sedimentation, shows a common discrete
580 distribution of ages with prominent clusters of c. 1.8, and 1.5 Ga and 579–545 Ma. The latter
581 cluster, occurring in the sediments of the Volyn and lower Valdai Series, is derived from the
582 Volyn flood basalts (Fig. 8). Also, the disappearance of Ca-plagioclases (Table S1) indicates
583 that the contribution of trap basalts to the volcano-sedimentary succession was terminated in
584 the lower Valdai Series. The maximum deposition ages obtained for seven Volyn Series
585 samples (Fig. 6; 579–545 Ma) document the sediment age decrease upward the profile and
586 constrain the age of Volyn flood basalt province (Fig. 8), in general agreement with the
587 previous age estimates of 573 ± 14 Ma for basalts, 571 ± 13 Ma for rhyolitic dacite
588 (Shumlyanskyy et al., 2016), and 551 ± 4 Ma for a tuff (Compston et al., 1995).
589
590 The detrital age distribution in the Volyn and Valdai Series is markedly different from the
591 underlying Vilchitsy Series (Fig. 6), probably reflecting a major reorganization of the
592 sediment supply routes related to the break-up of Rodinia (Fig. 8). The bulk mineralogy
593 change (Table S1) documents the same phenomenon. A potential source terrain can be found
594 within the Precambrian basement of Baltica, where numerous igneous bodies with 1.5 or 1.8
595 Ga ages exist (e.g., Bogdanova et al., 2008, 2015; Shumlyanskyy et al., 2015; Krzemińska et
596 al., 2017 and references therein). Narrow age spectra measured in the Ediacaran sediments
597 (Fig. 6) suggest a short delivery route from a catchment area preventing mixing between
598 detritus supplied by various crustal components. The sediment transport direction for the

599 Volyn and Valdai Series was from the SW (Fig. 8), as evidenced by basin geometry
600 (Rozanov and Lydka, 1987) and sedimentary facies distribution (Pacześna, 2010).
601
602 ***5.4. Ediacaran to Cambrian transition***
603 At the end of the Ediacaran no abrupt change in bulk rock mineralogy can be detected by
604 XRD: the mineral composition is gradually evolving, and only a decrease of the basaltic
605 source can be deduced. Also, the bimodal distribution of zircon ages in the Kobryn profile
606 continues into the rocks (sample Kob-54) that are interpreted as Cambrian based on trace
607 fossils (Elena Golubkova, pers. comm.).
608
609 Sample Kob-57, taken 15 m above, presents a completely different age spectrum, including a
610 broad 500–700 Ma Neoproterozoic cluster (Fig. 6). Similar major provenance shifts from the
611 bimodal (1.5 and 1.8 Ga) to polymodal distribution with a Neoproterozoic cluster were
612 reported from Estonia (Isozaki et al., 2014), the Russian part of the Baltic Monoclise
613 (Kuznetsov et al., 2011; Ivleva et al., 2016) and Scandinavia (lower Cambrian in Lorentzen et
614 al., 2017 vs. middle-upper Cambrian in Slàma and Pedersen, 2015; Sláma, 2016). Similarly,
615 the middle Cambrian sediments of the Okuniew IG-1 borehole (Podlasie Depression Poland,
616 SW part of the EEC; Valverde-Vaquero et al., 2000) and of the Syczyn OU1 borehole
617 (Lublin Basin; Porębski et al., 2019) contain a Neoproterozoic zircon cluster.
618
619 The complex age spectrum of sample Kob-57 with a dominant Neoproterozoic cluster seems
620 to herald the advance of a Neoproterozoic orogen at the margin of Baltica. There are at least
621 two possible orogenic sources of the Neoproterozoic zircons. The first is the Timanide belt
622 along the northern edge of Baltica (cf. Kuznetsov et al., 2011; Isozaki et al., 2014; Sláma and
623 Pedersen, 2015; Ivleva et al., 2016; Sláma, 2016). The second possible source terrain is

624 located around the SW corner of the present-day EEC and it is related to a peri-Gondwanan
625 Neoproterozoic terrane (Scythia) docked to the Baltica margin (Fig. 9) and giving rise to the
626 pre-Scythides orogen (Kheraskova et al., 2015). The latter option appears the most plausible
627 in the light of subsidence analysis published by Poprawa et al. (2018). Their study shows that
628 the majority of the SW Baltica margin remained relatively stable in the latest Ediacaran and
629 early Cambrian, whereas the Baltica's southern section, adjacent to the Scynthian Platform,
630 noted rapid subsidence in the latest Ediacaran. The subsidence curves show shapes indicative
631 of a flexural basin, suggesting the Baltica continental margin being overridden by a
632 collisional orogen.
633
634 ***5.5. Crustal evolution constrained by Hf isotopes***
635 Combined Hf zircon data from investigated samples suggest at least four episodes of new
636 continental crust generation at c. 1.8, 2.1–2.3, 2.8 and 3.3 Ga (Fig. 10). The intermediate
637 character of the source reservoirs with average composition of the continental crust
638 dominates, although more felsic components are tentatively identified as well. Considerable
639 mixing of the crustal reservoirs occurred at c. 1.8 Ga and 550–600 Ma. The data from Belarus
640 are similar to recent age-Hf isotope data from the Ukrainian, SW part of the EEC that
641 constrained four main crustal growth events at 1.5, 2.0–2.2, 3.15–3.20 and 3.75 Ga and a
642 minor 2.4–2.5 Ga event (Shumlyanskyy et al., 2015). The main difference is the timing of the
643 youngest crust-forming event, i.e., 1.8 Ga in Belarus versus 1.5 Ga in Ukraine.
644
645 A characteristic feature of samples analysed is their reasonable similarity to each other with a
646 main crust-forming event defined at 2.1–2.3 Ga and an evolution line corresponding to a
647 $^{176}Lu/^{177}Hf$ ratio of 0.010–0.016 (Figs. 7, 10). The latter points to crustal reservoirs of
648 intermediate composition, i.e. average composition of continental crust with some felsic

components. An exception makes more shallow apparent crustal evolution line in sample Vilch-6A with a $^{176}Lu/^{177}Hf$ ratio of 0.019 (Fig. 7a), suggesting of an intermediate to mafic crustal reservoir, representing a discrete crust-forming events at c. 3.3 Ga. However, this should be taken with caution due to limited data. This collectively suggests a relatively uniform source terrain throughout the Neoproterozoic that were located within the crust of the present-day EEC. These sources experienced subsequent reworking of crust at c. 1.8 Ga and 550–600 Ma. A stark contrast from the common characteristics is sample Kob-57 collected from rocks representing the uppermost Ediacaran or lower Cambrian. The lack of any trends or clustering within the data (Fig. 7f) may suggest insufficient number of measurements but also sedimentary mixing of zircons derived from exotic source terrains. The latter explanation appears plausible considering a possible derivation of Neoproterozoic zircons from the basement of the peri-Gondwanan Scythian Platform that was docked to the SW corner of Baltica in the latest Ediacaran (see above; Kheraskova et al., 2015).

6. Conclusions

The provenance record from the Meso- and Neoproterozoic sediments covering the Belarusian sector of the EEC reveals fairly uniform sources of sediments located on Paleoproterozoic crust typical of the EEC. An additional source was provided by Neoproterozoic intraplate volcanic rocks (Volyn volcanic province). Analysed samples show reasonable similarity to each other with a main crust-forming event defined at 2.1–2.3 Ga and an evolution line corresponding to crustal reservoirs of average composition of continental crust with some felsic components. An important change of detritus provenance is noted only at the transition from the Ediacaran to Cambrian or in the early Cambrian. This is shown by

673 significant input of late Neoproterozoic zircons derived from an orogenic source. The latter
674 was probably related to docking of an exotic terrane to the SW corner of Baltica.
675
676 **Acknowledgements:** Financial support for this project came from the Polish National
677 Science Centre MAESTRO grant 2013/10/A/ST10/00050. Hf isotope analyses were funded
678 by the Natural Environment Research Council [NERC grant NE/K008862/1 to B.D.]. Jiří
679 Sláma was supported by the Academy of Sciences of the Czech Republic institutional support
680 to the Institute of Geology, ASCR, RVO 67985831. State Enterprise "Scientific and
681 Industrial Centre for Geology" from Minsk, Belarus made available all core material used in
682 this study. Oksana Kuzmenkova, Alla Lapcevich, and Sergei Mankevich are thanked for their
683 help with the borehole selection and sampling. Izabela Kocjan is acknowledged for the zircon
684 separation and Zuzanna Ciesielska for the XRD measurements. Andrzej Łaptaś and Monika
685 Plech are thanked for graphical support. Comments from Associate Editor Tony Kemp, and
686 Reviewers Bernard Bingen and Anonymous are greatly appreciated and significantly
687 improved this article.
688

689 **7. References**

690 Bogdanova, S., Paskevich, I.K., Gorbatschev, R., Oryluk, M.I., 1996. Riphean rifting and
691 major Palaeoproterozoic crustal boundaries in the basement of the East European
692 Craton: Geology and geophysics. Tectonophysics 268, 1–21.
693 Bogdanova, S.V., Page, L.M., Skridlaite, G., Taran, L.N., 2001. Proterozoic tectonothermal
694 history in the western part of the East European Craton: $^{40}Ar/^{39}Ar$ geochronological
695 constraints. Tectonophysics 339, 39–66.

696 Bogdanova, S.V., Bingen, B., Gorbatschev, R., Kheraskova, T.N., Kozlov, V.I., Puchkov,
697 V.N., Volozh, Y.A., 2008. The East European Craton (Baltica) before and during the
698 assembly of Rodinia. Precambrian Research 160, 23–45.
699 Bogdanova, S., Gorbatschev, R., Skridlaite, G., Soesoo, A., Taran, L., Kurlovich, D., 2015.
700 Trans-Baltic Palaeoproterozoic correlations towards the reconstruction of
701 supercontinent Columbia/Nuna. Precambrian Research 259, 5–33.
702 Bouvier, A., Vervoort, J.D., Patchett, P.J., 2008. The Lu-Hf and Sm-Nd isotopic composition
703 of CHUR: constraints from unequilibrated chondrites and implications for the bulk
704 composition of terrestrial planets. Earth and Planetary Science Letters 273, 48–57.
705 Buchan, K.L., Mertanen, S., Park, R.G., Pesonen, L.J., Elming, S.Å., Abrahamsen, N.,
706 Bylund, G., 2000. Comparing the drift of Laurentia and Baltica in the Proterozoic: the
707 importance of key palaeomagnetic poles. Tectonophysics 319 (3), 167–198.
708 Chebanenko, I.I., Vyshnyakov, I.B., Vlasov, B.I., 1990. Geotectonics of the Volyno-Podolian
709 area. Naukova Dumka publisher, 244 pp. (in Russian).
710 Chumakov, N.M., Semikhatov, M.A., 1981. Riphean and Vendian of the USSR. Precambrian
711 Research 15 (3–4), 229–253.
712 Chumakov, N.M., 2010. Precambrian Glaciations and Associated Biospheric Events.
713 Stratigraphy and Geological Correlation 18 (5), 467–479.
714 Chumakov, N.M., 2015. The role of glaciations in the biosphere. Russian Geology and
715 Geophysics 56, 541–548.
716 Claesson, S., Bogdanova, S.V., Bibikova, E.V., Gorbatschev, R., 2001. Isotopic evidence for
717 Palaeoproterozoic accretion in the basement of the East European Craton.
718 Tectonophysics 339, 1–18.

719 Compston, W., Sambridge, M.S., Reinfrank, R.F., Moczydłowska, M., Vidal, G., Claesson, S.,
720 1995. Numerical ages of volcanic rocks and the earliest faunal zone within the Late
721 Precambrian of east Poland. Journal of the Geological Society 152, 599–611.
722 Condie, K.C., 2002. Breakup of a Paleoproterozoic supercontinent. Gondwana Research 5(1),
723 41–43.
724 Dhuime, B., Hawkesworth, Ch., Cawood, P., 2011. When Continents Formed. Science 331,
725 154–155.
726 Dickinson, W.R., Gehrels, G.E., 2009. Use of U–Pb ages of detrital zircons to infer
727 maximum depositional ages of strata: A test against a Colorado Plateau Mesozoic
728 database. Earth and Planetary Science Letters 288, 115–125.
729 Elming, S-Å, Mikhailova, N.P., Kravchenko, S.N., 1998. The consolidation of the East
730 European Craton: a palaeomagnetic analysis of Proterozoic rocks from the Ukrainian
731 Shield and tectonic reconstruction versus Fennoscandia. Geophysical Journal 20, 71–
732 74.
733 Ernst, R.E., Buchan, K.L., Hamilton, M.A., Okrugin, A.V., Tomshin, M.D., 2000. Integrated
734 paleomagnetism and U-Pb geochronology of mafic dikes of the eastern Anabar Shield
735 region, Siberia: Implications for Mesoproterozoic paleolatitude of Siberia and
736 comparison with Laurentia. The Journal of Geology 108 (4), 381–401.
737 Evans, D.A.D., Mitchell, R.N., 2011. Assembly and breakup of the core of
738 Palaeoproterozoic–Mesoproterozoic supercontinent Nuna. Geology 39, 443–446.
739 Gardiner, N. J., Johnson, T. E., Kirkland, C. L., Smithies, R. H., 2018. Melting controls on
740 the lutetium–hafnium evolution of Archaean crust. Precambrian Research 305, 479–
741 488.

742 Goryl, M., Marynowski, L., Brocks, J.J., Bobrovskiy, I., Derkowski, A., 2018. Exceptional
743 preservation of hopanoid and steroid biomarkers in Ediacaran sedimentary rocks of the
744 East European Craton. Precambrian Research 316, 38–47.
745 Heinonen, A.P., Andersen, T., Rämö, O.T., 2010. Re-evaluation of rapakivi petrogenesis:
746 Source constraints from the Hf isotope composition of zircon in the rapakivi granites
747 and associated mafic rocks of southern Finland. Journal of Petrology 51 (8), 1687–
748 1709.
749 Heinonen, A., Andersen, T., Rämö, O.T., Whitehouse, M., 2015. The source of Proterozoic
750 anorthosite and rapakivi granite magmatism: evidence from combined in situ Hf–O
751 isotopes of zircon in the Ahvenisto complex, southeastern Finland. Journal of the
752 Geological Society 172 (1), 103–112.
753 Hoskin, P.W.O., Black, L.P., 2000. Metamorphic zircon formation by solid-state
754 recrystallization of protolith igneous zircon. Journal of Metamorphic Geology 18, 423–
755 439.
756 Isozaki, Y., Põldvere, A., Bauertc, H., Nakahata, H., Aoki, K., Sakata, S., Hirata, T., 2014.
757 Provenance shift in Cambrian mid-Baltica: detrital zircon chronology of Ediacaran-
758 Cambrian sandstones in Estonia. Estonian Journal of Earth Sciences 63 (4), 251–256.
759 Ivleva, A.S., Podkovyrov, V.N., Ershova, V.B., Anfinson, O.A., Khudoley, A.K., Fedorov,
760 P.V., Maslov, A.V., Zdobin, D.Yu., 2016. Results of U–Pb LA–ICP–MS dating of
761 detrital zircons from Ediacaran–Early Cambrian deposits of the Eastern part of the
762 Baltic Monoclise. Doklady Earth Sciences 468, 593–597.
763 Johansson, Å., Waight, T., Andersen, T., Simonsen, S.L., 2016. Geochemistry and
764 petrogenesis of Mesoproterozoic A-type granitoids from the Danish island of
765 Bornholm, southern Fennoscandia. Lithos 244, 94–108.

766 Kelly, N.M., Harley, S.L., 2005. An integrated microtextural and chemical approach to zircon
767 geochronology: refining the Archaean history of the Napier Complex, east Antarctica.
768 Contributions to Mineralogy and Petrology 149, 57–84.
769 Kheraskova, T.N., Didenko, A.N., Bush, V.A., 2003. The Vendian-Early Paleozoic history of
770 the continental margin of eastern Paleogondwana, Paleoasian Ocean, and Central Asian
771 foldbelt. Russian Journal of Earth Sciences 5 (3), 165–184.
772 Kheraskova, T. N., Volozh, Yu. A., Antipov, M. P., Bykadorov, V. A., Sapozhnikov, R. B.,
773 2015. Correlation of Late Precambrian and Paleozoic events in the East European
774 Platform and the adjacent paleooceanic domains. Geotectonics 49, 27–52.
775 Krzemińska, E., Krzemiński, L., Petecki, Z., Wiszniewska, J., Salwa, S., Żaba, J., Gaidzik,
776 K., Williams, I.S., Rosowiecka, O., Taran, L., Johansson, Å., Pécskay, Z., Demaiffe,
777 D., Grabowski, J., Zieliński, G., 2017. Geological Map of Crystalline Basement in the
778 Polish part of the East European Platform 1:1 000 000. Państwowy Instytut
779 Geologiczny. Warszawa.
780 Kuzmenkova, O.F., Nosova, A.A., Shumlyansky, L.V., 2010. Comparison of Neoproterozoic
781 Volyn-Brest magmatic province with large world continental plate basalt provinces, the
782 nature of low- and high-Ti basite magmatism. Lithosphere 33, 3–16 (in Russian)
783 Kuzmenkova, O.F., Shumlyanskyy, L.V., Nosova, A.A., Voskoboynikova, T.V., Grakovich,
784 I.Yu., 2011. Petrology and correlation of trap formations of the Vendian in the adjacent
785 areas of Belarus and Ukraine. Litasfera 2 (35), 3–11.
786 Kuzmenkova, O.F., Laptsevich, A.G., Mankevich, S.S., 2016. Perspectives of the diamond
787 content of Vendian deposits of the Polesye Saddle of Belarus. Litosfera 44, 38–50 (in
788 Russian).
789 Kuznetsov, N.B., Orlov, S.Y., Miller, E.L., Shatsillo, A.V., Dronov, A.V., Soboleva, A.A.,
790 Udoratina, O.V., Gehrels, G.E., 2011. First U/Pb age results for detrital zircons from

791 Early Paleozoic and Devonian sandstones, South Priladozhje. Doklady of Earth
792 Sciences 438, 1–7.
793 Li, Z.X., Bogdanova, S.V., Collins, A.S., Davidson, A., De Waele, B., Ernst, R.E.,
794 Fitzsimons, I.C.W., Fuck, R.A., Gladkochub, D.P., Jacobs, J., Karlstrom, K.E., Lu, S.,
795 Natapov, L.M., Pease, V., Pisarevsky, S.A., Thrane, K., Vernikovsky, V., 2008.
796 Assembly, configuration, and break-up history of Rodinia: a synthesis. Precambrian
797 research 160 (1–2), 179–210.
798 Liivamägi, S., Środoń, J., Bojanowski, M., Gerdes, A., Stanek, J.J., Williams, L., Szczerba,
799 M., 2018. Paleosols on the Ediacaran basalts of the East European Craton: A unique
800 record of paleoweathering with minimum diagenetic overprint. Precambrian Research
801 316, 66–82.
802 Lorentzen, S., Augustsson, C., Nystuen, J.P., Berndt, J., Jahren, J., Schovsbo, N.H., 2017.
803 Provenance and sedimentary processes controlling the formation of lower Cambrian
804 quartz arenite along the southwestern margin of Baltica. Sedimentary Geology 375,
805 203–217.
806 Lubnina, N.V., Bogdanova, S.V., Shumlyanskyy, L.V., 2009. The East European Craton in
807 the Palaeoproterozoic: new paleomagnetic data on magmatic complexes in the
808 Ukrainian Shield. Geofizika 5, 56–64 (in Russian).
809 Makhnach, A.S., Veretennikov, N.V., Shkuratov, V.I., Bordon, V.E., 1976. Riphean and
810 Vendian of Belarus. Nauka i Tekhnika publisher, 360 pp. (in Russian).
811 Makhnach, A.S., Garetskiy, R.G., Matveev, A.V., Anoshko, Ya.I., 2001. Geology of Belarus.
812 Minsk, Institute of Geological Sciences, 815 pp. (in Russian).
813 Makhnach, A.S., Veretennikov, N.V., Shkuratov, V.I., Laptsevich, A.G., Piskun, L.V., 2005.
814 Stratigraphic chart of Vendian deposits of Belarus. Litasfera 22, 36–44 (in Russian).

Meert, J.G., Torsvik, T.H., 2003. The making and unmaking of a supercontinent: Rodinia revisited. Tectonophysics 375 (1–4), 261–288.

Nechaev, S.V., 1974. Geochronology of the Late Precambrian deposits of the south-western slope of the Russian platform. Abstract volume of the Conference on the Late Precambrian (Riphean) of the Russian platform. Nauka publisher, pp. 40–47. (in Russian).

Nosova, A.A., Kuzmenkova, O.F., Veretennikov, N.V., Petrova, L.G., Levskiy, L.K., 2008. Neoproterozoic Volyn-Brest magmatic province on western margin of the East European Craton: Peculiarities of intracratonic magmatism in the area of ancient suture zone. Petrologia 16, 115–147 (in Russian).

Pacześna, J., 2010. The evolution of late Ediacaran riverine-estuarine system in the Lublin-Podlasie slope of the East European Craton, southeastern Poland. Polish Geological Institute Special Papers 27, 1–96.

Pehr, K., Love, G.D., Kuznetsov, A., Podkovyrov, V., Junium, C.K., Shumlyanskyy, L., Sokur, T., Bekker, A., 2018. Ediacaran fauna flourished in oligotrophic and bacterially dominated marine environments. Nature communications 9, 1807.

Pisarevsky, S.A., Wingate, M.T., Powell, C.M., Johnson, S., Evans, D.A., 2003. Models of Rodinia assembly and fragmentation. Geological Society, London, Special Publications 206 (1), 35–55.

Pisarevsky, S.A., Elming, S.-Å., Pesonen, L.J., Li, Z.-X., 2014. Mesoproterozoic paleogeography: supercontinent and beyond. Precambrian Research 244, 207–225.

Popov, V., Iosifidi, A., Khramov, A., Tait, J., Bachtadse, V., 2002. Paleomagnetism of Upper Vendian sediments from the Winter Coast, White Sea region, Russia: implications for the paleogeography of Baltica during Neoproterozoic times. Journal of Geophysical Research 107 (B11), 1–0EPM10; 1–8.

840 Poprawa, P., Radkovets, N., Rauball, J., 2018. Ediacaran-Paleozoic subsidence history of the
841 Volyn-Podillya-Moldavia Basin (W and SW Ukraine, Moldova, NE Romania).
842 Geological Quarterly 62 (3), 459–486.
843 Porębski, S.J., Anczkiewicz. R., Paszkowski, M., Skompski, S., Kędzior, A., Mazur, S.,
844 Szczepański, S., Buniak, A., Mikołajewski, Z., 2019. Hirnantian icebergs in the
845 subtropical shelf of Baltica: Evidence from sedimentology and detrital zircon
846 provenance. Geology 47, 284–288.
847 Rogers, J.J., Santosh, M., 2002. Configuration of Columbia, a Mesoproterozoic
848 supercontinent. Gondwana Research 5 (1), 5–22.
849 Rozanov, A.Yu., Łydka, K., 1987. Paleogeography and Lithology of the Vendian and
850 Cambrian of the western East European Platform. Wydawnictwa Geologiczne,
851 Warsaw. 114 pp.
852 Rubatto, D., 2017. Zircon: The Metamorphic Mineral. Reviews in Mineralogy &
853 Geochemistry 83, 261–295.
854 Rundqvist, D.V., Mitrofanov, F.P., 1993. Precambrian Geology of the USSR, in:
855 Developments in Precambrian Geology, Windley, B.F. (Ed.), Elsevier, Amsterdam-
856 New York-London-Tokyo, 1440 pp.
857 Shumlyanskyy, L., 2012. Evolution of the Vendian flood basalt magmatism in the Volyn
858 region. Mineralogical Journal (Ukraine) 34 (4), 50–68 (in Ukrainian).
859 Shumlyanskyy, L., 2014. Geochemistry of the Osnitsk-Mikashevichy volcanoplutonic
860 complex of the Ukrainian shield. Geochemistry International 52, 912–924.
861 Shumlyanskyy, L., Hawkesworth, C., Dhuime, B., Billström, K., Claesson, S., Storey, C.,
862 2015. $^{207}Pb/^{206}Pb$ ages and Hf isotope composition of zircons from sedimentary rocks
863 of the Ukrainian shield: crustal growth of the south-western part of East European
864 craton from Archaean to Neoproterozoic. Precambrian Research 260, 39–54.

865 Shumlyanskyy, L., Nosova, A., Billström, K., Söderlund, U., Andréasson, P.-G.,
866 Kuzmenkova, O., 2016. The U-Pb zircon and baddeleyite ages of the Neoproterozoic
867 Volyn Large Igneous Province: implication for the age of the magmatism and the
868 nature of a crustal contaminant. GFF 138, 17–30.
869 Shumlyanskyy, L., Hawkesworth, C., Billström, K., Bogdanova, S., Mytrokhyn, O., Romer,
870 R., Dhuime, B., Claesson, S., Ernst, R., Whitehouse, M., Bilan, O., 2017. The origin of
871 the Palaeoproterozoic AMCG complexes in the Ukrainian Shield: new U-Pb ages and
872 Hf isotopes in zircon. Precambrian Research 292, 216–239.
873 Sinyakovskaya, I., Zaykov V., Kitagawa R., 2005. Types of Pyrophyllite Deposits in
874 Foldbelts. Resource Geology 55 (4), 405–418.
875 Sláma, J., Pedersen, R.B., 2015. Zircon provenance of SW Caledonian phyllites reveals a
876 distant Timanian sediment source. Journal of the Geological Society 172, 465–478.
877 Sláma, J., 2016. Rare late Neoproterozoic detritus in SW Scandinavia as a response to distant
878 tectonic processes. Terra Nova 28, 394–401.
879 Środoń, J., Drits, V.A., McCarty, D.K., Hsieh, J.C.C., Eberl, D.D., 2001. Quantitative XRD
880 analysis of clay-rich rocks from random preparations. Clays & Clay Minerals 49, 514–
881 528.
882 Środoń, J., Szulc, J., Anczkiewicz, A., Jewuła, K., Banaś, M., Marynowski, L., 2014.
883 Weathering, sedimentary, and diagenetic controls of mineral and geochemical
884 characteristics of the vertebrate-bearing Silesian Keuper. Clay Minerals 49, 569–594.
885 Šliaupa, S., Fokin, P., Lazauskiene, J., Stephenson, R., 2006. The Vendian-Early Palaeozoic
886 sedimentary basins of the East European craton. In: Gee, D.G., Stephenson, R.A. (Eds.)
887 European lithosphere dynamics. Geological Society Memoir 32, 449–462.

888 Torsvik, T.H., Smethurst, M.A., Van der Voo, R., Trench, A, Abrahamsen, N., Halvorsen, E.,
889 1992. Baltica A synopsis of Vendian-Permian palaeomagnetic data and their
890 palaeotectonic implications. Earth-Science Reviews 33 (2), 133–152.
891 Torsvik, T.H., Smethurst, M.A., Meert, J.G., Van der Voo, R., McKerrow, W.S., Brasier,
892 M.D., Sturt, B.A., Walderhaug, H.J., 1996. Continental break-up and collision in the
893 Neoproterozoic and Palaeozoic – a tale of Baltica and Laurentia. Earth-Science
894 Reviews 40 (3–4), 229–258
895 Torsvik, T.H., Rehnström, E.F., 2001. Cambrian palaeomagnetic data from Baltica:
896 implications for true polar wander and Cambrian palaeogeography. Journal of the
897 Geological Society 158 (2), 321–329.
898 Torsvik, T.H., 2003. The Rodinia jigsaw puzzle. Science 300 (5624), 1379–1381.
899 Valverde-Vaquero, P., Dörr, W., Belka, Z., Franke, W., Wiszniewska, J., Schastok, J., 2000.
900 U–Pb single-grain dating of detrital zircon in the Cambrian of central Poland:
901 implications for Gondwana versus Baltica provenance studies. Earth and Planetary
902 Science Letters 184, 225–240.
903 Weber, B., Scherer, E.E., Schulze, C., Valencia, V.A., Montecinos, P., Mezger, K., Ruiz, J.,
904 2010. U–Pb and Lu–Hf isotope systematics of lower crust from central-southern
905 Mexico–Geodynamic significance of Oaxaquia in a Rodinia Realm. Precambrian
906 Research 182 (1–2), 149–162.
907 Weil, A.B., Van der Voo, R., Mac Niocaill, C., Meert, J.G., 1998. The Proterozoic
908 supercontinent Rodinia: paleomagnetically derived reconstructions for 1100 to 800 Ma.
909 Earth and Planetary Science Letters 154 (1–4), 13–24.
910 Zhao, G., Cawood, P.A., Wilde, S.A., Sun, M., 2002. Review of global 2.1–1.8 Ga orogens:
911 implications for a pre-Rodinia supercontinent. Earth-Science Reviews 59 (1–4), 125–
912 162.

913 Zhao, G., Sun, M., Wilde, S.A., Li, S., 2004. A Paleo-Mesoproterozoic supercontinent:
914 assembly, growth and breakup. Earth-Sciences Reviews 67, 91–123.
915

916 **Figure captions**

917 **Fig. 1.** (a) The main structural elements of pre-Ediacaran Baltica (modified from Johansson
918 et al., 2009; Bogdanova et al., 2015). (b) Present day maximum extent of the Ediacaran
919 sediments (Kotlin) on investigated part of Baltica, the extent of underlying Volyn
920 sediments and volcanics (in worm's eye map manner; modified from Rozanov and
921 Łydka, 1987; Nosova et al., 2008; Kuzmenkova et al., 2010, 2016), and Rapakivi
922 granites (after Isozaki et al. 2014; Bogdanova et al., 2015; Krzemińska et al. 2015), and
923 of the boreholes sampled in this study. The borehole geographic coordinates: Vil'chytsy
924 – 53°47'N, 30°21'E; Bogushevsk – 54°50'N, 30°12'E; Lepel – 54°53'N, 28°42'E;
925 Kobryn – 52°13'N, 24°23'E; Pinsk – 52°07'N, 26°10'E.

926 **Fig. 2.** Correlation of the drilled sections with marked depths of studied samples. Maximum
927 depositional ages estimated in this study are given when applicable.

928 **Fig. 3.** Composite stratigraphic chart for the western part of Belarus. Compiled from
929 Chumakov and Semikhatov (1981), Rundqvist and Mitrofanov (1993), Makhnach et al.
930 (2005) and Pacześna (2010).

931 **Fig. 4**. Quantitative mineral composition of the subsequent rock series, averaged for all
932 investigated profiles: (a) quartz and weathering indices: kaolinite/dioctahedral 2:1 clay
933 (left) and quartz/sum primary minerals (right); (b) other primary minerals, including
934 sum of basaltic minerals (Ca-plagioclase, pyroxene, aluminoceladonite, saponite,
935 chlorite, chlorite-smectite, analcime, and clinoptilolite); (c) weathering (anatase,
936 hematite, kaolinite, and dioctahedral 2:1 clay) and authigenic (goethite, pyrite,
937 aopatite,siderite, dolomites, berthierine, gypsum, jarosite, barite) minerals.

938 **Fig. 5.** Representative cathodoluminescence (CL) images of the analysed zircons including
939 spot number, U-Pb age with ±2σ error (Ma) and ε_{Hf} with ±2σ error (in italic).

Fig. 6. Probability density plots presenting U-Pb age data yielded by zircons from Belarus, combined for A and B groups of zircons (see text for explanation).

Fig. 7. ε_{Hf} vs. time plots presenting results for each sample investigated. $^{206}Pb/^{238}U$ age for data <1000 Ma and $^{207}Pb/^{206}Pb$ age for data >1000 Ma. New crust evolution line according to Dhuime et al. (2011).

Fig. 8. Paleogeographic reconstruction of the Baltica paleocontinent during eruptions of the Volynian traps at c. 570 Ma. Detritus derivation from the SW margin of Baltica and Volynian trap basalts.

Fig. 9. Paleogeographic reconstruction of the Baltica paleocontinent during deposition of lower and middle Cambrian (Terreneuvian, c. 532 Ma) partly based on Šliaupa et al. (2006). Sourcing from an orogen/magmatic arc (Scythian orogen) approaching the SW Baltica edge.

Fig. 10. ε_{Hf} vs. time plot summarizing results for all samples. $^{206}Pb/^{238}U$ age for data <1000 Ma and $^{207}Pb/^{206}Pb$ age for data >1000 Ma. New crust evolution line according to Dhuime et al. (2011).

Table captions:

Table 1. Samples used for isotopic measurements of zircons.

Table 2. U-Pb ages and Hf isotope composition in investigated zircons.

Supplementary Data (online only)

Supplementary Data 1 (SD1). Detailed description of analytical methods.

Supplementary Data 2 (SD2). U-Pb zircon standards data.

Supplementary Data 3 (SD3). Hf zircon standards data.

Supplementary Data 4 (SD4). Summary of LA-ICP-MS U-Pb age data.

965 **Table S1.** Average quantitative XRD mineral composition of mudstones from different
966 stratigraphic units in five studied Belarussian wells. Weathering indices used in the text
967 are presented in the two columns on the right.
968 **Table S2.** Results of the U-Pb analyses of zircons.

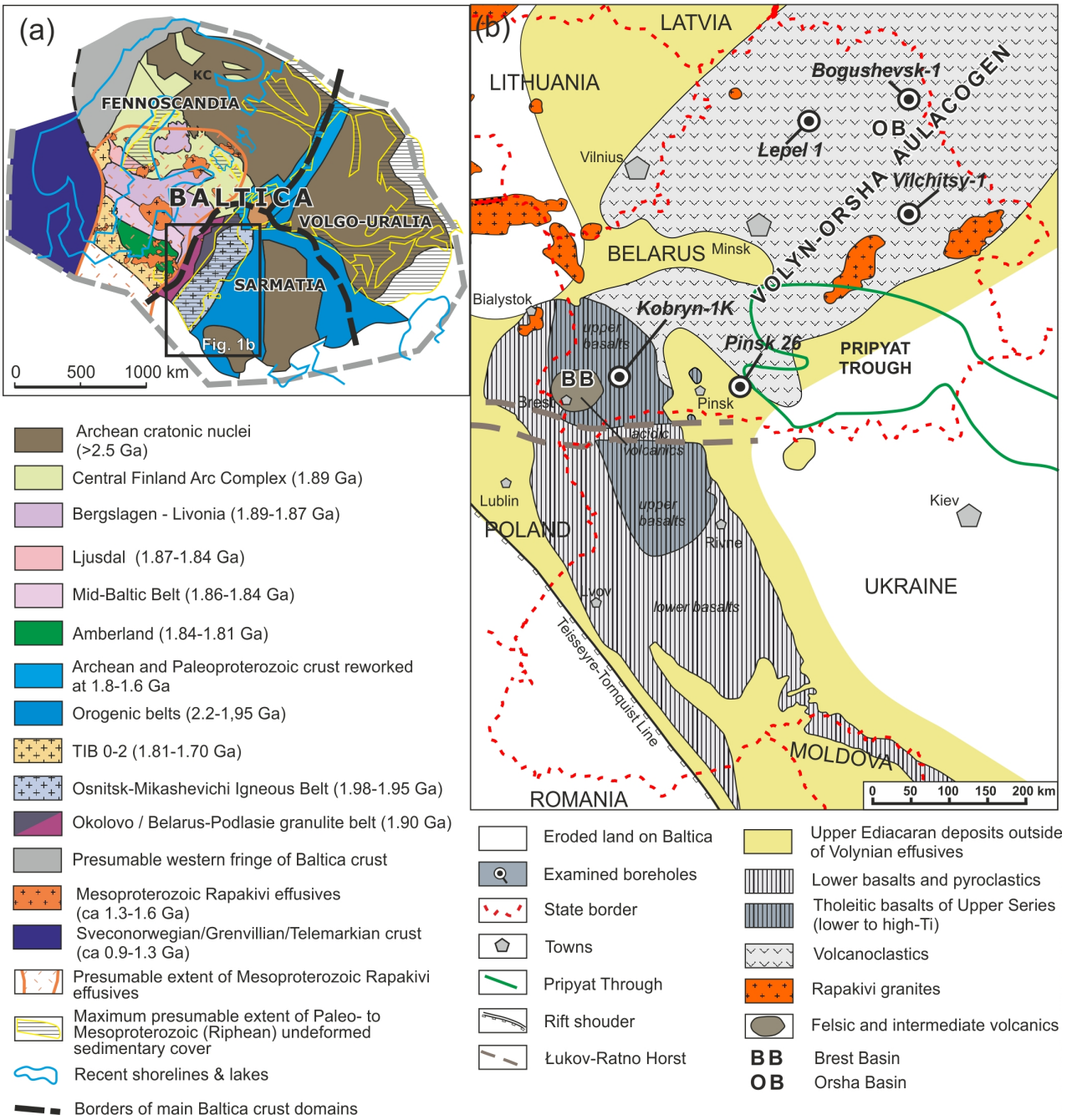
(a)
KC
FENNOSCANDIA
BALTICA
VOLGO-URALIA
SARMATIA
Fig. 1b
0 500 1000 km
(b)
LATVIA
LITHUANIA
Bogushevsk-1
OB
AULACOGEN
Łepel 1
Vilnius
Vilchitsy-1
BELARUS
Minsk
VOLYN-ORSHA
Bialystok
Kobryn-1K
upper basalts
Pinsk 26
PRIPYAT TROUGH
BB
Brest
Pinsk
lacidic volcanics
Lublin
Kiev
POLAND
upper basalts
Rivne
UKRAINE
Lvov
lower basalts
Teisseyre-Tornquist Line
MOLDOVA
ROMANIA
0 50 100 150 200 km
Archean cratonic nuclei (>2.5 Ga)
Central Finland Arc Complex (1.89 Ga)
Bergslagen - Livonia (1.89-1.87 Ga)
Ljusdal (1.87-1.84 Ga)
Mid-Baltic Belt (1.86-1.84 Ga)
Amberland (1.84-1.81 Ga)
Archean and Paleoproterozoic crust reworked at 1.8-1.6 Ga
Orogenic belts (2.2-1,95 Ga)
TIB 0-2 (1.81-1.70 Ga)
Osnitsk-Mikashevichi Igneous Belt (1.98-1.95 Ga)
Okolovo / Belarus-Podlasie granulite belt (1.90 Ga)
Presumable western fringe of Baltica crust
Mesoproterozoic Rapakivi effusives (ca 1.3-1.6 Ga)
Sveconorwegian/Grenvillian/Telemarkian crust (ca 0.9-1.3 Ga)
Presumable extent of Mesoproterozoic Rapakivi effusives
Maximum presumable extent of Paleo- to Mesoproterozoic (Riphean) undeformed sedimentary cover
Recent shorelines & lakes
Borders of main Baltica crust domains
Eroded land on Baltica
Examined boreholes
State border
Towns
Pripyat Through
Rift shouder
Łukov-Ratno Horst
Upper Ediacaran deposits outside of Volynian effusives
Lower basalts and pyroclastics
Tholeitic basalts of Upper Series (lower to high-Ti)
Volcanoclastics
Rapakivi granites
Felsic and intermediate volcanics
BB Brest Basin
OB Orsha Basin

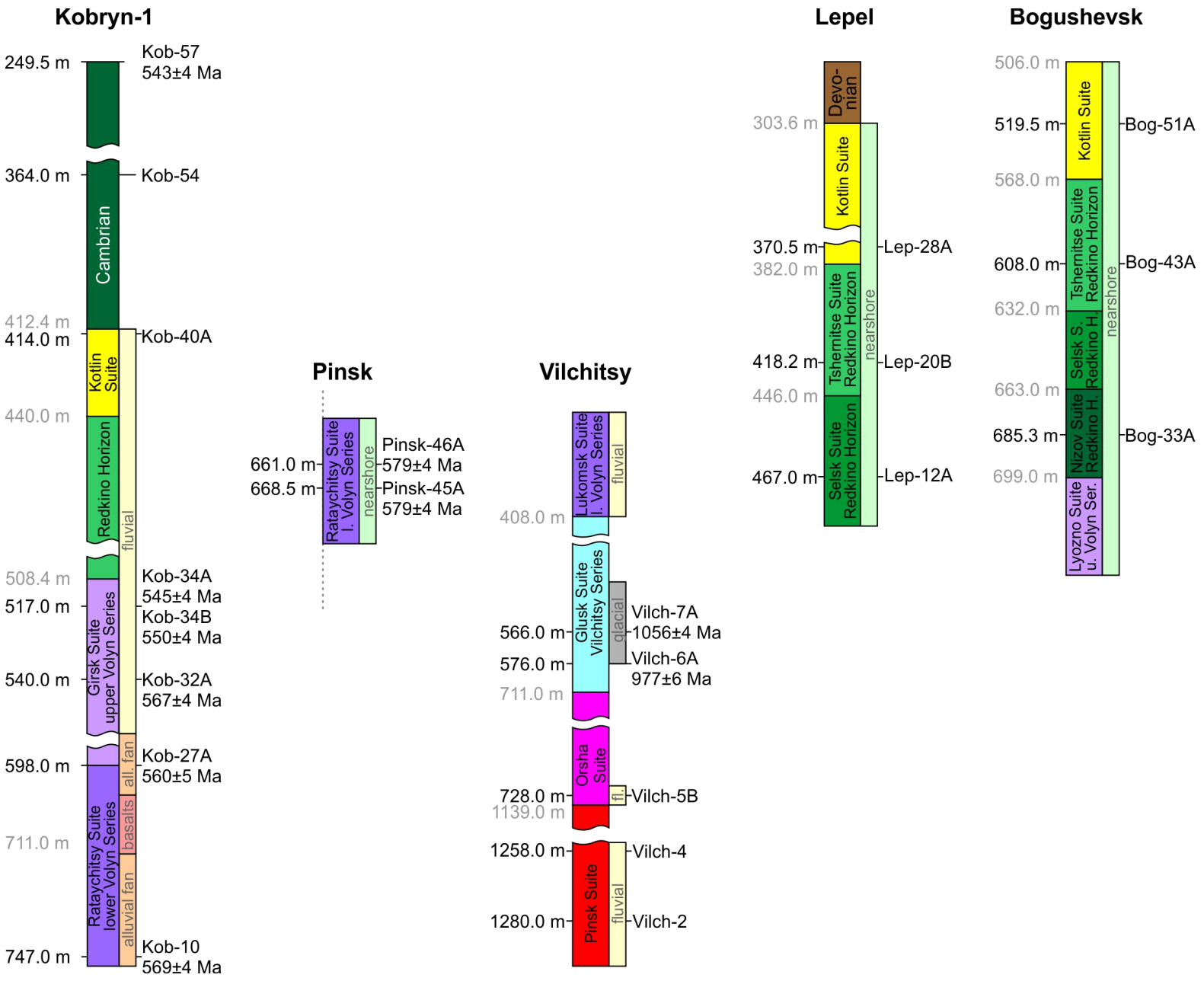
Kobryn-1
249.5 m
Kob-57
543±4 Ma
364.0 m
Kob-54
Cambrian
412.4 m
414.0 m
Kob-40A
Kotlin Suite
440.0 m
Redkino Horizon
fluvial
508.4 m
Kob-34A
545±4 Ma
517.0 m
Kob-34B
550±4 Ma
Girsk Suite
upper Volyn Series
540.0 m
Kob-32A
567±4 Ma
598.0 m
Kob-27A
560±5 Ma
all. fan
basalts
711.0 m
Ratavchitsy Suite
lower Volyn Series
alluvial fan
747.0 m
Kob-10
569±4 Ma
Pinsk
661.0 m
668.5 m
Ratavchitsy Suite
l. Volyn Series
nearshore
Pinsk-46A
579±4 Ma
Pinsk-45A
579±4 Ma
Vilchitsy
408.0 m
Lukomsk Suite
l. Volyn Series
fluvial
566.0 m
576.0 m
711.0 m
Glusk Suite
Vilchitsy Series
glacial
Vilch-7A
1056±4 Ma
Vilch-6A
977±6 Ma
Orsha Suite
728.0 m
1139.0 m
fl.
Vilch-5B
1258.0 m
Vilch-4
Pinsk Suite
fluvial
1280.0 m
Vilch-2
Lepel
303.6 m
Devo-
nian
Kotlin Suite
370.5 m
382.0 m
Lep-28A
Tshernitse Suite
Redkino Horizon
nearshore
418.2 m
Lep-20B
446.0 m
Selsk Suite
Redkino Horizon
467.0 m
Lep-12A
Bogushevsk
506.0 m
519.5 m
Kotlin Suite
Bog-51A
568.0 m
Tshernitse Suite
Redkino Horizon
608.0 m
Bog-43A
632.0 m
Selsk S.
Redkino H.
663.0 m
Nizov Suite
Redkino H.
685.3 m
Bog-33A
699.0 m
Lyozno Suite
u. Volyn Ser.
nearshore

BELARUS

ERATHEM	System	SYSTEM	Horizon	Series (Group)	Formation (Suite)	max thickness (m)
Paleozoic	lower Cambrian	Cambrian	Lontova	Baltic	Stradech / Lontova	119
			Rovno		Rytsk / Ruda-mina	39
Neoproterozoic	Ediacaran	VENDIAN	Kotlin	Valdai	Kotlin	220
			Redkino		Tshernitse	64
					Selsk	57
					Nizov	47
	Cryogenian		Lyozno	Volyn	Lyozno / Girsk / Vidibor	50-70 / 110-
					Luk-omsk / Kletsk / Ratay-chitsy	80-340 / 177-
					Gorbashi	30
				Vilchitsy	Glusk	483
					Blon	245
	Tonian	RIPHEAN	Lapichi	Belarus	Lapichi	82
			Polissia		Orsha	620
					Rudnya / Pinsk	300 / 460
					Rogachev	40
				Sherovitchi	Bortnikov	35
				Babruysk	Mishkovitchi	160
					Luchkov	158
Mesoproterozoic						

542
550
560
635
720
1000
1300
1350
1600

stratigraphic gap

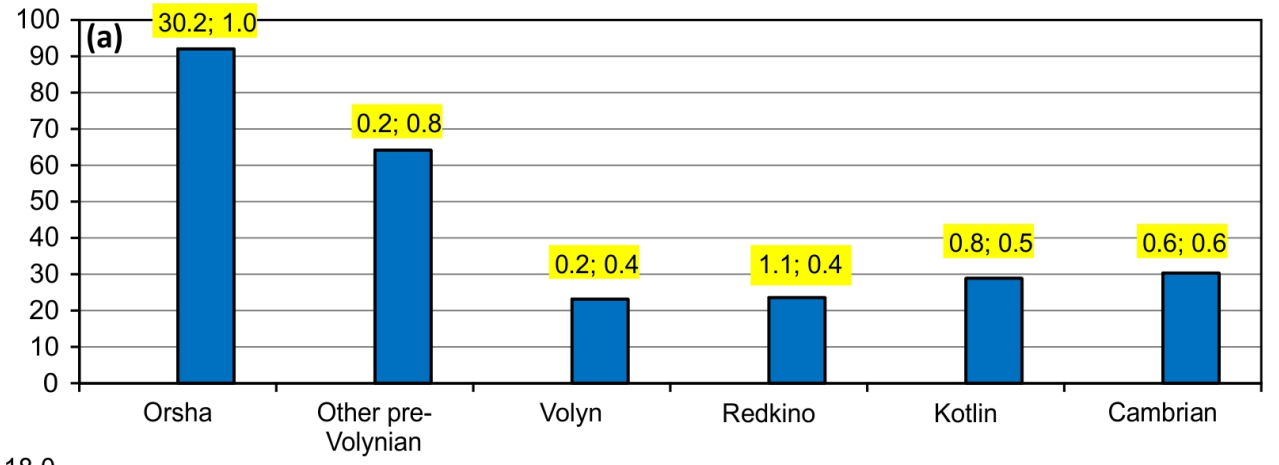
(a)
100
90
80
70
60
50
40
30
20
10
0
30.2; 1.0
0.2; 0.8
0.2; 0.4
1.1; 0.4
0.8; 0.5
0.6; 0.6
Orsha
Other pre-Volynian
Volyn
Redkino
Kotlin
Cambrian

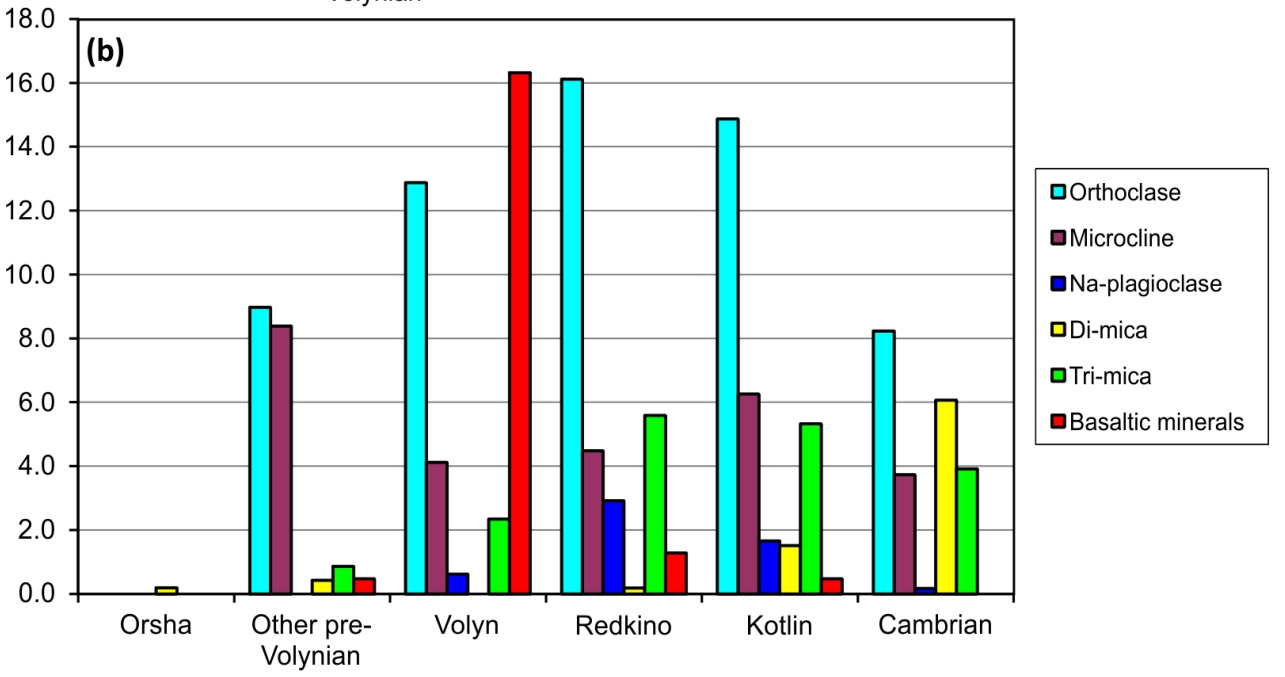
(b)
18.0
16.0
14.0
12.0
10.0
8.0
6.0
4.0
2.0
0.0
Orsha
Other pre-Volynian
Volyn
Redkino
Kotlin
Cambrian
Orthoclase
Microcline
Na-plagioclase
Di-mica
Tri-mica
Basaltic minerals

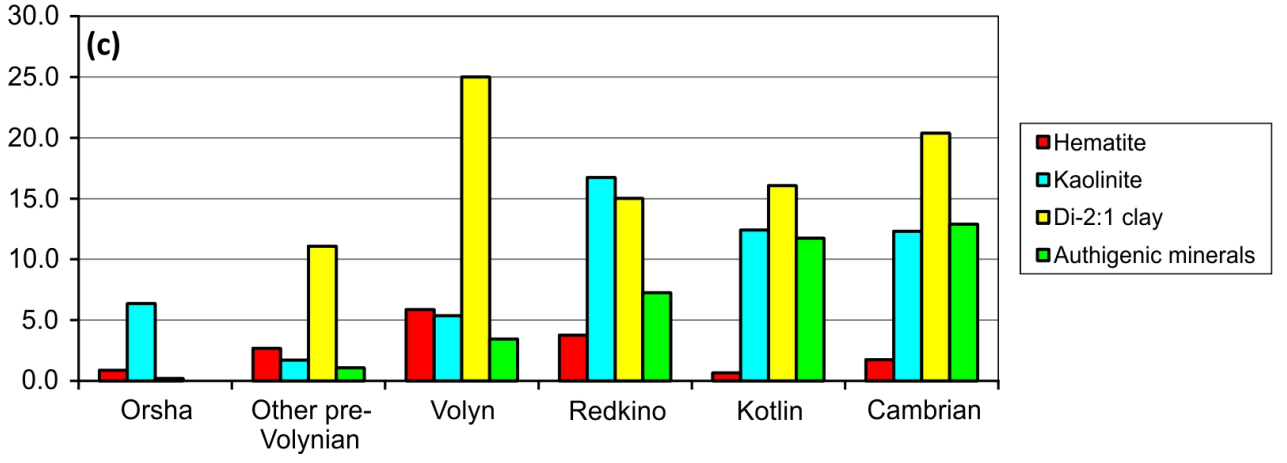
(c)
30.0
25.0
20.0
15.0
10.0
5.0
0.0
Orsha
Other pre-Volynian
Volyn
Redkino
Kotlin
Cambrian
Hematite
Kaolinite
Di-2:1 clay
Authigenic minerals


188
1984±25
175
1971±26
158
1967±26
140
1714±32
120
1953±27
Vilch-2, Pinsk Suite
300
1982±25
307
1956±29
334
1963±28
Vilch-4
Pinsk Suite
87
1356±24
95
2086±23
169
1885±23
190
1782±23
150
1994±23
Vilch-5B, Orsha Suite
329
1331±39
330
2770±24
357
954±12
209
2504±21
-6.5±0.9
210
1420±35
-10.2±0.7
216
1967±19
-2.6±0.9
232
980±11
-0.9±0.8
238
978±9
2.0±0.6
8
1488±25
-3.1±0.8
10
1503±25
3.1±0.7
13
584±8
-10.2±0.8
15
576±8
-13.2±0.7
Pinsk-46A
Rataychitsy Suite
30
1489±36
-2.8±0.7
269
2707±16
-4.2±0.5
390
1973±20
5.2±0.6
Vilch-6A
Glusk Suite
250
2038±17
-4.4±0.6
215
1564±30
-1.8±0.8
232
1416±39
-5.4±0.7
247
1556±36
-3.6±1.0
213
1622±39
-1.6±0.8
299
2366±31
-7.2±1.0
Lep-12A
Selsk Suite
408
1480±36
-4.0±0.6
410
708±13
-11.5±0.8
417
1778±31
4.4±0.6
414
1804±29
0.1±0.7
490
1798±30
4.0±0.7
452
570±8
-0.6±0.9
491
1508±32
-2.8±0.5
Kob-34B
Girsk Suite
215
1802±17
-12.3±0.9
230
2717±14
0.1±1.0
250
605±7
-3.1±0.8
256
1806±17
-12.4±1.5
348
635±7
-5.5±0.8
317
586±7
-20.0±1.0
287
1851±23
2.3±1.0
307
1931±36
5.8±0.7
299
1828±25
2.9±0.5
347
1934±46
5.1±0.6
389
1541±30
-9.2±0.8
419
1642±26
-0.4±0.6
Bog-33A
Nizov Suite
337
3409±21
0.3±0.9
Kob-57
lower Cambrian
$^{206}Pb/^{238}U$ or $^{207}Pb/^{206}Pb$ age ± 2SE
εHf ± 2SE
scale bars 100 μm

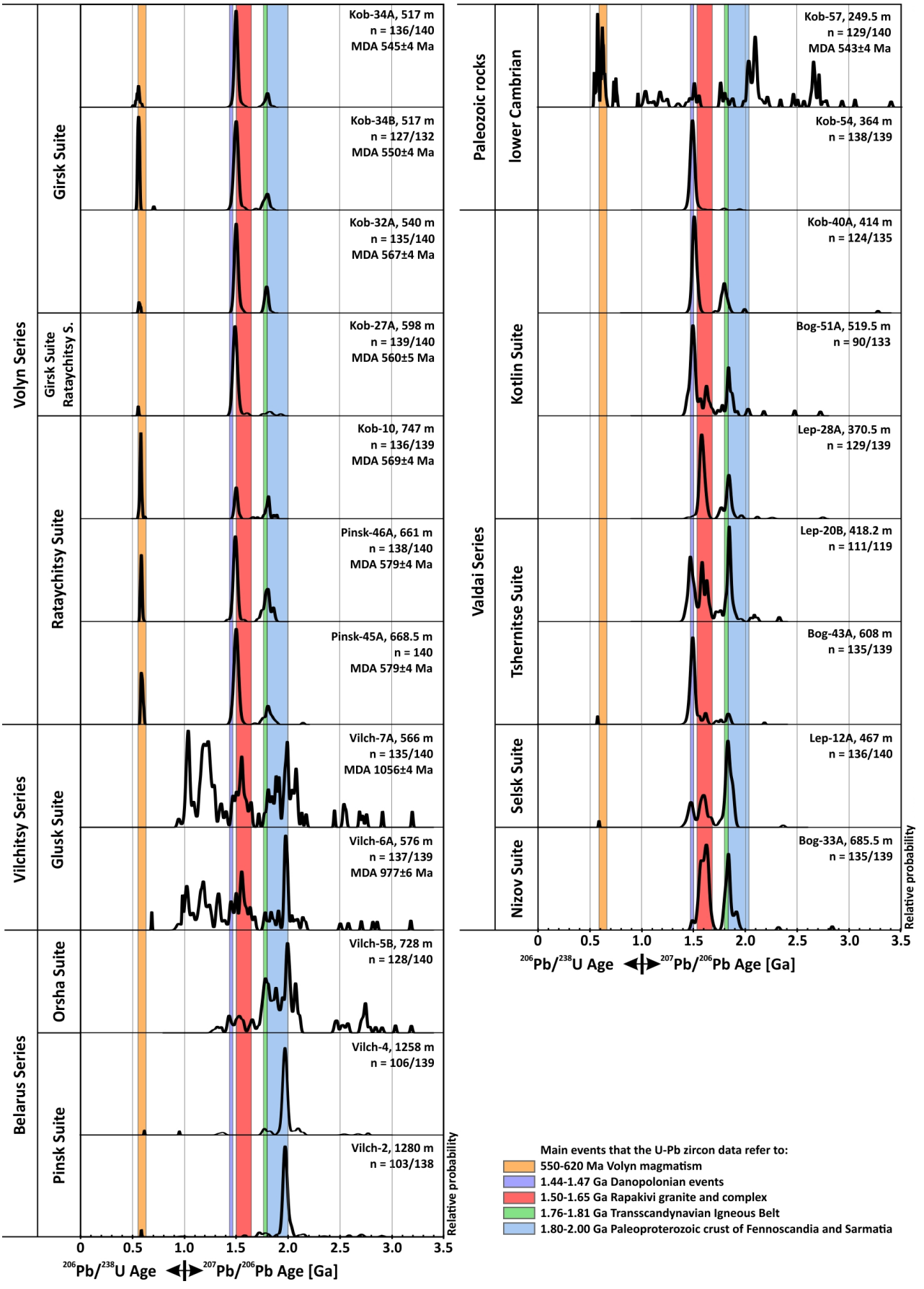
Volyn Series
Girsk Suite
Girsk Suite Rataychitsy S.
Rataychitsy Suite
Vilchitsy Series
Glusk Suite
Belarus Series
Orsha Suite
Pinsk Suite
Paleozoic rocks
lower Cambrian
Valdai Series
Kotlin Suite
Tshernitse Suite
Selsk Suite
Nizov Suite
Kob-34A, 517 m
n = 136/140
MDA 545±4 Ma
Kob-34B, 517 m
n = 127/132
MDA 550±4 Ma
Kob-32A, 540 m
n = 135/140
MDA 567±4 Ma
Kob-27A, 598 m
n = 139/140
MDA 560±5 Ma
Kob-10, 747 m
n = 136/139
MDA 569±4 Ma
Pinsk-46A, 661 m
n = 138/140
MDA 579±4 Ma
Pinsk-45A, 668.5 m
n = 140
MDA 579±4 Ma
Vilch-7A, 566 m
n = 135/140
MDA 1056±4 Ma
Vilch-6A, 576 m
n = 137/139
MDA 977±6 Ma
Vilch-5B, 728 m
n = 128/140
Vilch-4, 1258 m
n = 106/139
Vilch-2, 1280 m
n = 103/138
Kob-57, 249.5 m
n = 129/140
MDA 543±4 Ma
Kob-54, 364 m
n = 138/139
Kob-40A, 414 m
n = 124/135
Bog-51A, 519.5 m
n = 90/133
Lep-28A, 370.5 m
n = 129/139
Lep-20B, 418.2 m
n = 111/119
Bog-43A, 608 m
n = 135/139
Lep-12A, 467 m
n = 136/140
Bog-33A, 685.5 m
n = 135/139
Relative probability
0
0.5
1.0
1.5
2.0
2.5
3.0
3.5
206Pb/238U Age
207Pb/206Pb Age [Ga]
Main events that the U-Pb zircon data refer to:
550-620 Ma Volyn magmatism
1.44-1.47 Ga Danopolonian events
1.50-1.65 Ga Rapakivi granite and complex
1.76-1.81 Ga Transscandynavian Igneous Belt
1.80-2.00 Ga Paleoproterozoic crust of Fennoscandia and Sarmatia

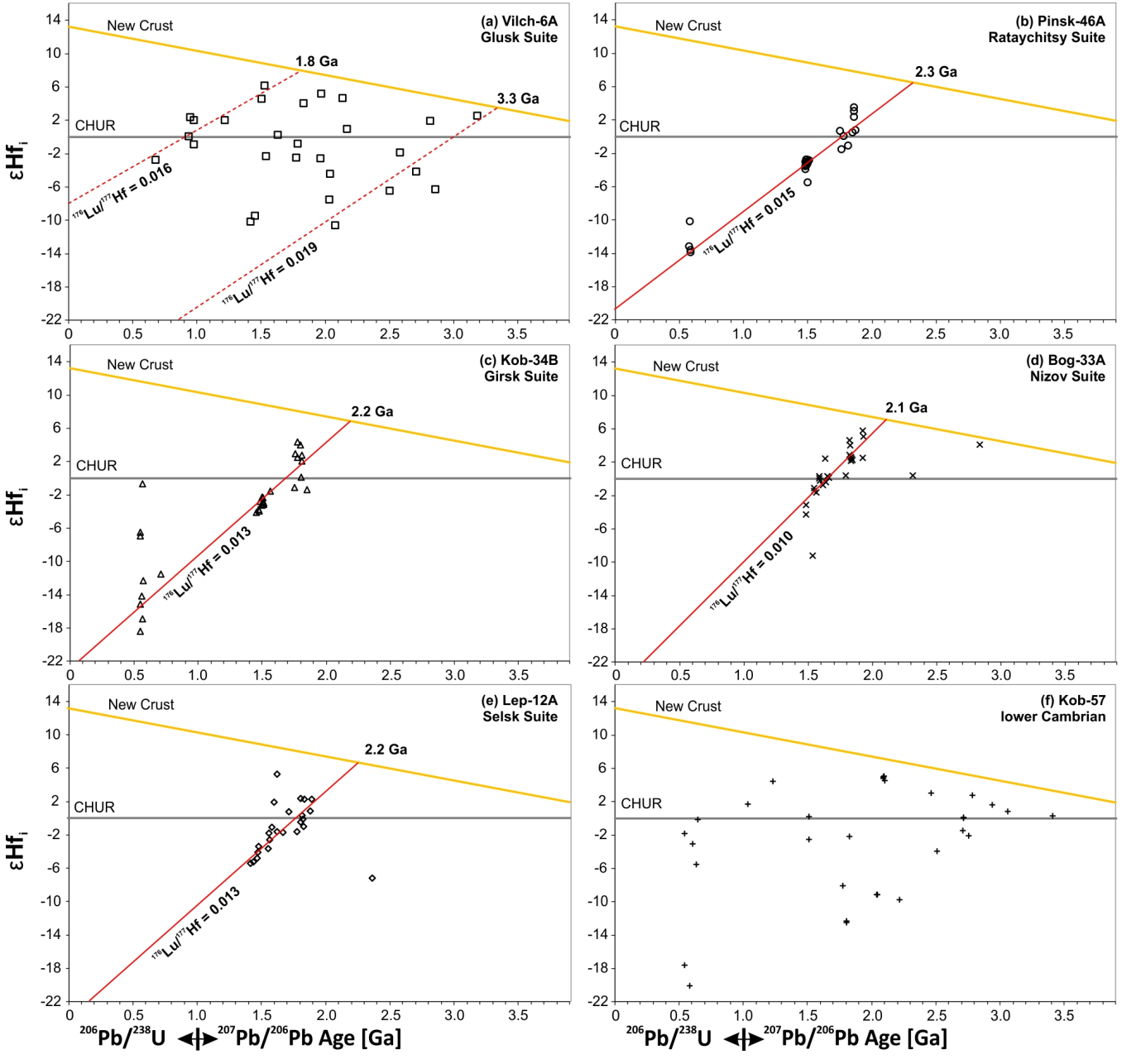
(a) Vilch-6A
Glusk Suite
(b) Pinsk-46A
Rataychitsy Suite
(c) Kob-34B
Girsk Suite
(d) Bog-33A
Nizov Suite
(e) Lep-12A
Selsk Suite
(f) Kob-57
lower Cambrian
New Crust
CHUR
1.8 Ga
3.3 Ga
2.3 Ga
2.2 Ga
2.1 Ga
176Lu/177Hf = 0.016
176Lu/177Hf = 0.019
176Lu/177Hf = 0.015
176Lu/177Hf = 0.013
176Lu/177Hf = 0.010
εHfi
206Pb/238U ◄┼► 207Pb/206Pb Age [Ga]

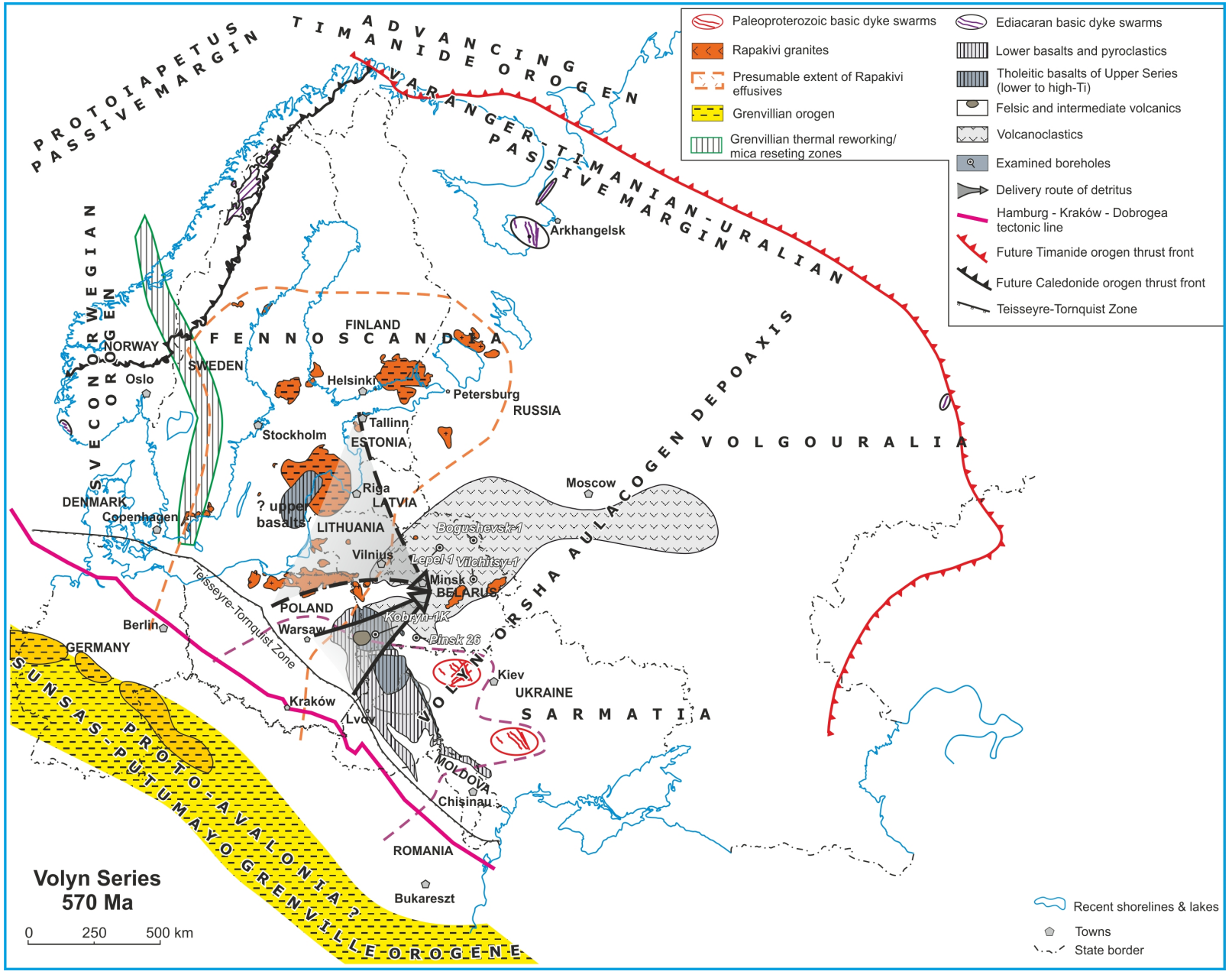
PROTOIAPETUS PASSIVE MARGIN
TIMANIDE OROGEN
VARANGER-TIMANIAN-URALIAN PASSIVE MARGIN
SVECONORWEGIAN OROGEN
FENNOSCANDIA
VOLGOURALIA
MOSCOW-ORSHA AULACOGEN DEPOAXIS
SARMATIA
VOLYN-ORSHA AULACOGEN
SUNSAS-PUTUMAYO-GRENVILLE-OROGENE?
NORWAY
SWEDEN
FINLAND
RUSSIA
DENMARK
ESTONIA
LATVIA
LITHUANIA
BELARUS
POLAND
GERMANY
UKRAINE
MOLDOVA
ROMANIA
Oslo
Copenhagen
Stockholm
Helsinki
Petersburg
Tallinn
Riga
Vilnius
Minsk
Warsaw
Berlin
Kraków
Lviv
Kiev
Chisinau
Bukareszt
Arkhangelsk
Moscow
? upper basalts
Bogushevsk-1
Lepel-1
Vilchitsy-1
Kobryn-1K
Pinsk 26
Teisseyre-Tornquist Zone
Volyn Series
570 Ma
0
250
500 km
Paleoproterozoic basic dyke swarms
Rapakivi granites
Presumable extent of Rapakivi effusives
Grenvillian orogen
Grenvillian thermal reworking/ mica reseting zones
Ediacaran basic dyke swarms
Lower basalts and pyroclastics
Tholeitic basalts of Upper Series (lower to high-Ti)
Felsic and intermediate volcanics
Volcanoclastics
Examined boreholes
Delivery route of detritus
Hamburg - Kraków - Dobrogea tectonic line
Future Timanide orogen thrust front
Future Caledonide orogen thrust front
Teisseyre-Tornquist Zone
Recent shorelines & lakes
Towns
State border

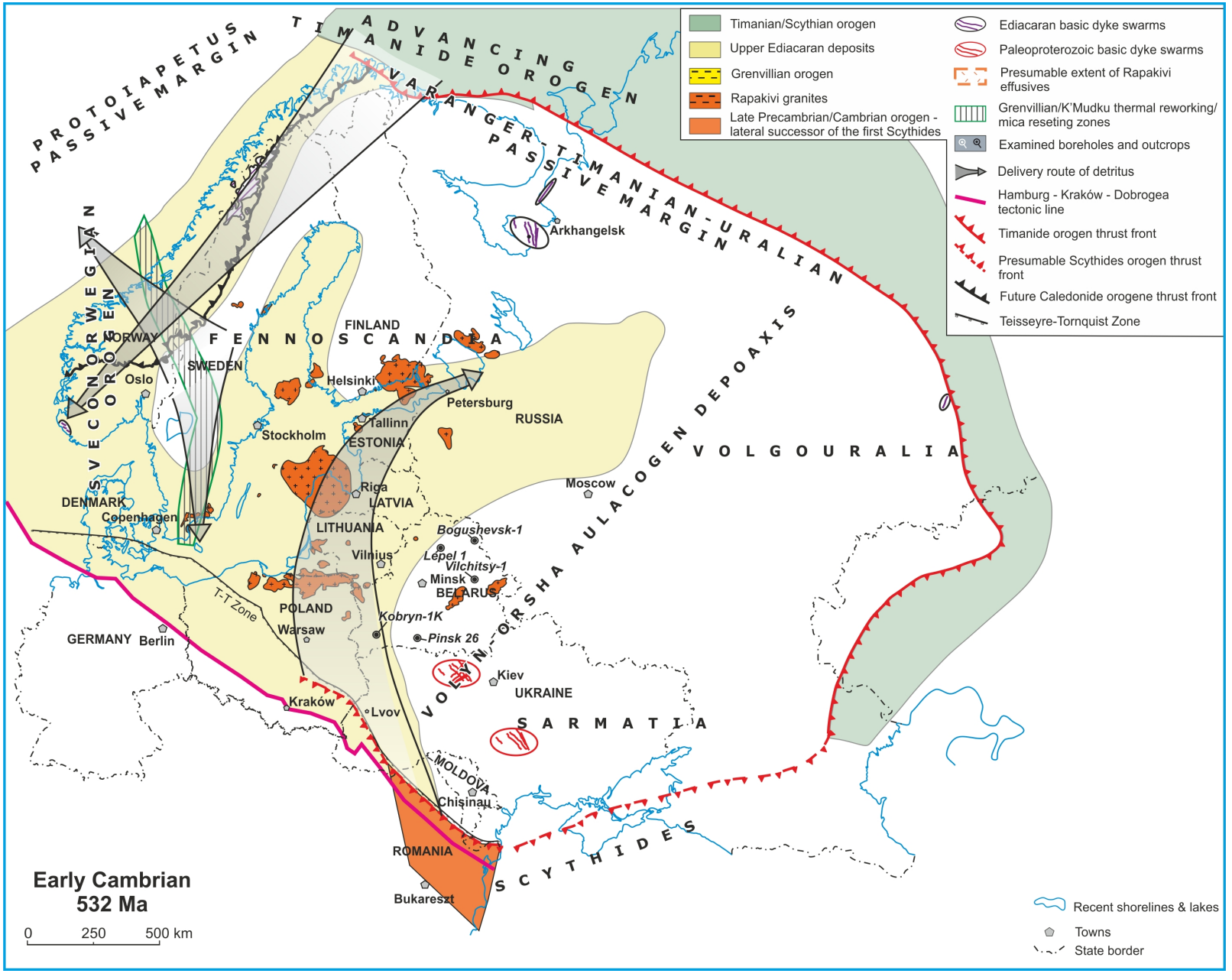
Timanian/Scythian orogen
Upper Ediacaran deposits
Grenvillian orogen
Rapakivi granites
Late Precambrian/Cambrian orogen - lateral successor of the first Scythides
Ediacaran basic dyke swarms
Paleoproterozoic basic dyke swarms
Presumable extent of Rapakivi effusives
Grenvillian/K'Mudku thermal reworking/ mica reseting zones
Examined boreholes and outcrops
Delivery route of detritus
Hamburg - Kraków - Dobrogea tectonic line
Timanide orogen thrust front
Presumable Scythides orogen thrust front
Future Caledonide orogene thrust front
Teisseyre-Tornquist Zone
PROTOIAPETUS PASSIVE MARGIN
TIMANIDE OROGEN
ADVANCING
VARANGER-TIMANIAN-URALIAN PASSIVE MARGIN
SVECONORWEGIAN OROGEN
FENNOSCANDIA
VOLGOURALIA
MOLDANUBIAN-MOESIAN-SCYTHIAN PLATFORM
VOLGA-SARMATIA
SCYTHIDES
AULACOGEN DEPOAXIS
PRIPYAT-DNIEPER-DONETS AULACOGEN
NORWAY
SWEDEN
FINLAND
RUSSIA
DENMARK
GERMANY
POLAND
LATVIA
ESTONIA
LITHUANIA
BELARUS
UKRAINE
MOLDOVA
ROMANIA
Oslo
Copenhagen
Stockholm
Helsinki
Tallinn
Petersburg
Riga
Vilnius
Minsk
Warsaw
Berlin
Kraków
Lvov
Kiev
Chisinau
Bukareszt
Moscow
Arkhangelsk
Bogushevsk-1
Lépel 1
Vilchitsy-1
Kobryn-1K
Pinsk 26
T-T Zone
Early Cambrian
532 Ma
0
250
500 km
Recent shorelines & lakes
Towns
State border

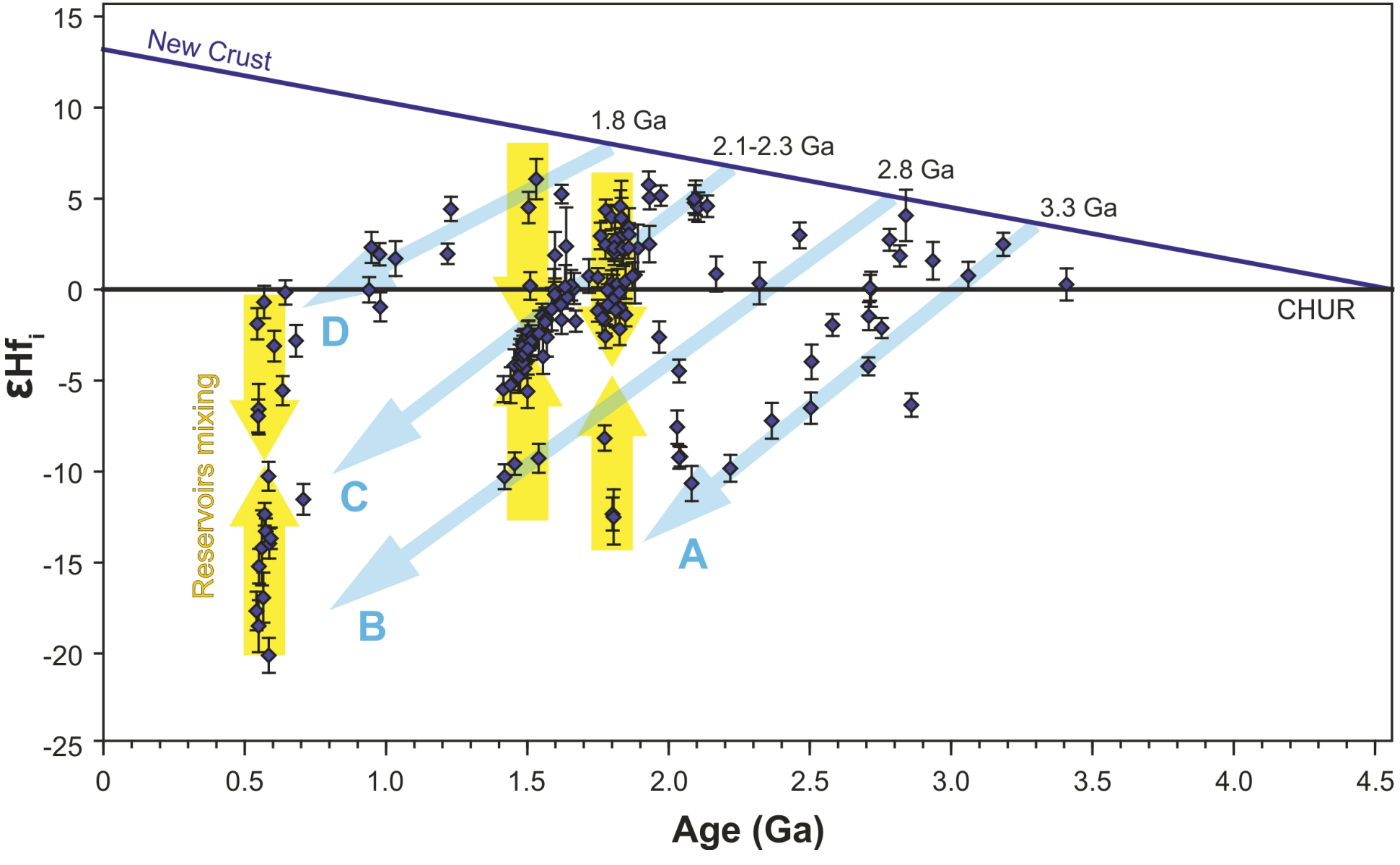
New Crust
1.8 Ga
2.1-2.3 Ga
2.8 Ga
3.3 Ga
CHUR
D
C
B
A
Reservoirs mixing
εHf$_i$
Age (Ga)
15
10
5
0
-5
-10
-15
-20
-25
0
0.5
1.0
1.5
2.0
2.5
3.0
3.5
4.0
4.5

Table 1. Samples used for isotopic measurements of zircons.

Abbreviation	Borehole name	Depth [m]	Lithology	Stratigraphic interval
Kob-57	Kobryn-1	249.5	coarse-grained sandstone	lower Cambrian
Kob-54	Kobryn-1	364.0	glauconite-bearing quartz arenite	lower Cambrian
Kob-40A	Kobryn-1	414.0	subarkose	Kotlin Suite
Kob-34A	Kobryn-1	517.0	tuff	Girsk Suite
Kob-34B	Kobryn-1	517.0	arkose	Girsk Suite
Kob-32A	Kobryn-1	540.0	arkose/wacke	Girsk Suite
Kob-27A	Kobryn-1	598.0	soft brown tuff	Girsk Suite / Rataychitsy Suite
Kob-10	Kobryn-1	747.0	volcanogenic sandstone	Rataychitsy Suite
Pinsk-46A	Pinsk	661.0	tuffite	Rataychitsy Suite
Pinsk-45A	Pinsk	668.5	sandy tuffite	Rataychitsy Suite
Vilch-7A	Vilchitsy	566.0	tillite	Glusk Suite
Vilch-6A	Vilchitsy	576.0	tillite	Glusk Suite
Vilch-5B	Vilchitsy	728.0	quartz arenite	Orsha Suite
Vilch-4	Vilchitsy	1258.0	sandstone	Pinsk Suite
Vilch-2	Vilchitsy	1280.0	sandstone	Pinsk Suite
Lep-28A	Lepel	370.5	arkosic sandstone	Kotlin Suite
Lep-20B	Lepel	418.2	subarkose	Tshernitse Suite
Lep-12A	Lepel	467.0	arkose	Selsk Suite
Bog-51A	Bogushevsk	519.5	arkose	Kotlin Suite
Bog-43A	Bogushevsk	608.0	arkose/wacke	Tshernitse Suite
Bog-33A	Bogushevsk	685.3	quartz arenite/subarkose	Nizov Suite

Supplementary Data SD1. Detailed description of analytical methods.

U-Pb measurements

The sample selection was primarily based on the presence of zircons that may constrain timing of volcanic activity coeval with sedimentation, in addition to the detrital zircons, present in all separated zircon populations and dated for provenance. All selected samples contained euhedral zircons, including needle-shaped acicular crystals typical for rapidly crystallized, porphyritic, sub-volcanic intrusions or high-level granites (cf. Corfu et al., 2003), that potentially may constrain maximum depositional ages of Riphean and Ediacaran sediments. Analytical strategy included selecting c. 40 most euhedral grains with sharp edges (named group A), whenever possible, and c. 100 grains representing random detrital population for provenance analysis (named group B), particularly in terms of geotectonic setting of the potential source terrains.

Zircons were separated by routine methods including crushing and sieving, followed by electromagnetic and heavy liquids separations. Zircons were mounted on adhesive tape and carbon-coated for imaging of the morphology by using Scanning Electron Microscopy at the Institute of Petrology and Structural Geology, Charles University in Prague. Then zircons were mounted in epoxy resin and polished for CL imaging prior to U-Pb measurements.

A Thermo Scientific Element 2 sector field ICP-MS coupled to a 193 nm ArF excimer laser (Teledyne Cetac Analyte Excite laser) at the Institute of Geology of the Czech Academy of Sciences, Prague, Czech Republic, was used to measure the Pb/U and Pb isotopic ratios in zircons. The laser was fired at a repetition rate of 5 Hz and fluence of 3.17–3.66 J/cm^2 with 20–25-micron spot size, depending on the zircon grain size. He carrier gas was flushed through the two-volume ablation cell at a flow rate of 0.7 L/min and mixed with 0.66 L/min Ar and 0.004 L/min N prior to introduction into the ICP. The in-house glass signal homogenizer (design of Tunheng and Hirata, 2004) was used for mixing all the gases and aerosol resulting in smooth, spike-free signal. The signal was tuned for maximum sensitivity of Pb and U, Th/U ratio close to unity and low oxide level, commonly below 0.2 %. Typical acquisitions consisted of 15 second of blank measurement followed by measurement of U, Th and Pb signals from the ablated zircon for another 35 seconds. The total of 420 mass scans data were acquired in time resolved – peak jumping – pulse counting / analogue mode with 1 point measured per peak for masses ^{204}Pb + Hg, ^{206}Pb, ^{207}Pb, ^{208}Pb, ^{232}Th, ^{235}U, and ^{238}U. Due

to a non-linear transition between the counting and analogue acquisition modes of the ICP instrument, the raw data were pre-processed using a purpose-made Excel macro. As a result, the intensities of ^{238}U were left unchanged if measured in a counting mode and recalculated from ^{235}U intensities if the ^{238}U was acquired in analogue mode. Data reduction was then carried out off-line using the Iolite data reduction package version 3.4 with VizualAge utility (Petrus and Kamber, 2012). Full details of the data reduction methodology can be found in Paton et al. (2010). The data reduction included correction for gas blank, laser-induced elemental fractionation of Pb and U and instrument mass bias. For the data presented here, blank intensities and instrumental bias were interpolated using an automatic spline function while down-hole inter-element fractionation was corrected using an exponential function. No common Pb correction was applied to the data due to the high Hg contamination of the commercially available He carrier gas, which precludes accurate correction of the interfering ^{204}Hg on the very small signal of ^{204}Pb (common lead).

Residual elemental fractionation and instrumental mass bias were corrected by normalization to the natural zircon reference material Plešovice (Sláma et al., 2008). The excess variance (Paton et al., 2010) of Plešovice zircon was calculated in Isoplot and quadratically added to the measurement uncertainties of all unknowns including validation zircon reference materials GJ-1 {nr. 63} (Jackson et al., 2004) and 91500 (Wiedenbeck et al., 1995). These two were periodically analysed during the measurement for quality control. The values obtained from analyses performed over many days (discordant GJ-1: mean concordia age of 600 ± 3 Ma (2σ), mean $^{207}Pb/^{206}Pb$ age of 608 ± 2 Ma (2σ); near-concordant 91500: mean concordia age of 1065 ± 5 Ma (2σ); see the STD data and plots in the electronic supplementary material) correspond perfectly and are less than 1% accurate within the published reference values (GJ-1: $^{206}Pb/^{238}U$ age of 600.5 ± 0.4 Ma, Schaltegger et al., 2015 and $^{207}Pb/^{206}Pb$ age of 608.53 ± 0.4 Ma, Jackson et al., 2004 respectively; 91500: $^{207}Pb/^{206}Pb$ age of 1065.4 ± 0.3 Ma, Wiedenbeck et al., 1995). The zircon U–Pb ages are presented as concordia (pooled) age and probability density plots generated with the ISOPLOT program v. 4.16 (Ludwig, 2008).

Maximum depositional ages were calculated using from 2 to 5 youngest zircons following Dickinson and Gehrels (2009). These are presented as concordia ages calculated from the youngest zircons with <2.0 % discordance.

Lu-Hf measurements

The Lu-Hf analyses were performed at the University of Bristol (Bristol Isotope Group) using a ThermoFinnigan Neptune plus multicollector inductively-coupled plasma mass spectrometer (MC-ICP-MS) coupled with a Photon-Machine Analyte G2 Excimer laser (193 nm wavelength). Ablation was performed using 50 μm and 40 μm spot sizes, a laser frequency of 4 Hz, and the energy density of the laser beam was c. 5.5 J/cm^2. A typical analysis was 90 seconds, including a 30 seconds background measurement and a 60 seconds ablation period. Correction for the interferences and mass bias followed the Bristol routine procedure (Hawkesworth and Kemp, 2006; Kemp et al., 2009). The correction for the isobaric interference of Yb and Lu on ^{176}Hf was made following a method detailed in Fisher et al. (2011). For Yb, the interference-free ^{171}Yb was corrected for mass bias effects using an exponential law and ^{173}Yb/^{171}Yb = 1.132685 (Chu et al., 2002). The mass bias-corrected ^{171}Yb was monitored during the run and the magnitude of the ^{176}Yb interference on ^{176}Hf was calculated using ^{176}Yb/^{171}Yb = 0.901864 (Chu et al., 2002). For Lu, the interference-free ^{175}Lu was corrected for mass bias effects assuming βLu = βYb and using an exponential law. The mass bias-corrected ^{176}Lu was monitored during the run and the magnitude of the ^{176}Lu interference on ^{176}Hf was calculated using ^{176}Lu/^{175}Lu = 0.02655 (Vervoort et al., 2004). Interference-corrected ^{176}Hf/^{177}Hf were corrected for mass bias using an exponential law and ^{179}Hf/^{177}Hf = 0.7325 (Patchett et al., 1981). To facilitate data comparison between labs, a final correction was applied to ^{176}Hf/^{177}Hf ratios to account for the ca. 80 ppm difference between the JMC-475 solution value measured in Bristol (0.282137±6) and the accepted value of 0.282160 for this standard (Blichert-Toft et al., 1997). ^{176}Hf/^{177}Hf initial values were calculated using the ^{176}Lu decay constant of Söderlund et al. (2004) and the U-Pb crystallisation ages of the zircons. Uncertainties over crystallisation ages were taken into account for the calculation of initial Hf isotope ratios. The accuracy and long-term reproducibility of the measurements were gauged by analyzing three zircon reference standards: Plešovice (^{176}Hf/^{177}Hf = 0.282478±23, n = 21), Mud Tank (^{176}Hf/^{177}Hf = 0.282506±19, n = 21) and TEMORA 2 (^{176}Hf/^{177}Hf = 0.282683±22, n = 8). All errors are given at 2 s.d. level. ^{176}Hf/^{177}Hf initial values were calculated using the ^{176}Lu decay constant of Söderlund et al. (2004). New crust evolution curve of Dhuime et al. (2011), and chondritic values from Bouvier et al. (2008) were used for model age calculations.

References

Blichert-Toft, J., Chauvel, C., Albarède, F., 1997. Separation of Hf and Lu for high-precision isotope analysis of rock samples by magnetic sector-multiple collector ICP-MS. Contributions to Mineralogy and Petrology 127, 248–260.

Bouvier, A., Vervoort, J.D, Patchett, P.J., 2008. The Lu-Hf and Sm-Nd isotopic composition of CHUR: constraints from unequilibrated chondrites and implications for the bulk composition of terrestrial planets. Earth and Planetary Science Letters 273, 48–57.

Chu, N.-Ch., Taylor, R.N., Chavagnac, V., Nesbitt, R.W., Boella, R.M., Milton, J.A., German, Ch.R., Bayon, G., Burton, K., 2002. Hf isotope ratio analysis using multi-collector inductively coupled plasma mass spectrometry: an evaluation of isobaric interference corrections. Journal of Analytical Atomic Spectrometry 17, 1567–1574.

Corfu, F., Hanchar, J.M., Hoskin, P.W.O., Kinny, P., 2003. Atlas of zircon textures. In: Hanchar, J.M., Hoskin, P.W.P. (eds.) Zircon. Mineralogical Society of America. Reviews in Mineralogy and Geochemistry 53, pp. 469–500.

Dhuime, B., Hawkesworth, Ch., Cawood, P., 2011. When Continents Formed. Science 331, 154–155.

Dickinson, W.R., Gehrels, G.E., 2009. Use of U–Pb ages of detrital zircons to infer maximum depositional ages of strata: A test against a Colorado Plateau Mesozoic database. Earth and Planetary Science Letters 288, 115–125.

Fisher, Ch.M., Hanchar, J.M., Samson, S.D., Dhuime, B.D., Blichert-Toft, J., Vervoort, J.D., Lam, R., 2011. Synthetic zircon doped with hafnium and rare earth elements: A reference material for in situ hafnium isotope analysis. Chemical Geology 286, 32–47.

Hawkesworth, C.J., Kemp, A.I.S., 2006. Using hafnium and oxygen isotopes in zircons to unravel the record of crustal evolution. Chemical Geology 226, 144–162.

Jackson, S.E., Pearson, N.J., Griffin, W.L., Belousova, E.A., 2004. The application of laser ablation-inductively coupled plasma-mass spectrometry to in situ U-Pb zircon geochronology. Chemical Geology 211, 47–69.

Kemp, A.I.S., Foster, G.L., Scherstén, A., Whitehouse, M.J., Darling, J., Storey, C., 2009. Concurrent Pb–Hf isotope analysis of zircon by laser ablation multi-collector ICP-MS, with implications for the crustal evolution of Greenland and the Himalayas. Chemical Geology 261, 244–260.

Ludwig, K.R., 2008. Isoplot 3.70. A geochronological toolkit for Microsoft Excel. Berkley Geochronology Center Special Publication No. 4.

Patchett, P.J., Tatsumoto, M., 1981. A routine high-precision method for Lu-Hf isotope geochemistry and chronology. Contributions to Mineralogy and Petrology 75, 263–267.

Paton, C., Woodhead, J.D., Hellstrom, J.C., Hergt, J.M., Greig, A., Maas, R., 2010. Improved laser ablation u-pb zircon geochronology through robust downhole fractionation correction. Geochemistry Geophysics Geosystems, 11.

Petrus, J.A., Kamber, B.S., 2012. VizualAge: A Novel Approach to Laser Ablation ICP-MS U-Pb Geochronology Data Reduction. Geostandards and Geoanalytical Research 36, 247–270.

Schaltegger, U., Schmitt, A.K., Horstwood, M.S.A., 2015. U–Th–Pb zircon geochronology by ID-TIMS, SIMS, and laser ablation ICP-MS: Recipes, interpretations, and opportunities. Chemical Geology 402, 89–110.

Sláma, J., Kosler, J., Condon, D.J., Crowley, J.L., Gerdes, A., Hanchar, J.M., Horstwood, M.S.A., Morris, G.A., Nasdala, L., Norberg, N., Schaltegger, U., Schoene, B., Tubrett, M.N., Whitehouse, M.J., 2008. Plesovice zircon – a new natural reference material for U-Pb and Hf isotopic microanalysis. Chemical Geology 249, 1–35.

Söderlund, U., Patchett, J.P., Vervoort, J.D., Isachsen, C.E., 2004. The ^{176}Lu decay constant determined by Lu–Hf and U–Pb isotope systematics of Precambrian mafic intrusions. Earth and Planetary Science Letters 219, 311–324.

Tunheng, A., Hirata, T., 2004. Development of signal smoothing device for precise elemental analysis using laser ablation-ICP-mass spectrometry. Journal of Analytical Atomic Spectrometry 19, 932.

Vervoort, J. D., Patchett, P.J., Söderlund, U., Baker, M., 2004. Isotopic composition of Yb and the determination of Lu concentrations and Lu/Hf ratios by isotope dilution using MC-ICPMS. Geochemistry, Geophysics, Geosystems, 5, Q11002, doi: 10.1029/2004GC000721

Wiedenbeck, M., Alle, P., Corfu, F., Griffin, W.L., Meier, M., Oberli, F., Vonquadt, A., Roddick, J.C., Speigel, W., 1995. 3 natural zircon standards for U-Th-Pb, Lu-Hf, trace-element and REE analyses. Geostandards Newsletter 19, 1–23.

Supplementary Data SD4. Summary of LA-ICP-MS U-Pb age data.

1. Sandstone Vilch-2 (Vilchitsy borehole, depth 1280 m); Belarus Series, Pinsk Suite

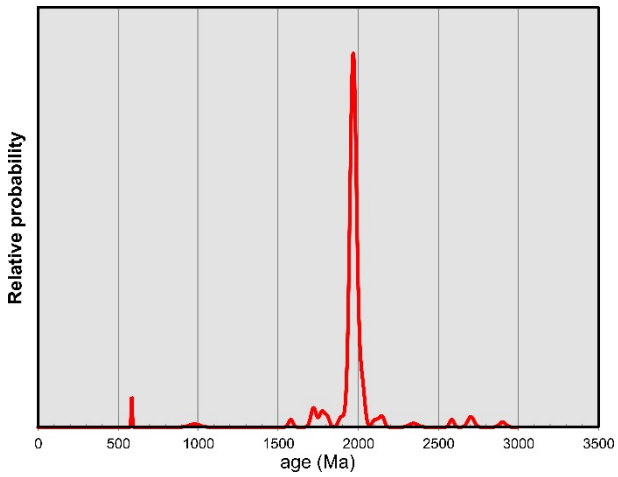

Detrital zircon age spectrum (probability density plot) (n = 103) for the Vilch-2 sample.

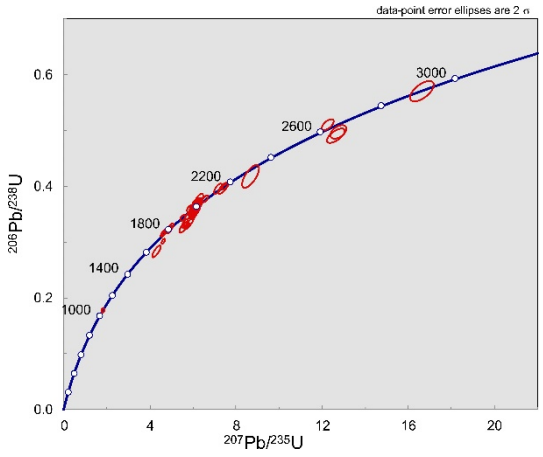

U-Pb isotopic data obtained from the detrital zircon population from the Vilch-2 sample.

2. Sandstone Vilch-4 (Vilchitsy borehole, depth 1258 m); Belarus Series, Pinsk Suite

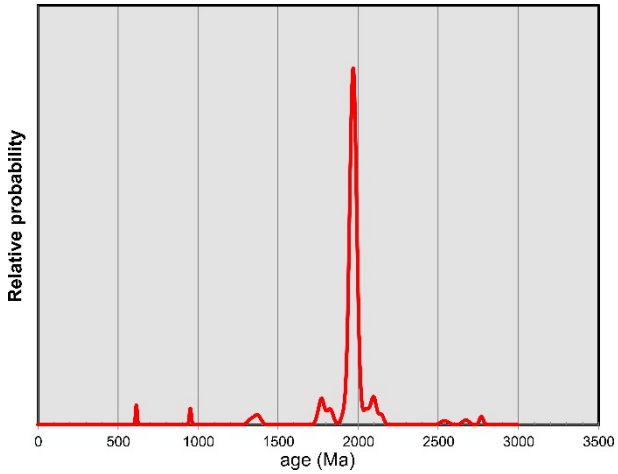

Detrital zircon age spectrum (n = 106) for the Vilch-4 sample.

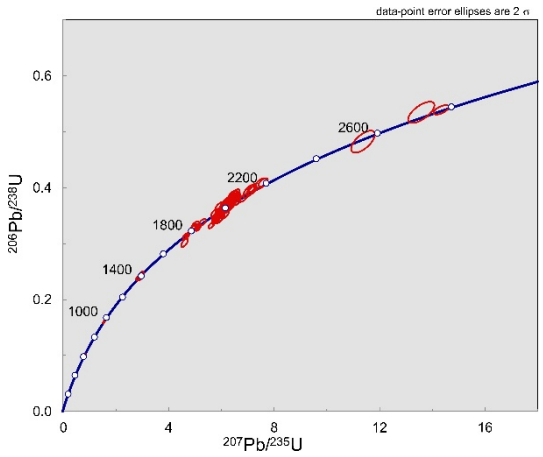

U-Pb isotopic data obtained from the detrital zircon population from the Vilch-4 sample.

3. Quartz arenite Vilch-5B (Vilchitsy borehole, depth 728 m); Belarus Series, Orsha Suite

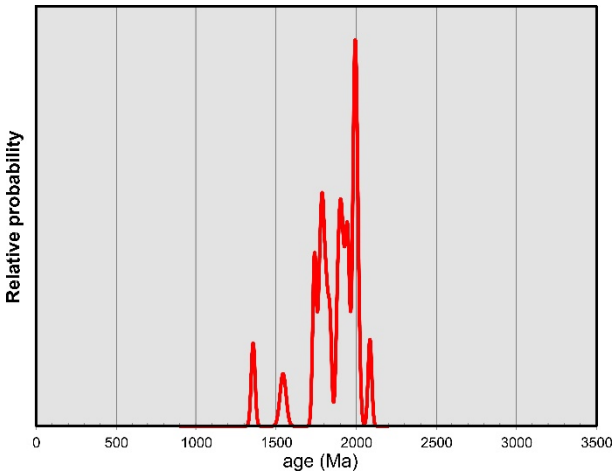

Detrital zircon age spectrum (n = 24) for the group A zircons from the Vilch-5B sample.

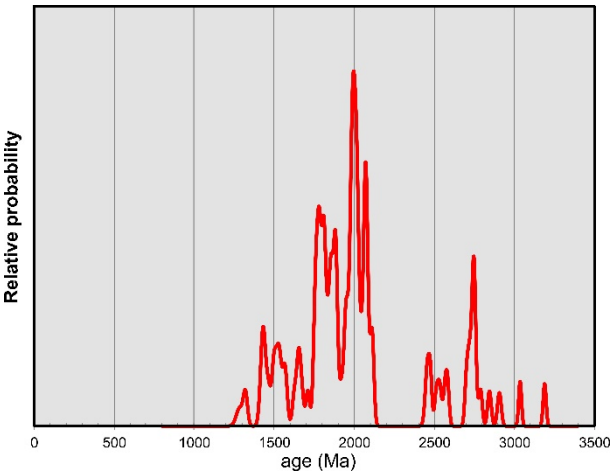

Detrital zircon age spectrum (n = 104) for the group B zircons from the Vilch-5B sample

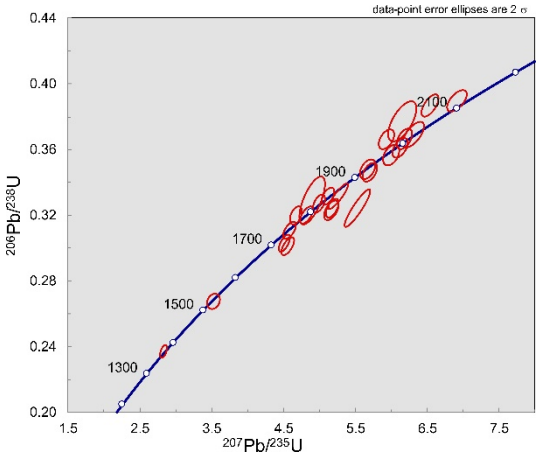

U-Pb isotopic data obtained from the detrital zircon population of the group A in the Vilch-5B sample.

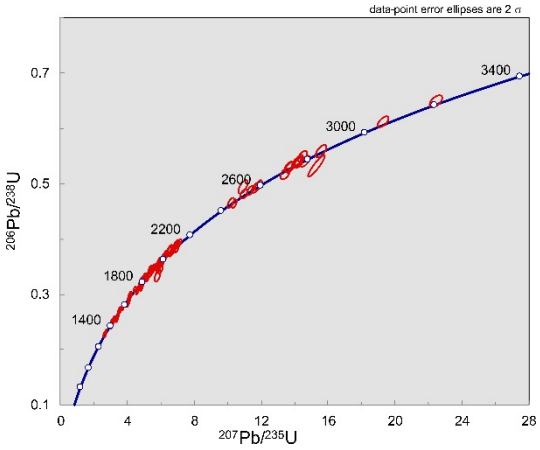

U-Pb isotopic data obtained from the detrital zircon population of the group B in the Vilch-5B sample.

4. Tillite Vilch-6A (Vilchitsy borehole, depth 576.0 m); Vilchitsy Series, Glusk Suite

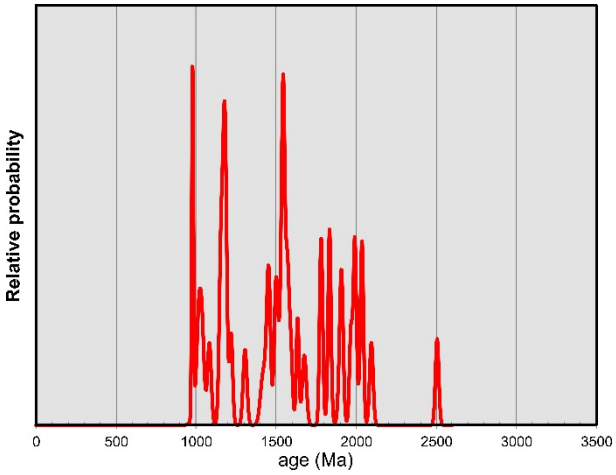

Detrital zircon age spectrum (n = 41) for the group A zircons from the Vilch-6A sample.

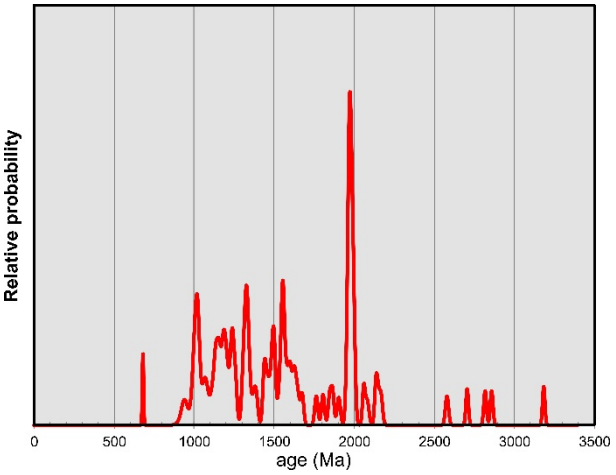

Detrital zircon age spectrum (n = 96) for the group B zircons from the Vilch-6A sample.

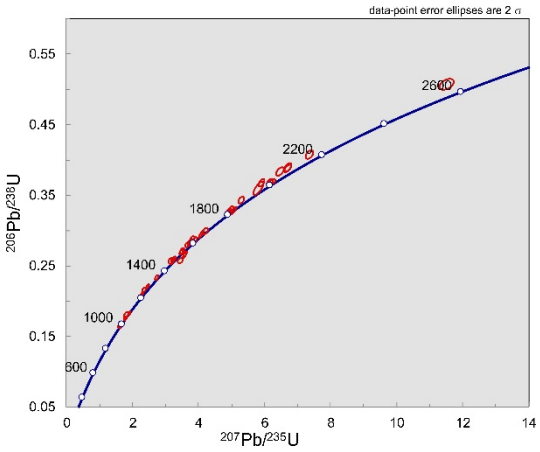

U-Pb isotopic data obtained from the detrital zircon population of the group A in the Vilch-6A sample.

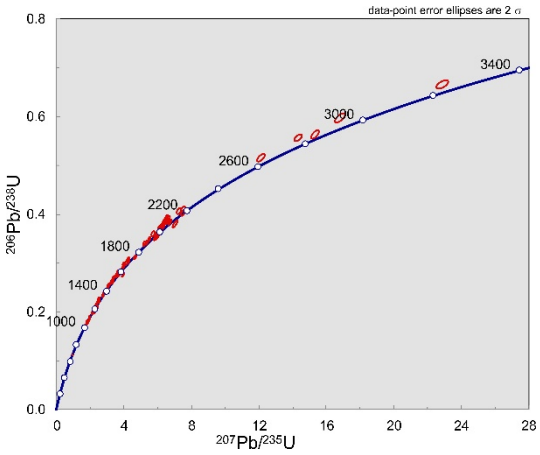

U-Pb isotopic data obtained from the detrital zircon population of the group B in the Vilch-6A sample.

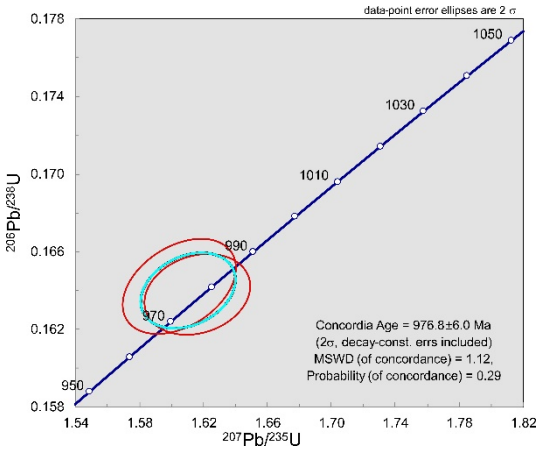

U-Pb isotopic data obtained from the youngest detrital zircons, constraining maximum depositional age for the Vilch-6A sample.

5. Tillite Vilch-7A (Vilchitsy borehole, depth 566.0 m); Vilchitsy Series, Glusk Suite

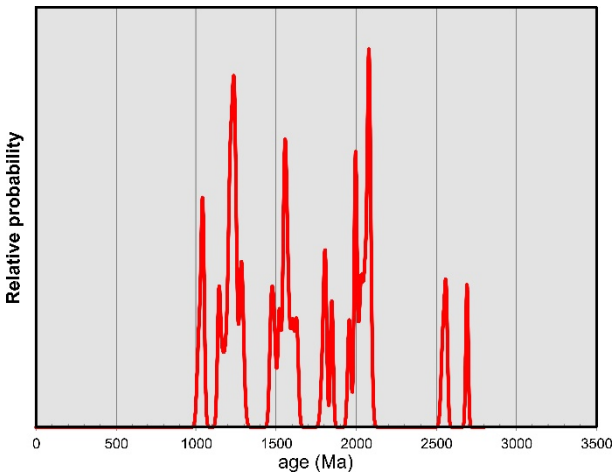

Detrital zircon age spectrum (n = 39) for the group A zircons from the Vilch-7A sample.

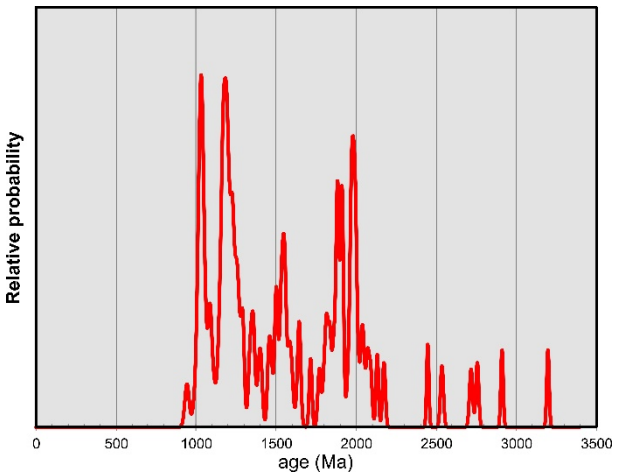

Detrital zircon age spectrum (n = 96) for the group B zircons from the Vilch-7A sample.

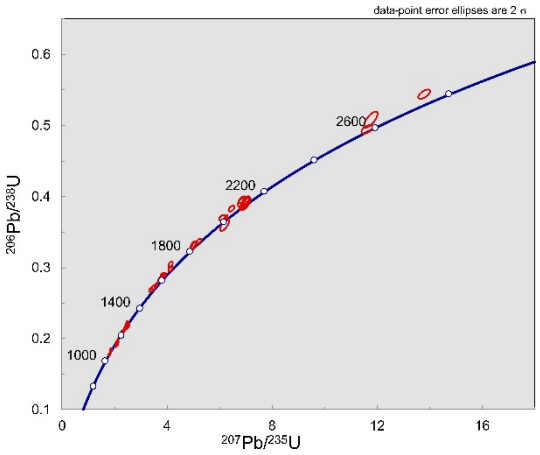

U-Pb isotopic data obtained from the detrital zircon population of the group A in the Vilch-7A sample.

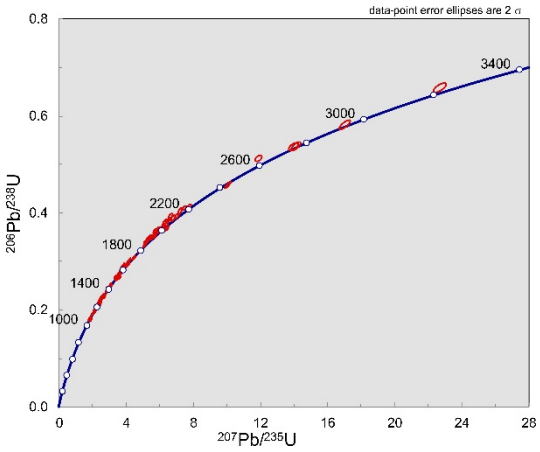

U-Pb isotopic data obtained from the detrital zircon population of the group B in the Vilch-7A sample.

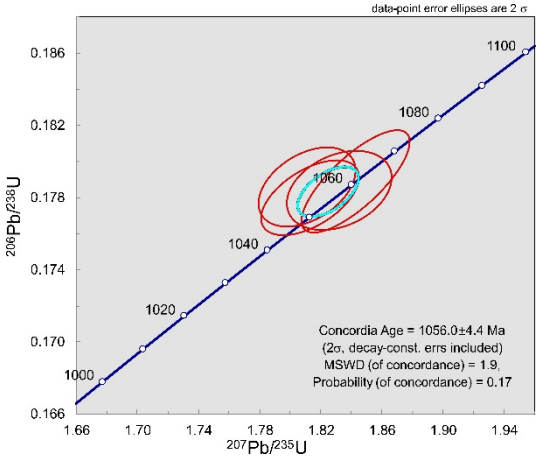

U-Pb isotopic data obtained from the youngest detrital zircons, constraining maximum depositional age for the Vilch-7A sample.

6. Sandy tuffite Pinsk-45A (Pinsk borehole, depth 668.5 m); Volyn Series, Rataychitsy Suite

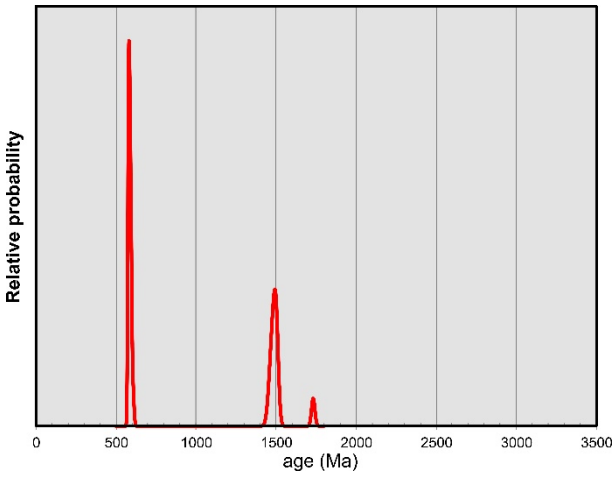

Detrital zircon age spectrum (n = 12) for the group A zircons from the Pinsk-45A sample.

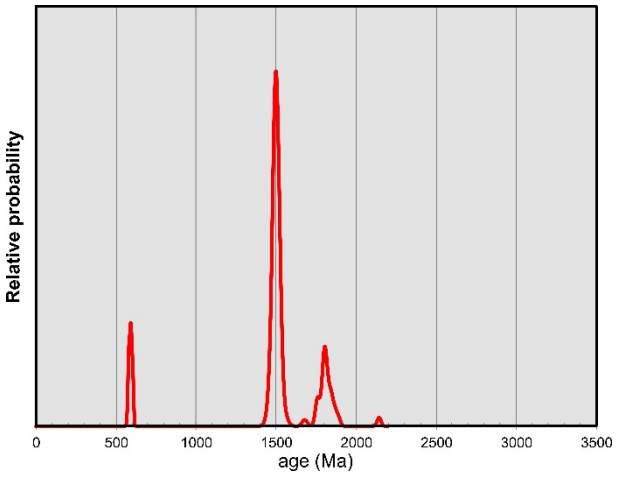

Detrital zircon age spectrum (n = 117) for the group B zircons from the Pinsk-45A sample.

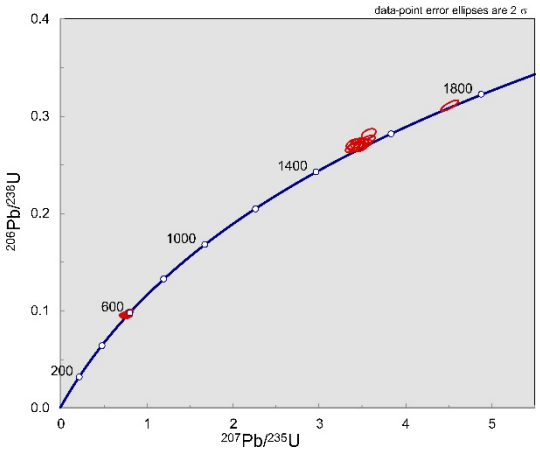

U-Pb isotopic data obtained from the detrital zircon population of the group A in the Pinsk-45A sample.

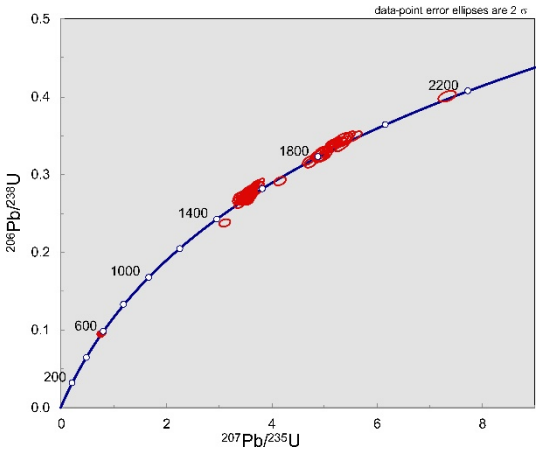

U-Pb isotopic data obtained from the detrital zircon population of the group B in the Pinsk-45A sample.

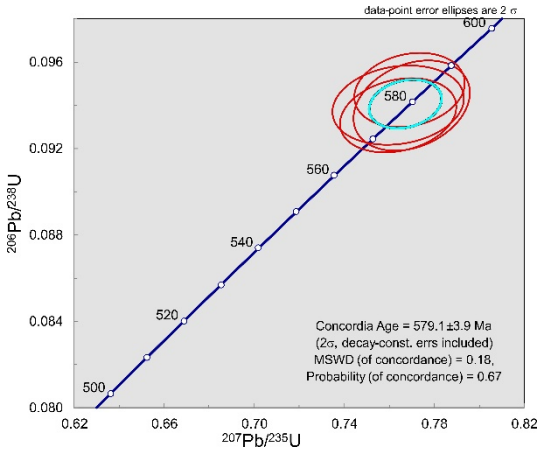

U-Pb isotopic data obtained from the youngest detrital zircons, constraining maximum depositional age for the Pinsk-45A sample.

7. Tuffite Pinsk-46A (Pinsk borehole, depth 661 m); Volyn Series, Rataychitsy Suite

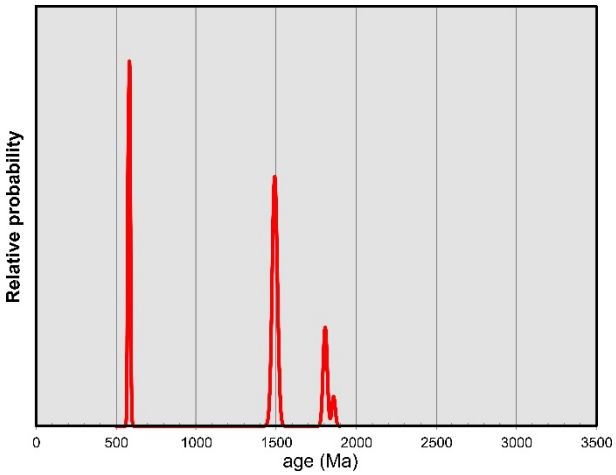

Detrital zircon age spectrum (n = 27) for the group A zircons from the Pinsk-46A sample.

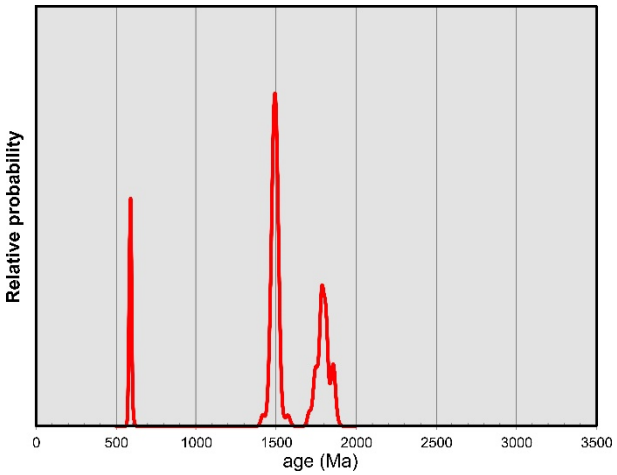

Detrital zircon age spectrum (n = 111) for the group B zircons from the Pinsk-46A sample.

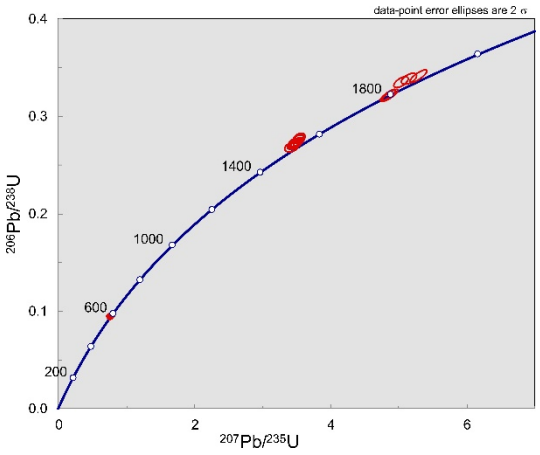

U-Pb isotopic data obtained from the detrital zircon population of the group A in the Pinsk-46A sample.

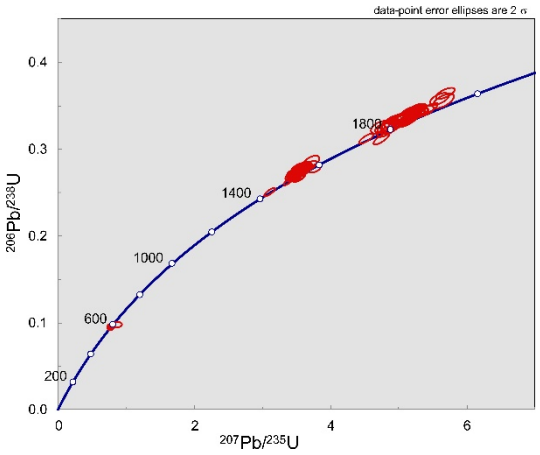

U-Pb isotopic data obtained from the detrital zircon population of the group B in the Pinsk-46A sample.

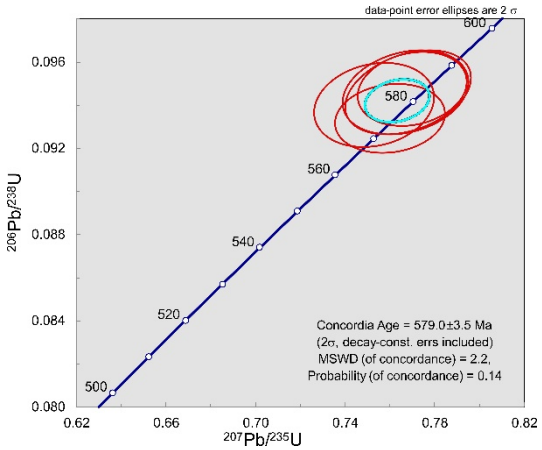

U-Pb isotopic data obtained from the youngest detrital zircons, constraining maximum depositional age for the Pinsk-46A.

8. Volcanogenic sandstone Kob-10 (Kobryn borehole, depth 747 m); Volyn Series, Rataychitsy Suite

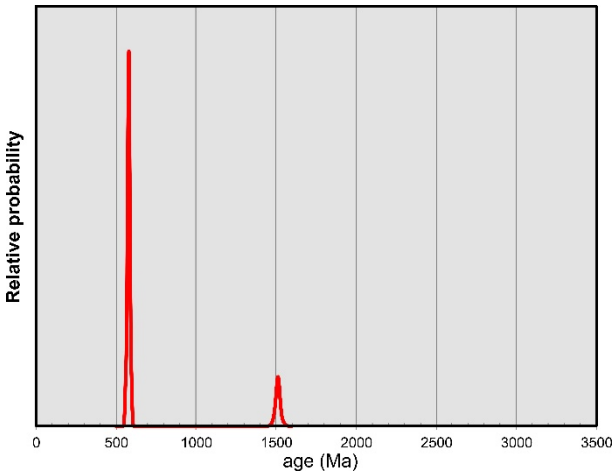

Detrital zircon age spectrum (n = 37) for the group A zircons from the Kob-10 sample.

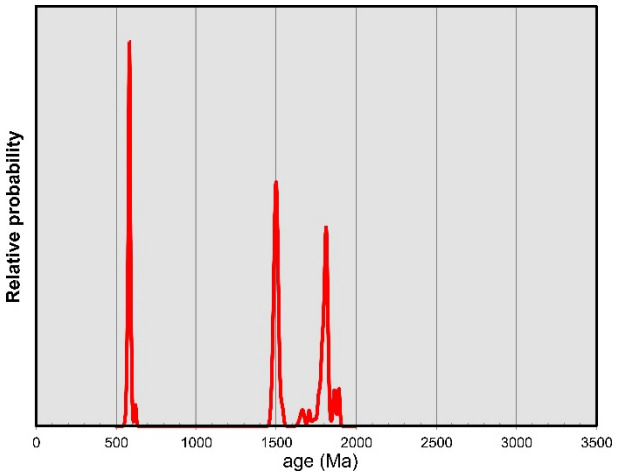

Detrital zircon age spectrum (n = 99) for the group B zircons from the Kob-10 sample.

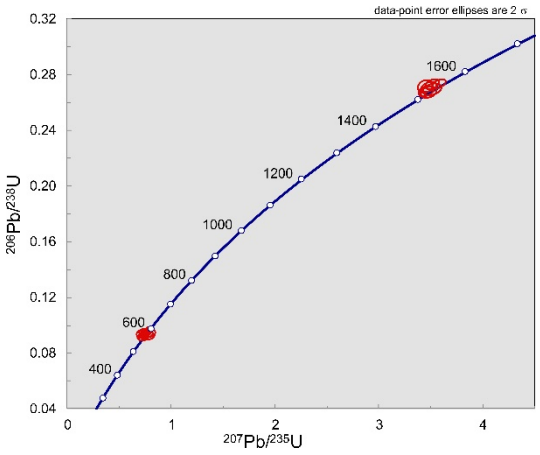

U-Pb isotopic data obtained from the detrital zircon population of the group A in the Kob-10 sample.

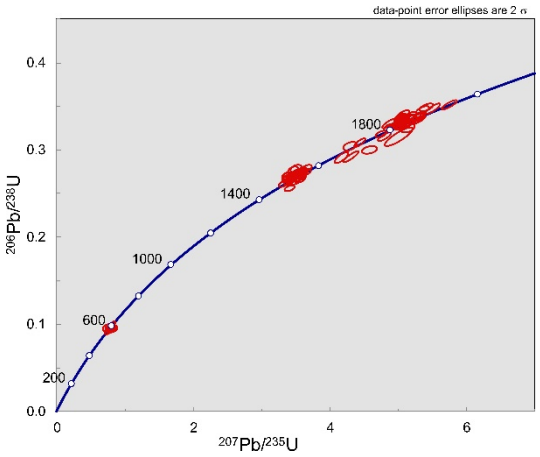

U-Pb isotopic data obtained from the detrital zircon population of the group B in the Kob-10 sample.

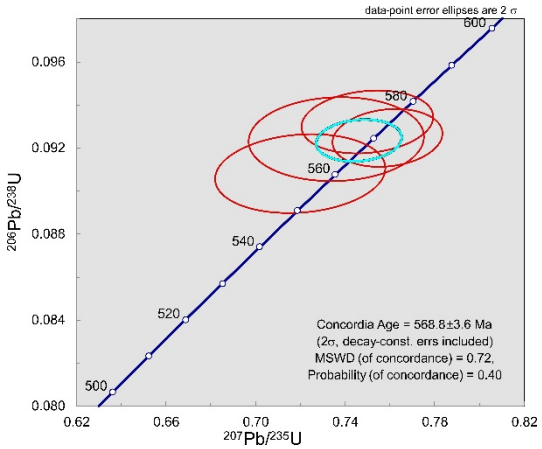

U-Pb isotopic data obtained from the youngest detrital zircons, constraining maximum depositional age for the Kob-10 sample.

9. Soft brown tuff Kob-27A (Kobryn borehole, depth 598 m); Volyn Series, Girsk Suite / Rataychitsy Suite

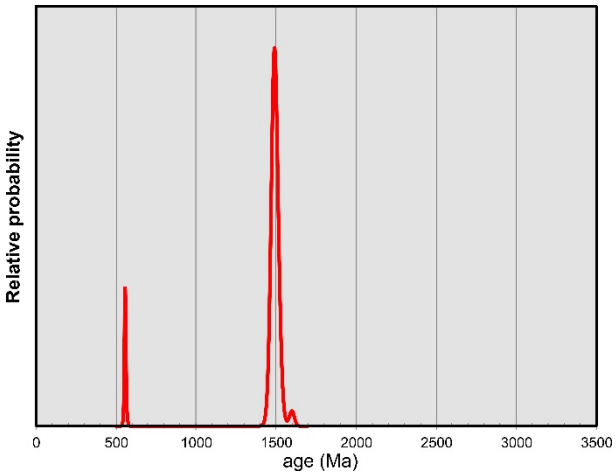

Detrital zircon age spectrum (n = 40) for the group A zircons from the Kob-27A sample.

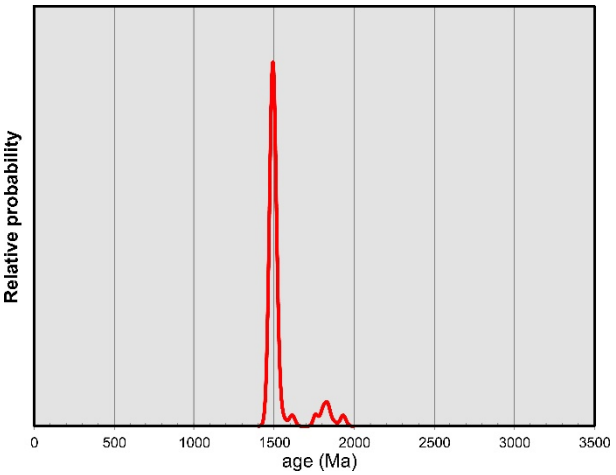

Detrital zircon age spectrum (n = 99) for the group B zircons from the Kob-27A sample.

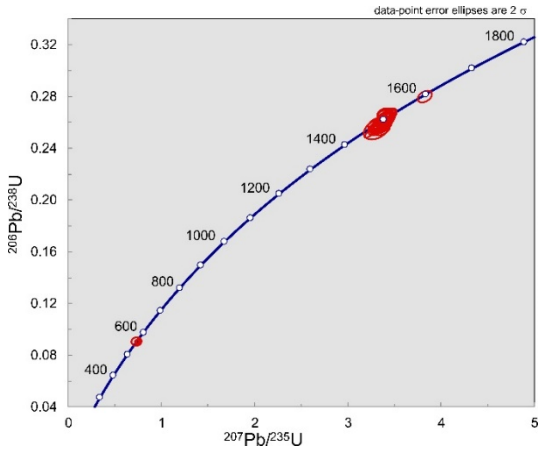

U-Pb isotopic data obtained from the detrital zircon population of the group A in the Kob-27A sample.

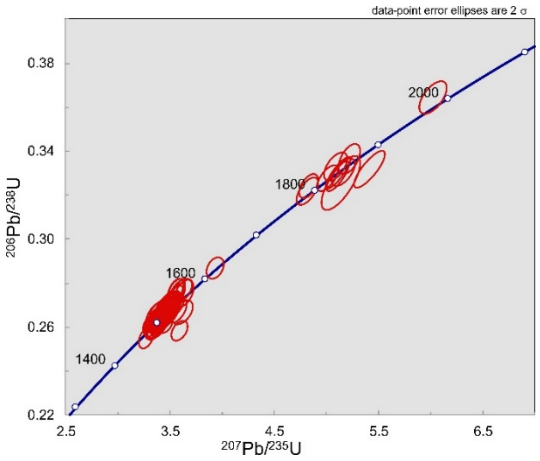

U-Pb isotopic data obtained from the detrital zircon population of the group B in the Kob-27A sample.

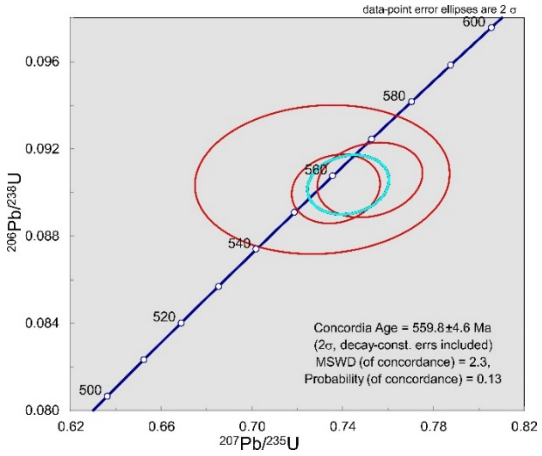

U-Pb isotopic data obtained from the youngest detrital zircons, constraining maximum depositional age for the Kob-27A sample.

10. Arkose/wacke Kob-32A (Kobryn borehole, depth 540 m); Volyn Series, Girsk Suite

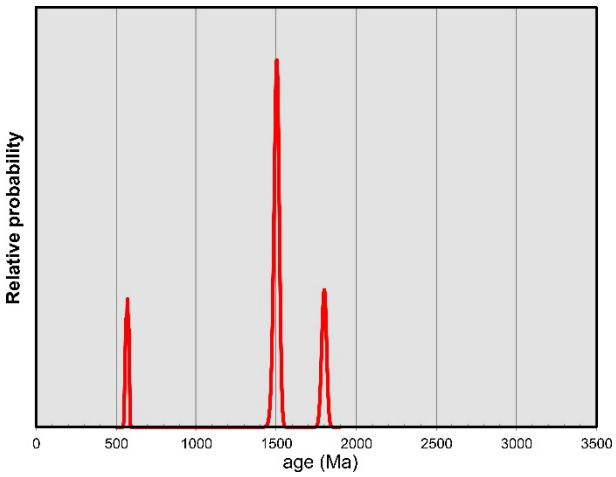

Detrital zircon age spectrum (n = 36) for the group A zircons from the Kob-32A sample.

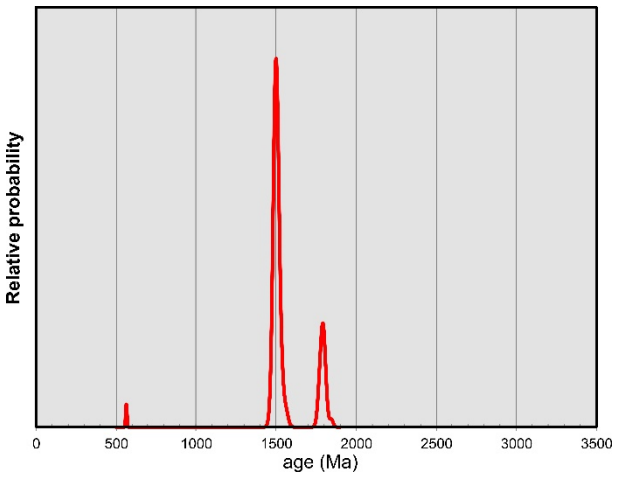

Detrital zircon age spectrum (n = 99) for the group B zircons from the Kob-32A sample.

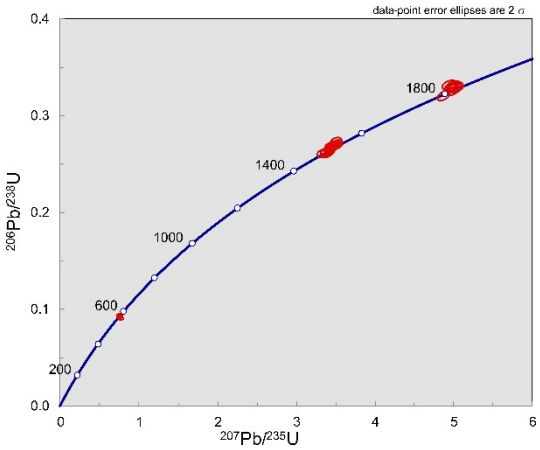

U-Pb isotopic data obtained from the detrital zircon population of the group A in the Kob-32A sample.

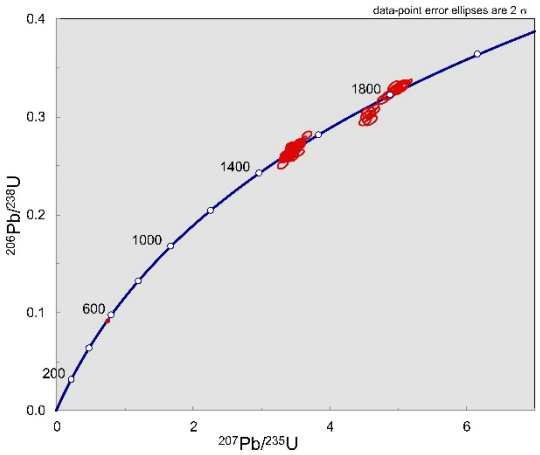

U-Pb isotopic data obtained from the detrital zircon population of the group B in the Kob-32A sample.

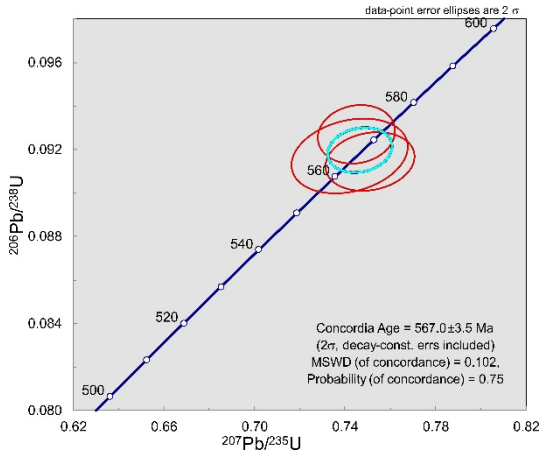

U-Pb isotopic data obtained from the youngest detrital zircons, constraining maximum depositional age for the Kob-32A sample.

11. Tuff Kob-34A (Kobryn borehole, depth 517 m); Volyn Series, Girsk Suite

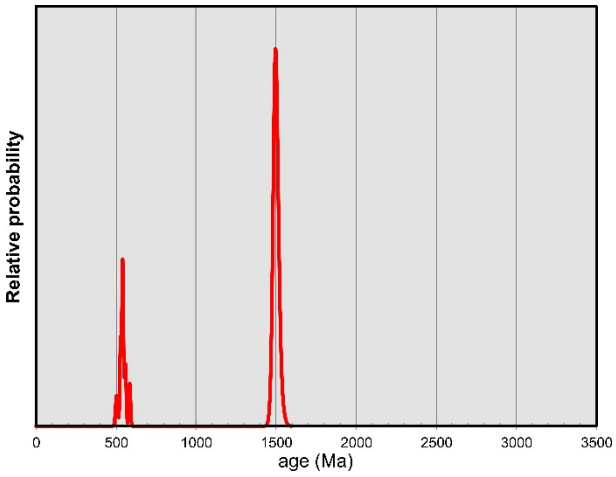

Detrital zircon age spectrum (n = 39) for the group A zircons from the Kob-34A sample.

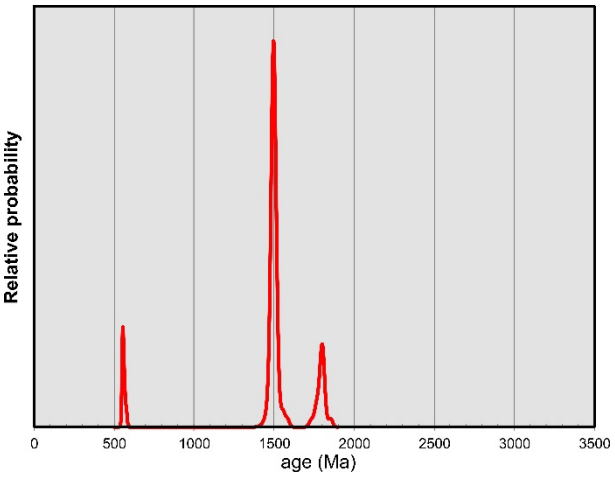

Detrital zircon age spectrum (n = 97) for the group B zircons from the Kob-34A sample.

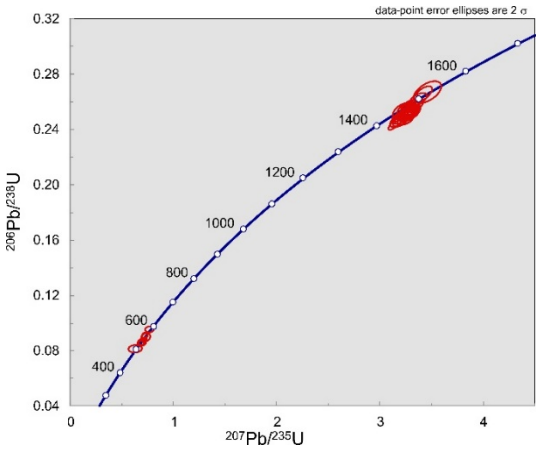

U-Pb isotopic data obtained from the detrital zircon population of the group A in the Kob-34A sample.

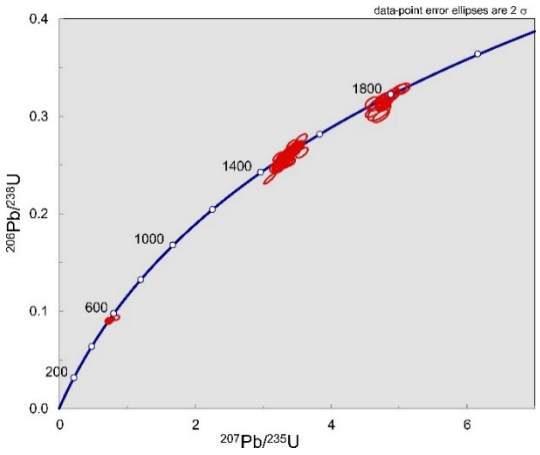

U-Pb isotopic data obtained from the detrital zircon population of the group B in the Kob-34A sample.

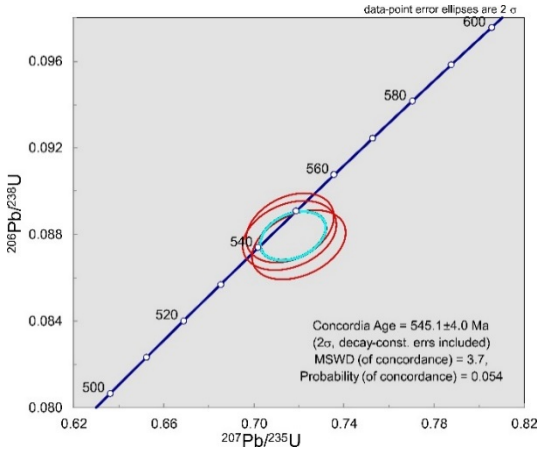

U-Pb isotopic data obtained from the youngest detrital zircons, constraining maximum depositional age for the Kob-34A sample.

12. Arkose Kob-34B (Kobryn borehole, depth 517 m); Volyn Series, Girsk Suite

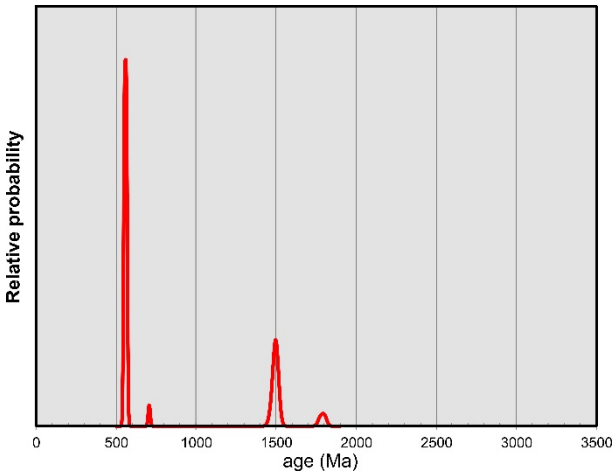

Detrital zircon age spectrum (n = 41) for the group A zircons from the Kob-34B sample.

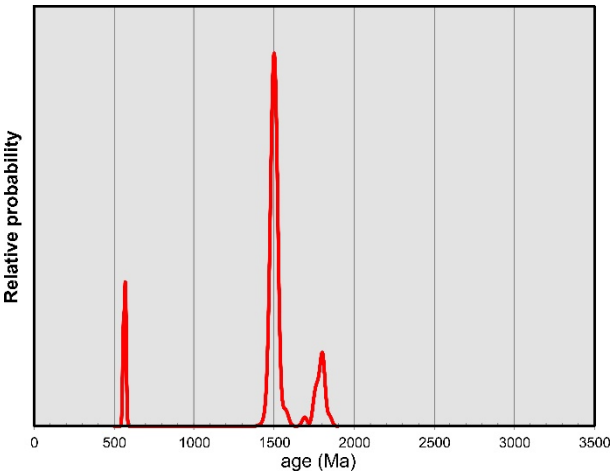

Detrital zircon age spectrum (n = 86) for the group B zircons from the Kob-34B sample.

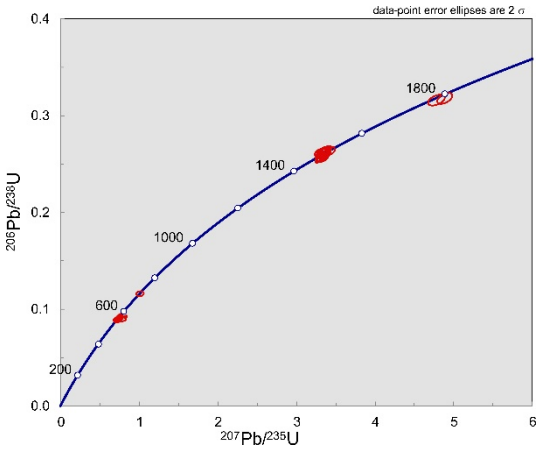

U-Pb isotopic data obtained from the detrital zircon population of the group A in the Kob-34B sample.

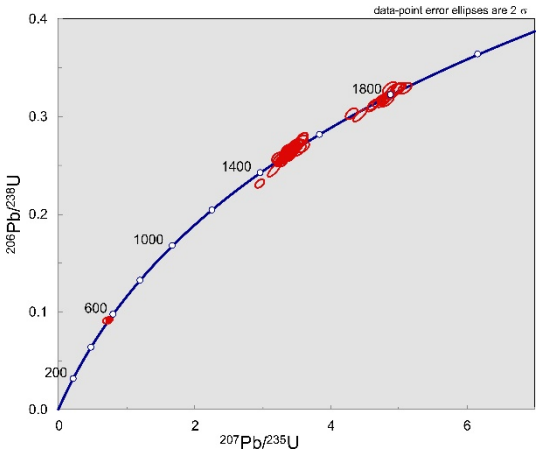

U-Pb isotopic data obtained from the detrital zircon population of the group B in the Kob-34B sample.

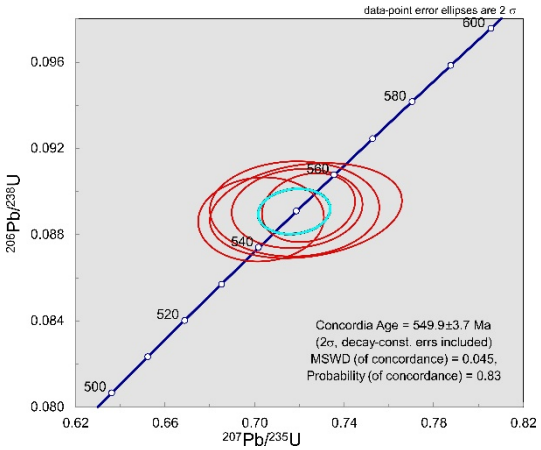

U-Pb isotopic data obtained from the youngest detrital zircons, constraining maximum depositional age for the Kob-34B sample.

13. Quartz arenite/subarkose Bog-33A (Bogushevsk borehole, depth 685.3 m); Valdai Series, Nizov Suite.

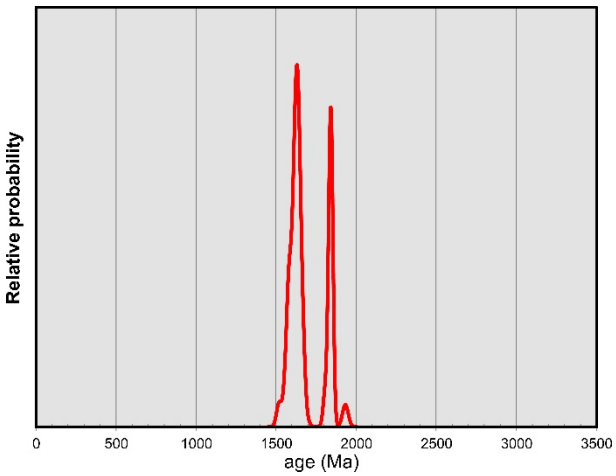

Detrital zircon age spectrum (n = 42) for the group A zircons from the Bog-33A sample.

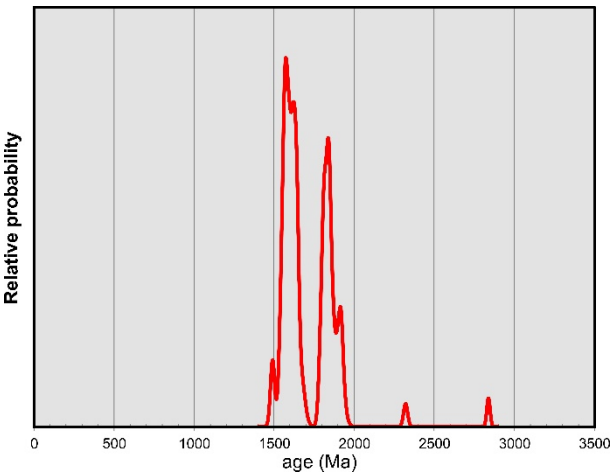

Detrital zircon age spectrum (n = 93) for the group B zircons from the Bog-33A sample.

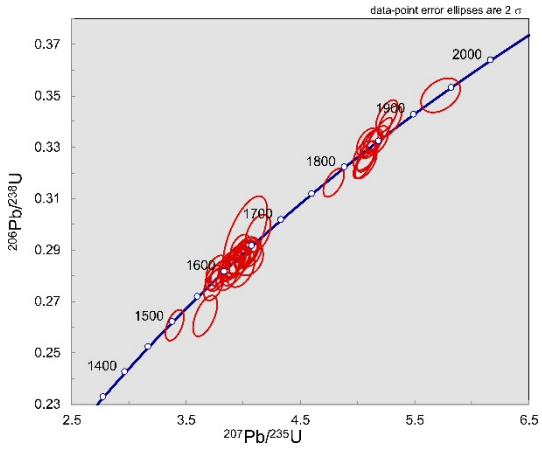

U-Pb isotopic data obtained from the detrital zircon population of the group A in the Bog-33A sample.

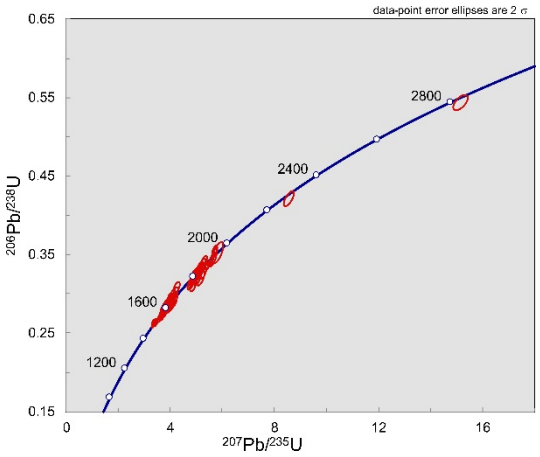

U-Pb isotopic data obtained from the detrital zircon population of the group B in the Bog-33A sample.

14. Arkose Lep-12A (Lepel borehole, depth 467 m); Valdai Series, Selsk Suite.

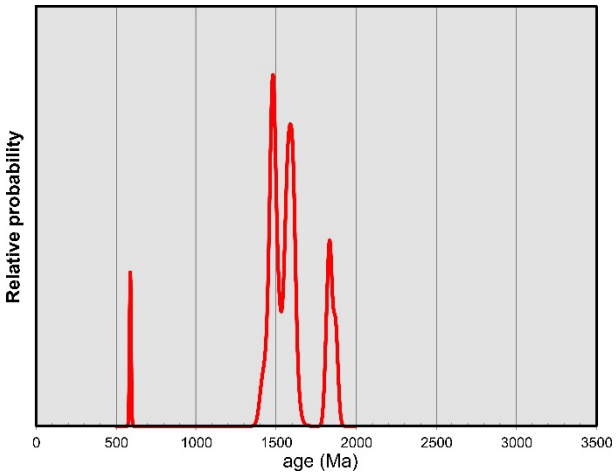

Detrital zircon age spectrum (n = 31) for the group A zircons from the Lep-12A sample.

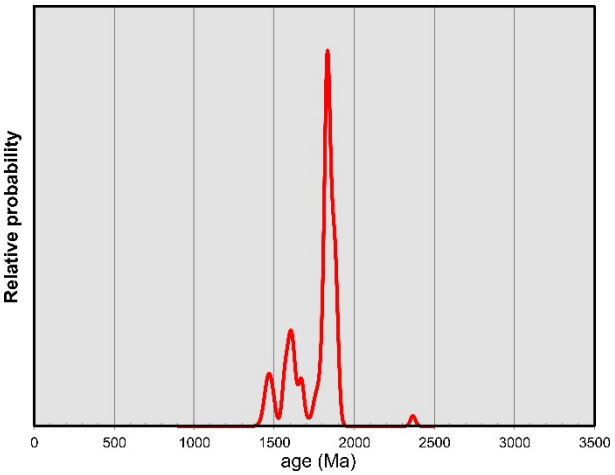

Detrital zircon age spectrum (n = 105) for the group B zircons from the Lep-12A sample.

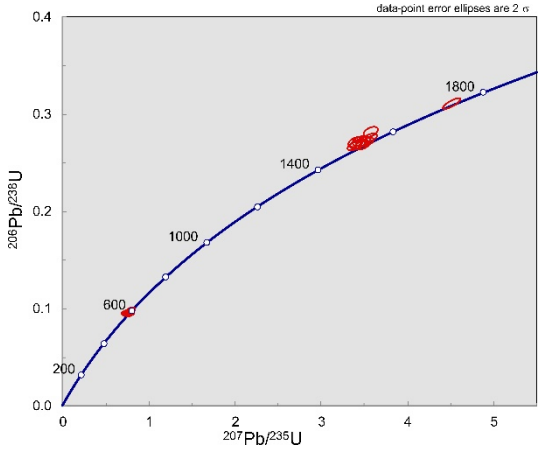

U-Pb isotopic data obtained from the detrital zircon population of the group A in the Lep-12A sample.

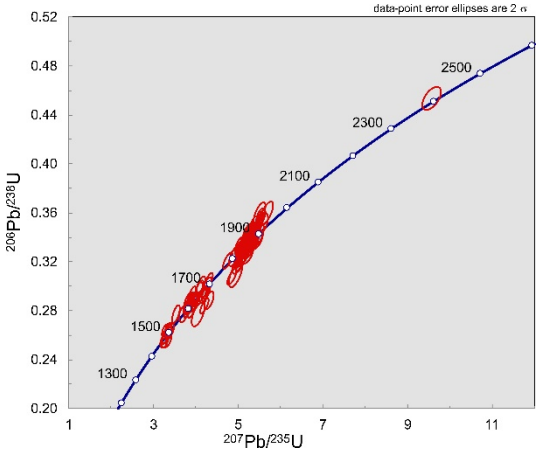

U-Pb isotopic data obtained from the detrital zircon population of the group B in the Lep-12A sample.

15. Arkose/wacke Bog-43A (Bogushevsk borehole, depth 608 m); Valdai Series, Tshernitse Suite.

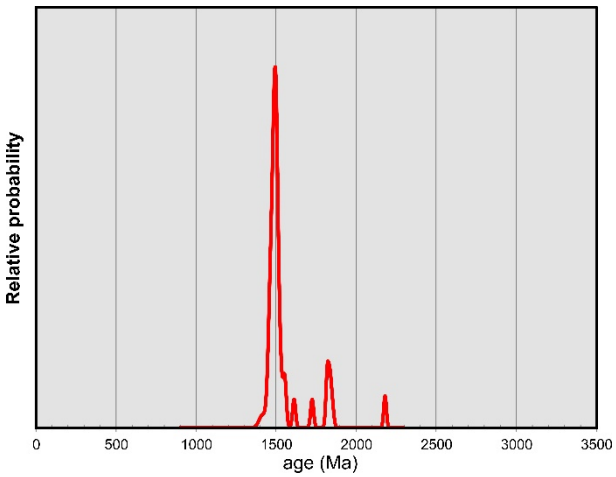

Detrital zircon age spectrum (n = 39) for the group A zircons from the Bog-43A sample.

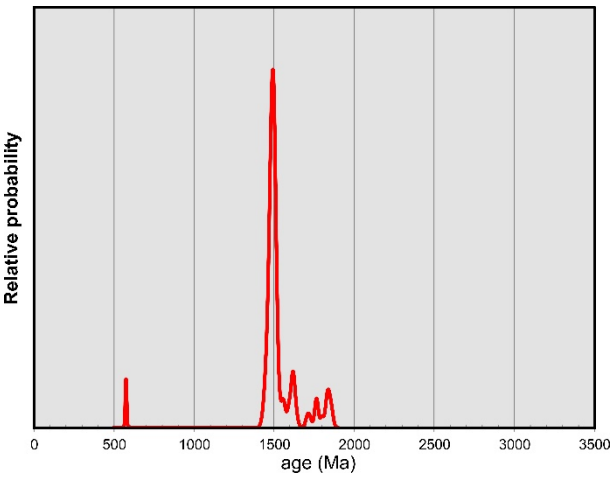

Detrital zircon age spectrum (n = 96) for the group B zircons from the Bog-43A sample.

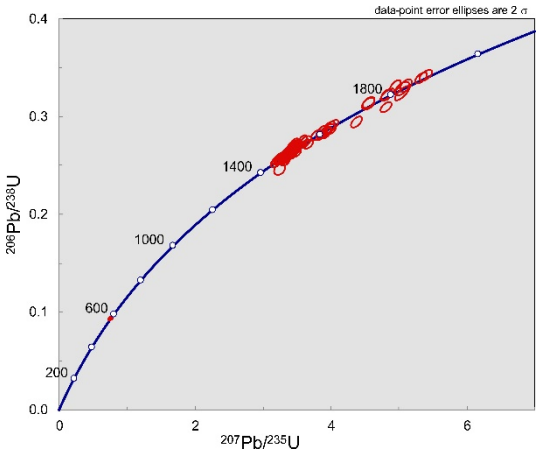

U-Pb isotopic data obtained from the detrital zircon population of the group A in the Bog-43A sample.

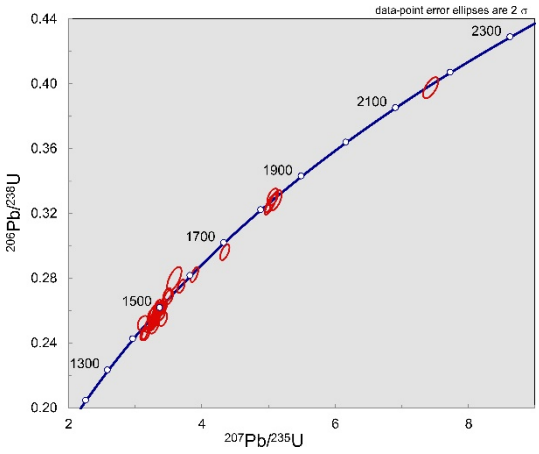

U-Pb isotopic data obtained from the detrital zircon population of the group B in the Bog-43A sample.

16. Subarkose Lep-20B (Lepel borehole, depth 418.2 m); Valdai Series, Tshernitse Suite.

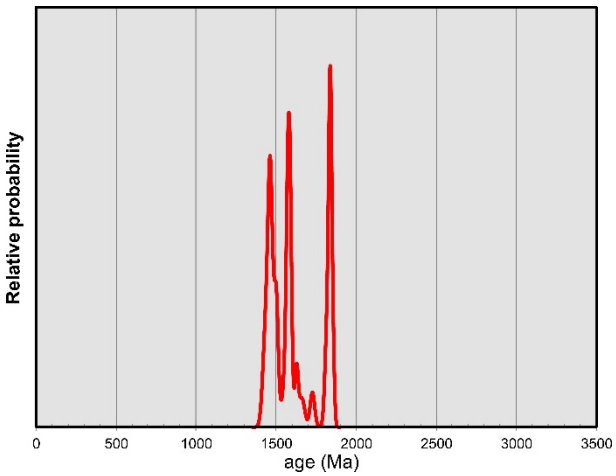

Detrital zircon age spectrum (n = 37) for the group A zircons from the Lep-20B sample.

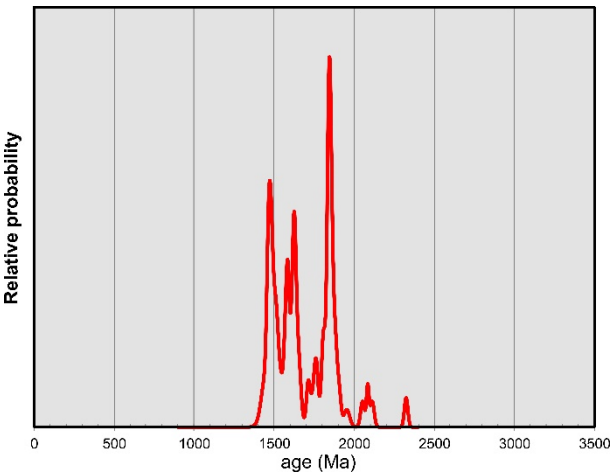

Detrital zircon age spectrum (n = 74) for the group B zircons from the Lep-20B sample.

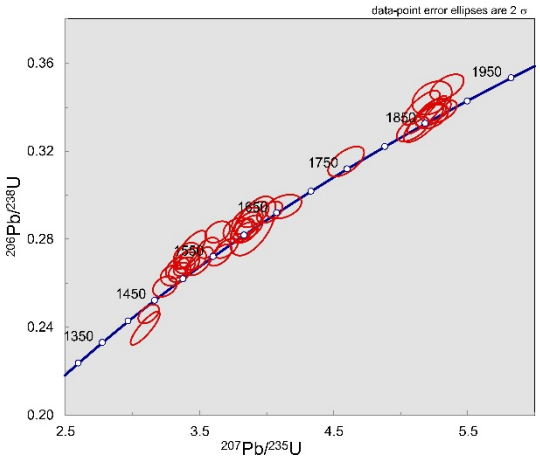

U-Pb isotopic data obtained from the detrital zircon population of the group A in the Lep-20B sample.

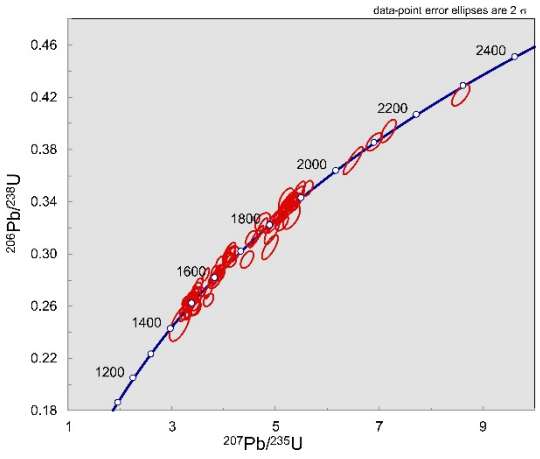

U-Pb isotopic data obtained from the detrital zircon population of the group B in the Lep-20B sample.

17. Arkosic sandstone Lep-28A (Lepel borehole, depth 370.5 m); Valdai Series, Kotlin Suite.

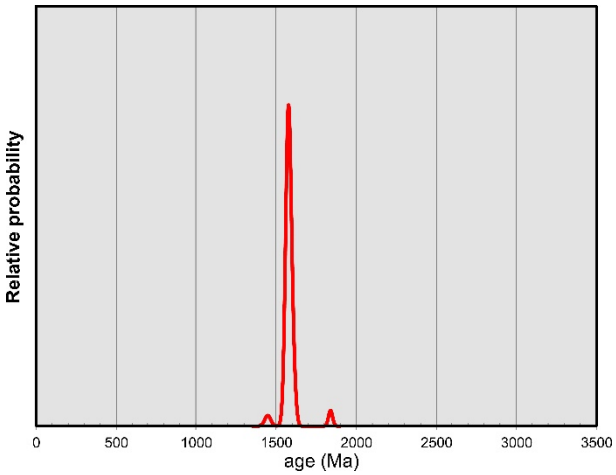

Detrital zircon age spectrum (n = 33) for the group A zircons from the Lep-28A sample.

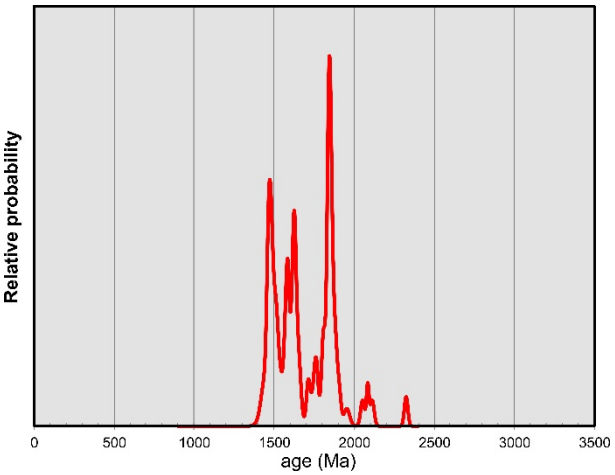

Detrital zircon age spectrum (n = 96) for the group B zircons from the Lep-28A sample.

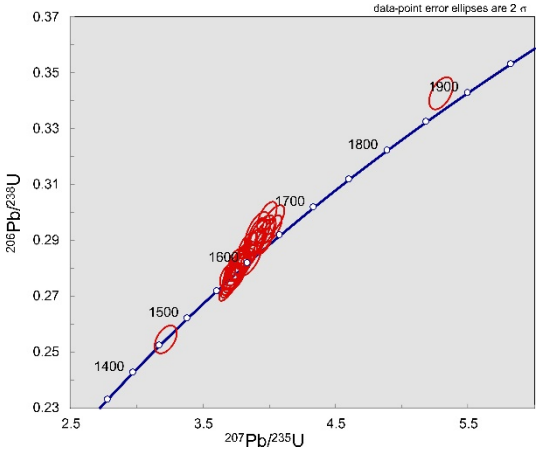

U-Pb isotopic data obtained from the detrital zircon population of the group A in the Lep-28A sample.

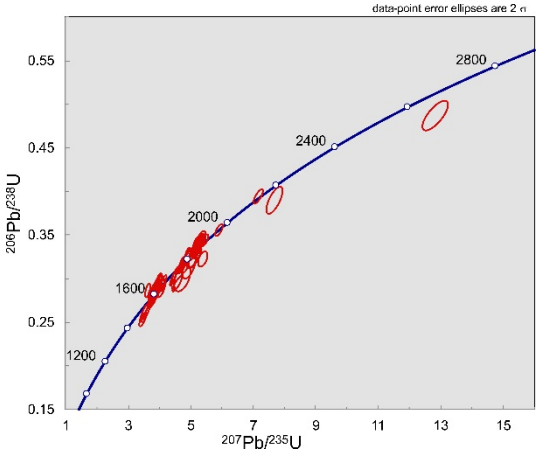

U-Pb isotopic data obtained from the detrital zircon population of the group B in the Lep-28A sample.

18. Arkose Bog-51A (Bogushevsk borehole, depth 519.5 m); Valdai Series, Kotlin Suite.

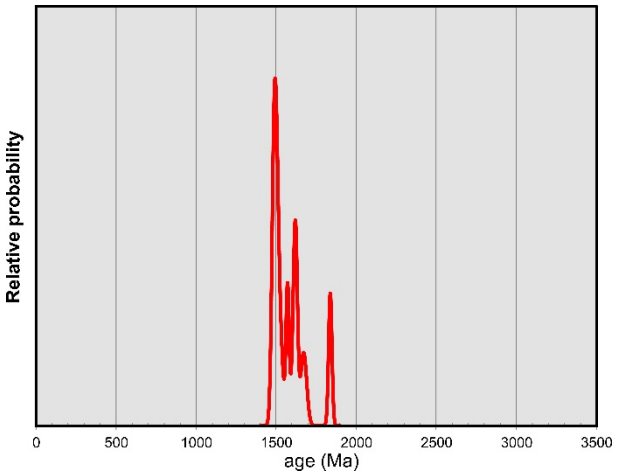

Detrital zircon age spectrum (n = 10) for the group A zircons from the Bog-51A sample.

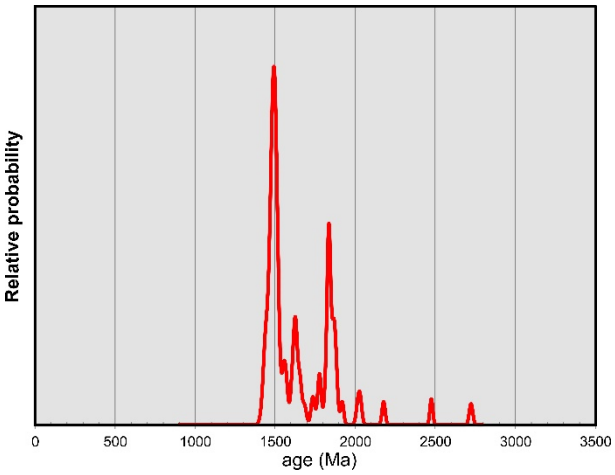

Detrital zircon age spectrum (n = 80) for the group B zircons from the Bog-51A sample.

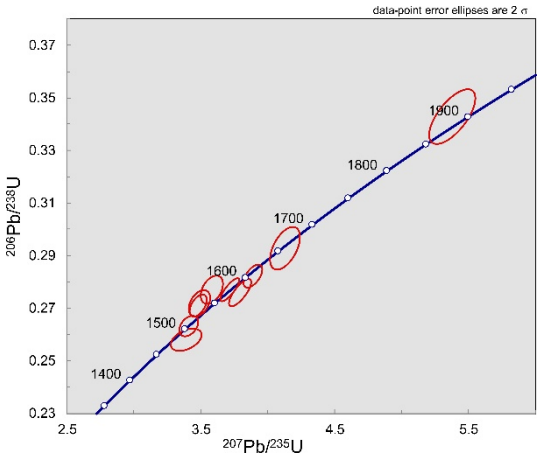

U-Pb isotopic data obtained from the detrital zircon population of the group A in the Bog-51A sample.

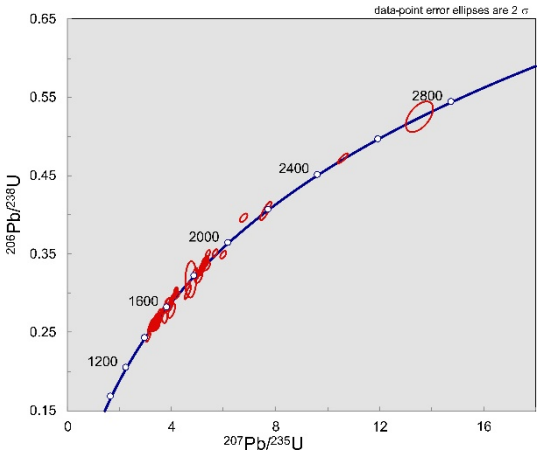

U-Pb isotopic data obtained from the detrital zircon population of the group B in the Bog-51A sample.

19. Subarkose Kob-40A (Kobryn borehole, depth 414 m); Valdai Series, Kotlin Suite.

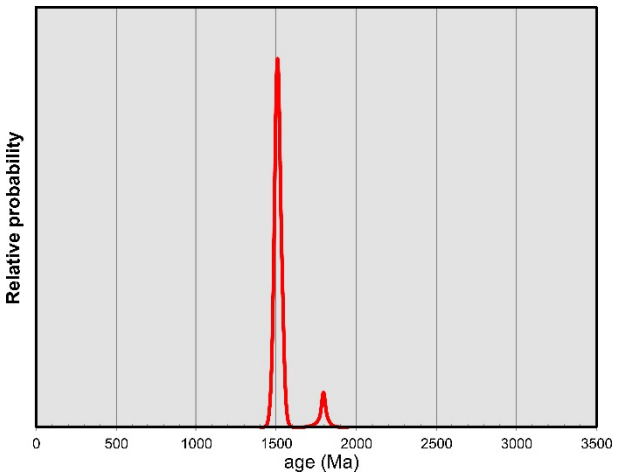

Detrital zircon age spectrum (n = 40) for the group A zircons from the Kob-40A sample.

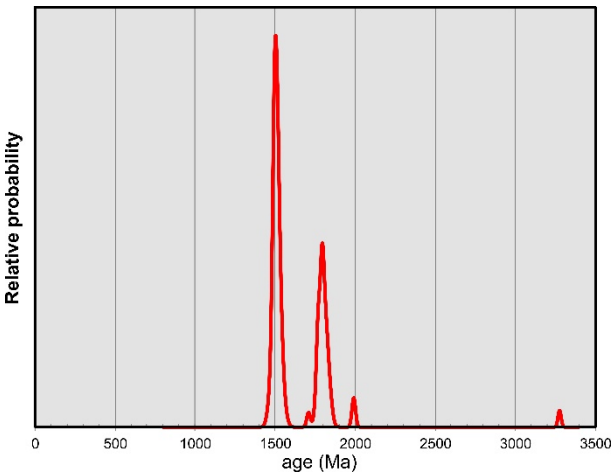

Detrital zircon age spectrum (n = 84) for the group B zircons from the Kob-40A sample.

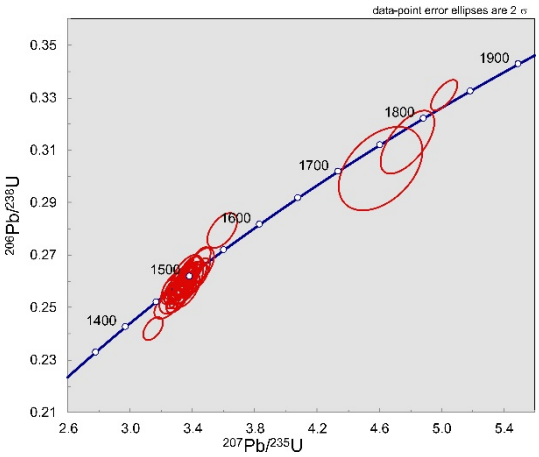

U-Pb isotopic data obtained from the detrital zircon population of the group A in the Kob-40A sample.

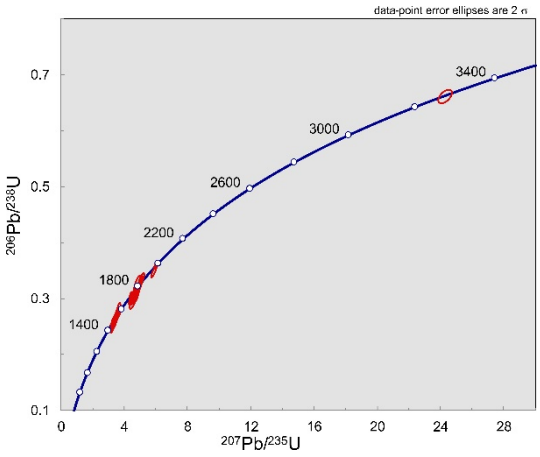

U-Pb isotopic data obtained from the detrital zircon population of the group B in the Kob-40A sample.

20. Glauconite-bearing quartz arenite Kob-54 (Kobryn borehole, depth 364 m), Early Cambrian

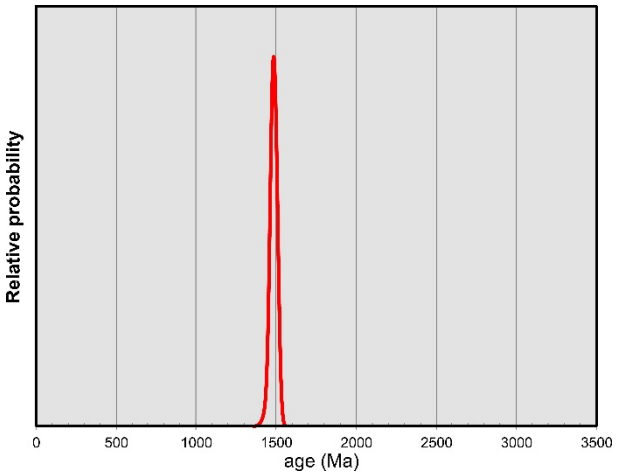

Detrital zircon age spectrum (n = 27) for the group A zircons from the Kob-54 sample.

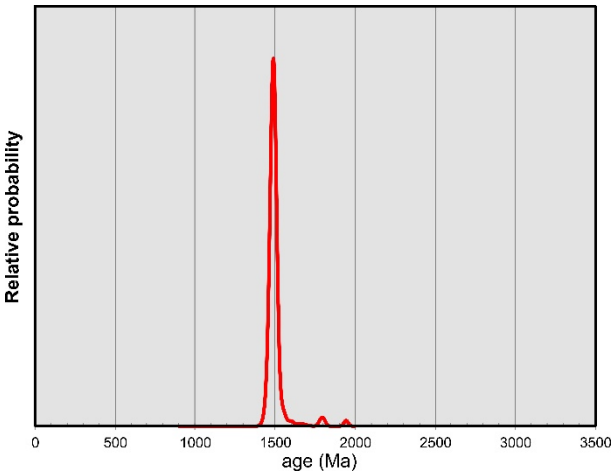

Detrital zircon age spectrum (n = 111) for the group B zircons from the Kob-54 sample.

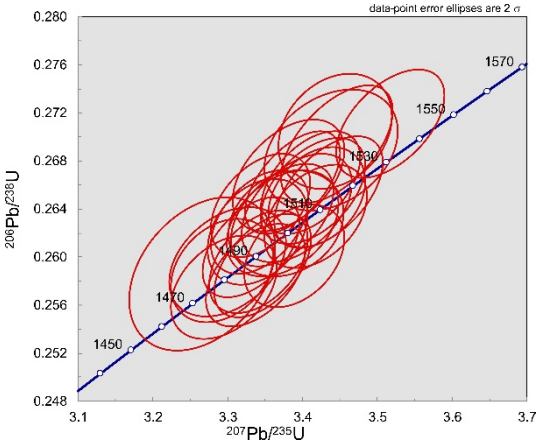

U-Pb isotopic data obtained from the detrital zircon population of the group A in the Kob-54 sample.

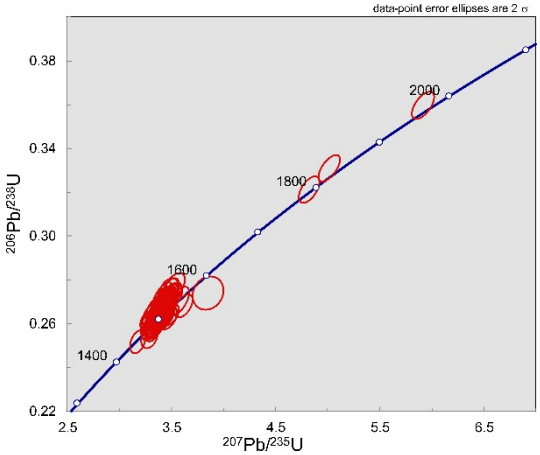

U-Pb isotopic data obtained from the detrital zircon population of the group B in the Kob-54 sample.

21. Coarse-grained sandstone Kob-57 (Kobryn borehole, depth 249.5 m), Early Cambrian

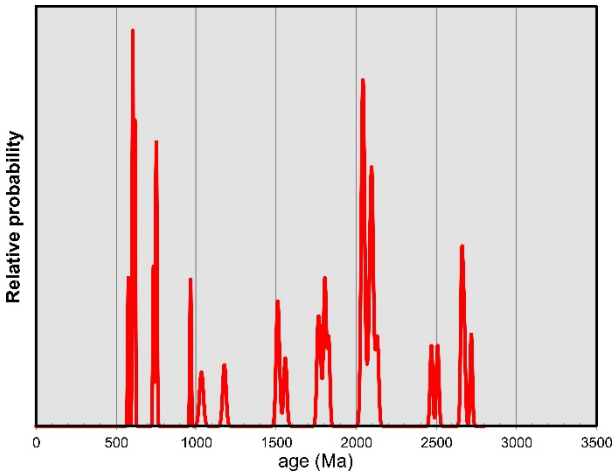

Detrital zircon age spectrum (n = 37) for the group A zircons from the Kob-57 sample.

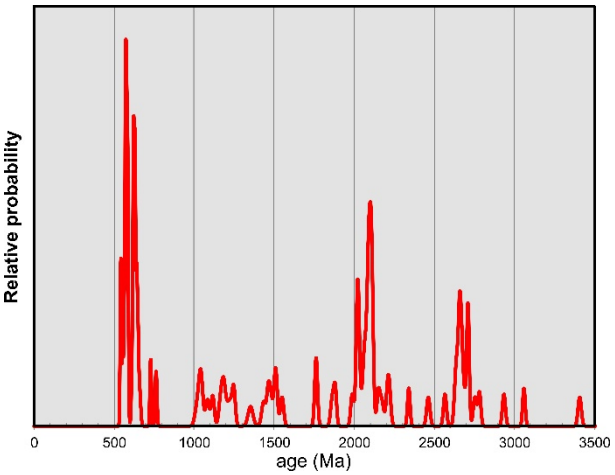

Detrital zircon age spectrum (n = 92) for the group B zircons from the Kob-57 sample.

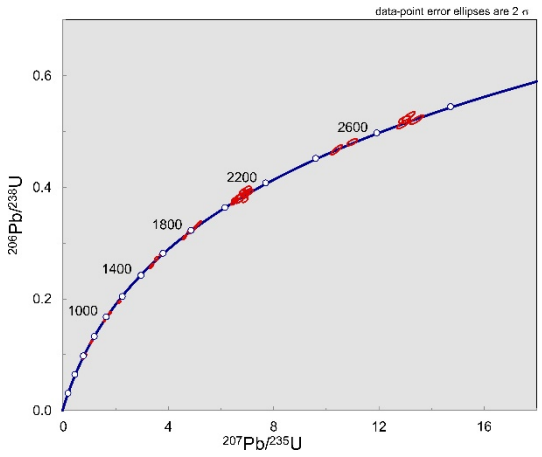

U-Pb isotopic data obtained from the detrital zircon population of the group A in the Kob-57 sample.

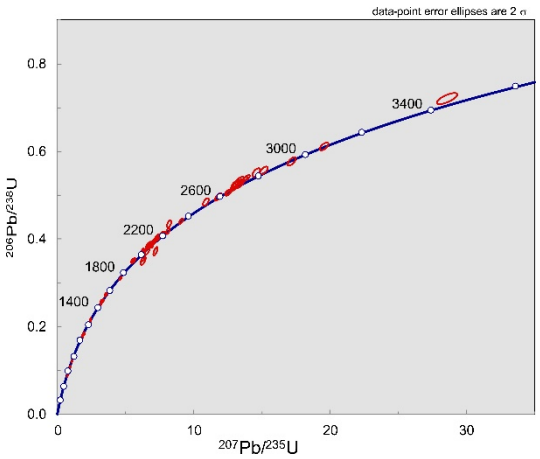

U-Pb isotopic data obtained from the detrital zircon population of the group B in the Kob-57 sample.

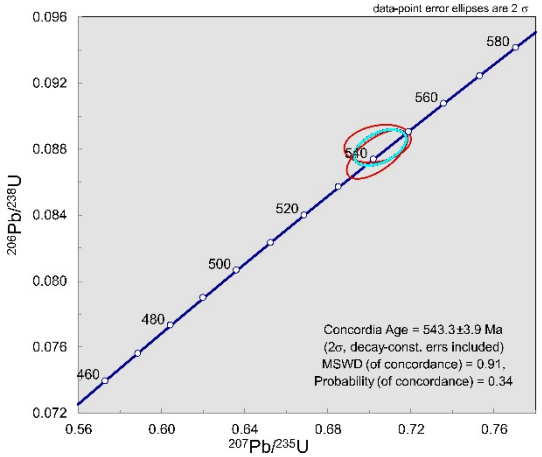

U-Pb isotopic data obtained from the youngest detrital zircons, constraining maximum depositional age for the Kob-57 sample.